Title: Radio frequency energy harvesting for autonomous systems

Name: Ivan K. Ivanov

RADIO FREQUENCY ENERGY HARVESTING FOR AUTONOMOUS SYSTEMS

by

IVAN K. IVANOV

A thesis submitted to the University of Bedfordshire in partial fulfilment of the requirements for the degree of Doctor of Philosophy

April 2018

Declaration of Authorship

I, Ivan Ivanov

declare that this thesis and the work presented in it are my own and has been generated by me as the result of my own original research.

Radio Frequency Energy Harvesting for Autonomous Systems

I confirm that:

1. This work was done wholly or mainly while in candidature for a research degree at this University;
2. Where any part of this thesis has previously been submitted for a degree or any other qualification at this University or any other institution, this has been clearly stated;
3. Where I have cited the published work of others, this is always clearly attributed;
4. Where I have quoted from the work of others, the source is always given. With the exception of such quotations, this thesis is entirely my own work;
5. I have acknowledged all main sources of help;
6. Where the thesis is based on work done by myself jointly with others, I have made clear exactly what was done by others and what I have contributed myself;
7. Either none of this work has been published before submission, or parts of this work have been published as indicated in Section 4.2.

Name of candidate: Signature:

Date:

Abstract

Radio Frequency Energy Harvesting (RFEH) is a technology which enables wireless power delivery to multiple devices from a single energy source. The main components of this technology are the antenna and the rectifying circuitry that converts the RF signal into DC power. The devices which are using Radio Frequency (RF) power may be integrated into Wireless Sensor Networks (WSN), Radio Frequency Identification (RFID), biomedical implants, Internet of Things (IoT), Unmanned Aerial Vehicles (UAVs), smart meters, telemetry systems and may even be used to charge mobile phones. Aside from autonomous systems such as WSNs and RFID, the multi-billion portable electronics market – from GSM phones to MP3 players – would be an attractive application for RF energy harvesting if the power requirements are met. To investigate the potential for ambient RFEH, several RF site surveys were conducted around London. Using the results from these surveys, various harvesters were designed and tested for different frequency bands from the RF sources with the highest power density within the Medium Wave (MW), ultra- and super-high (UHF and SHF) frequency spectrum. Prototypes were fabricated and tested for each of the bands and proved that a large urban area around Brookmans park radio centre is suitable location for harvesting ambient RF energy.

Although the RFEH offers very good efficiency performance, if a single antenna is considered, the maximum power delivered is generally not enough to power all the elements of an autonomous system. In this thesis we present techniques for optimising the power efficiency of the RFEH device under demanding conditions such as ultra-low power densities, arbitrary polarisation and diverse load impedances. Subsequently, an energy harvesting ferrite rod rectenna is designed to power up a wireless sensor and its transmitter, generating dedicated Medium Wave (MW) signals in an indoor environment. Harvested power management, application scenarios and practical results are also presented.

Acknowledgements

I would like to express my sincere gratitude to many people who supported me during the course of my studies.

I would like to first say a very big thank you to my first supervisor Dr. Ben Allen for all the support and encouragement he gave me from the beginning until the very end of my study. Thanks to Dr. Vladan Velisavljevic for his support and supervisory role and also to Dr. Masood UrRehman for his input. My deep appreciation goes also to David Jazani. His excellent support during the field trials has made an invaluable contribution towards my PhD.

I am grateful to all my friends and colleagues in Milton Keynes who were always so helpful in numerous ways during my time at UCMK. I am happy that I have had the opportunity to meet them.

Last but not the least, I would like to thank my family for supporting me throughout writing this thesis. They are the most important people in my world and I dedicate this thesis to them.

Publications

1. **Ivanov, I**., Rehman, M. U., & Allen, (2016) B. Printed Microstrip Antenna for Harvesting Energy from Mobile Phone Base Stations. In *Antennas and Propagation (EuCAP), 2016 10th European Conference on* (pp. 2–6).

2. Allen, B., Jazani, D., Dyo, V., Ajmal, T., & **Ivanov, I**. (2014). Design and optimisation of compact RF energy harvesting device for smart applications. *Electronics Letters*, *50*(2), 111–113.

3. Dyo, V., Allen, B., Jazani, D., **Ivanov, I**., & Ajmal, T. (2013). Design of a ferrite rod antenna for harvesting energy from medium wave broadcast signals. *The Journal of Engineering*, 1–8.

4. **Ivanov, I**, Allen, B., Rehman, M. U. (2013). Radio Frequency Energy Harvesting from medium waves AM broadcast signals. *ARSR-SWICOM 2013 Conference*

Table of contents

List of Figures

List of Tables

Acronyms

3G	Third Generation
4G	Fourth Generation
AC	Alternating Current
ADS	Advanced Design Software
AM	Amplitude Modulation
BW	Bandwidth
CDMA	Code Division Multiple Access
CEPT	European Conference of Postal and Telecommunications Administrations
CMOS	Complementary Metal Oxide Semiconductor
CMPA	Circular Microstrip Patch Antenna
CPS	Coplanar Stripline
CSI	Channel Station Information
CUT	Coil Under Test
DAB	Digital Audio Broadcast
DC	Direct Current
DC-DC	Direct Current to Direct Current
DTV	Digital Television
DVB	Digital Video Broadcast
EH	Energy Harvesting
EIRP	Effective Isotropic Radiated Power
ELF	Extremely Low Frequency
EM	Electromagnetic
EMF	Electromagnetic Field
ERP	Effective Radiated Power
ESR	Effective Series Resistance
EV	Electric Vehicle
FEA	Finite Element Analysis
FM	Frequency Modulation
FSPA	Folded Shorted Patch Antenna
GaAs	Gallium Arsenide
GEO	Geostationary Earth Orbit

GPS	Global Positioning System
GSM	Global System for Mobile Communications or Groupe Spécial Mobile
HB	Harmonic Balance
HFSS	High Frequency Structural Simulator
IoT	Internet of Things
IEEE	Institute of Electrical and Electronic Engineers
IGBT	Insulated Gate Bipolar Transistor
IPT	Inductive Power Transfer
ISM	Industrial, Scientific, Medical
LCD	Liquid Crystal Display
LED	Light Emitting Diode
LF	Low Frequency
Li-ion	Lithium Ion
LTE	Long Term Evolution
LTSpice	Simulator of electronic circuits, produced by Linear Technology
LW	Long Wave
MDP	Markov Decision Process
MESFET	Metal Semiconductor Field Effect Transistor
MIM	Metal-insulator-metal
MIT	Microstrip Impedance Transformer
MOSFET	Metal Oxide Semiconductor Field Effect Transistor
MPPT	Maximum Power Point Tracking
MSF	Longwave time broadcast
MW	Medium Wave
NiCd	Nickel Cadmium
NiMH	Nickel Metal Hydride
NMOS	N-Type Metal Oxide Semiconductor
OCV	Open Circuit Voltage
PA	Power Amplifier
PCB	Printed Circuit Board
PMOS	P-Type Metal Oxide Semiconductor
PSU	Power Supply Unit
PTFE	Polytetrafluoroethylene

QS	Quasi Static
RC	Resistance, Capacitance (electric circuit)
RF	Radio Frequency
RF-DC	Radio Frequency to Direct Current
RFEH	Radio Frequency Energy Harvesting
RFID	Radio Frequency Identification
RLC	Resistance, Inductance, Capacitance (electric circuit)
RX	Receiver
SDR	Software Defined Radio
SHF	Super High Frequencies
SLA	Sealed Lead Acid
SNR	Signal to Noise Ratio
SPICE	National Instruments Model Parameters
SPS	Solar Power Satellite
SRF	Self-resonant Frequency
SWIPT	Simultaneous Wireless Information and Power Transfer
SWR	Standing Wave Ratio
TCF77	German longwave time signal
TETRA	Terrestrial Trunked Radio
TV	Television
TX	Transmission
UAV	Unmanned Aerial Vehicle
UHF	Ultra High Frequency
UK	United Kingdom
UMTS	Universal Mobile Telecommunications System
USA	United States of America
VHF	Very High Frequencies
VNA	Vector Network Analyser
VSWR	Voltage Standing Wave Ratio
WiMAX	Worldwide Interoperability for Microwave Access
WLAN	Wireless Local Area Network
WPT	Wireless Power Transfer
WSN	Wireless Sensor Network

Chapter 1 Introduction

1.1. Aim and objectives

Radio Frequency Energy Harvesting (RFEH) is an emerging and essential technology because of its advantages over the more popular optical [1], mechanical [2] and thermal [3] harvesting technologies. The aim of this research is to investigate and develop effective RFEH methods and devices, capable of producing enough power for the operation of low power autonomous systems such as Wireless Sensor Networks (WSN), IoT devices, Radio-frequency Identification (RFID) systems etc.

Harvesting the surrounding energy is a well-known technique. Most exploitable ambient energy sources can be found in solar radiation, thermal sources and physical motion, and they have been already harvested using photovoltaic panels [4], thermoelectric [5] and kinetic energy harvesters [6], respectively. However, none of them provide a continuous power due to the nature of their energy sources. Collecting energy from radio waves is a feasible energy harvesting method, in which the power harvested will be present until the source signal is interrupted.

The main objectives of this research are to:

- Investigate potential applications;
- Investigate suitability of the available electromagnetic sources:
    - TV and Radio broadcast transmitters;
    - Mobile phone base stations;
    - ISM band communications;
    - Wi-Fi transmitters;
    - Special purpose communications, such as point-to-point communication links etc.

• Select the most suitable sources by applying temporal, geographical and frequency domain analysis of the available RF sources. This includes link loss analyses at the frequencies on which RF transmissions are available.

• Investigate candidate antenna designs such as:

- Dipole array;
- Ferrite Rod antenna (LF);
- Microstrip (Patch) antennas;
- Microstrip Yagi-Uda antennas;
- Bowtie microstrip antenna;
- Folded dipole with reflector.

• Develop and compare experimental prototypes of selected antenna designs.

• Determine effectiveness of RFEH devices in terms of power, size and efficiency trade-off.

• Evaluate the effectiveness of candidate RF-DC converter circuits through simulation and experimentation. A simple and straightforward model of an RF-DC converter will be proposed, that can then be used to translate it into an equivalent circuit which can be simulated by a general purpose simulator such as LTspice [7].

The power can be transferred using inductive coupling at very short distances, inductive power transfer for mid-distances and RF power transfer for long distances. Wireless Power Transfer (WPT) is a technology that can deliver power to locations, which are not accessible for the conventional energy harvesting methods.

There are several approaches for applying wireless power supply. Near-field inductive coupling typically works on less than few centimetres, however, it is characterised by high efficiencies [8], [9]. Inductive coupling methods are not relying on radio propagation properties. They work at distances much shorter than the wavelength of the energy source signal. This approach is popular in wireless

charging of the rechargeable battery of consumer products, such as electric shavers or toothbrushes.

Magnetic coupling between two devices (usually coils) enables energy transfer in the near-field. Transmitters and receivers used in this technology are typically huge [10], [11] and energy can only be transferred over short ranges where the distances are comparable to the receiver and emitter physical sizes. The highest power efficiency available is only reached close to an optimal operating point [12]. Up to 70% transfer efficiency can be achieved, considering the loss between the transmitter and receiver, at distances of not more than 1 m, however, the overall system efficiency with this method is under 20%.

Energy can also be transferred by using the properties of High Frequency (HF) field. High power RF energy has been transferred over distances of more than a kilometre with power efficiencies of more than 70% [13]. The same technique is also used for transferring power for High Frequency Radio-Frequency Identification (HF RFID) devices [14] at ranges of less than 10 m using HF radio spectrum.

1.2. System description

The key components of RFEH technology are the antenna and the rectifying circuitry that converts the RF signal into a DC signal (Figure 1.1). The load can be a DC energy storage device (battery, capacitor, etc.) or, a directly powered device. In both cases, load parameters such as resistance and capacitance are often not constant. The requirements for a rectifier's characteristics would be defined by analysing the signals at the antenna's output (or rectifier input) and the load's input.

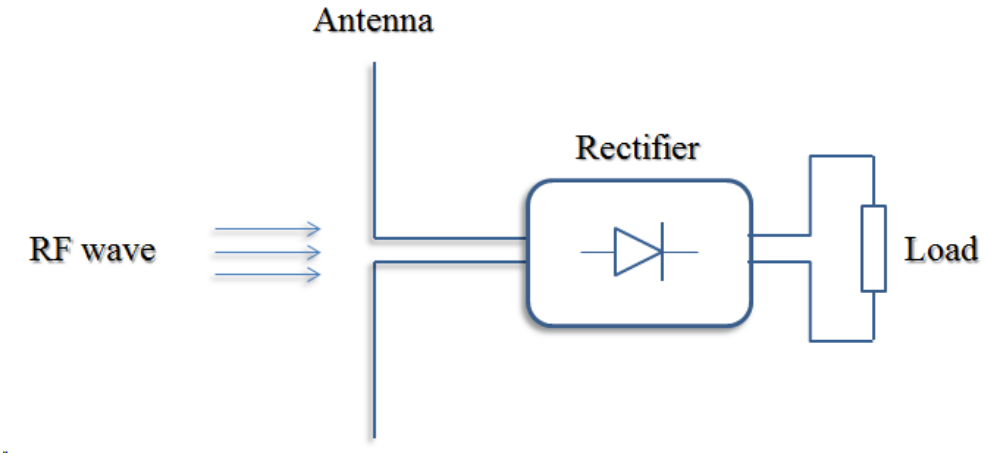

Figure 1.1 Block diagram of RF energy harvester

Analysing the component's specifications of an RFEH system is an important aspect of its overall optimisation process. Therefore, to analyse such a system in terms of power efficiency, two more components should be added to the diagram shown in Figure 1.1 – matching network and DC-to-DC charge pump. The importance of these two components will be demonstrated in Chapter 5

Figure 1.2 illustrates the typical high level configuration suitable for power efficiency analyses. It is important to highlight that, as in any other energy harvesting system, the goal is to maximise the rectified power available to the load terminals for a given incident RF signal power. This work focuses on optimizing the complete system, therefore all system blocks will be taken into account.

Figure 1.2 RF Energy Harvester system block diagram

Increasing the power conversion efficiency of RF-DC circuitry in RF energy harvesting circuits extends the range and reliability of autonomous networks. Multi-frequency waveforms are one technique that assists in overcoming the energy-harvesting circuit diode voltage threshold, which limits the energy-

conversion efficiency at low RF input powers typically encountered by sensors at the fringe of their coverage area.

As shown in expression (1), each block contributes some conversion loss to the overall system efficiency.

$$P_{DC} = \eta_M \eta_P \eta_{CP} \eta_{DC} P_{inc} \quad (1)$$

where, P_{DC} is output DC power, η_P is the parasitic and η_M is the matching efficiency, η_{CP} is the RF-DC conversion efficiency, η_{DC} is the DC-to-DC conversion efficiency, and P_{inc} is the incident RF power.

1.3. RF energy sources

Multiple sources of RF electromagnetic energy occur on different frequencies in many directions. With the impact of mobile communications and digital broadcast transmissions the RF electromagnetic environment has become more suitable for harvesting RF Energy than ever before. Ambient RF energy sources are available on many frequencies and with different power densities. However, when the target is to use it as a source for powering elements of an autonomous system the right choice of the RF source is of extreme importance. In order to select the most appropriate transmission for a particular application, it requires key parameters of the candidate signals to be investigated, such as frequency, power, coverage, location and the transmitter's duty cycle.

In many of the todays urban environments, there are a variety of RF electromagnetic sources, such as Digital Video Broadcast (DVB) stations, GSM downlink base stations, Medium Wave (MW) broadcast stations, Wi-Fi networks, etc. Presenting the frequency spectrum as a complex range of frequency bands as shown in Figure 1.3, helps to compare the RF energy sources available to the

ambient sources which have already been successfully used as alternative power sources for many years.

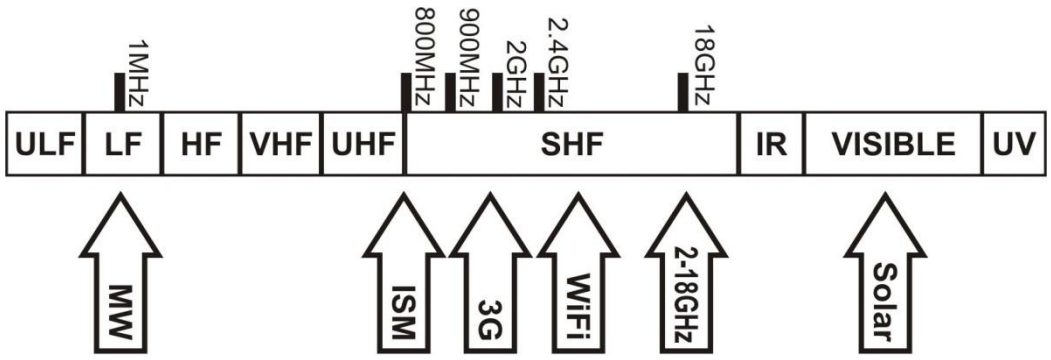

Figure 1.3 Examples of sources of ambient energy

The obvious need of collecting ambient RF energy using dedicated RF power transmissions is the reuse of RF energy emitted by radio transmitters, such as WiFi networks and mobile base stations. The number of these RF transmissions will continue to increase with the expansion of the of mobile devices. For instance, considering the number of WiFi access points and wireless user devices such as tablets and laptops, we can conclude that the energy transmitted by such devices have multiplied recently. As a result, in particular urban environments, we can scan and discover tens, and in some cases hundreds of WiFi signals at a single location.

The number of WiFi networks over the years detected by one of the submission-based catalogues of wireless networks [15] is shown in Figure 1.4.

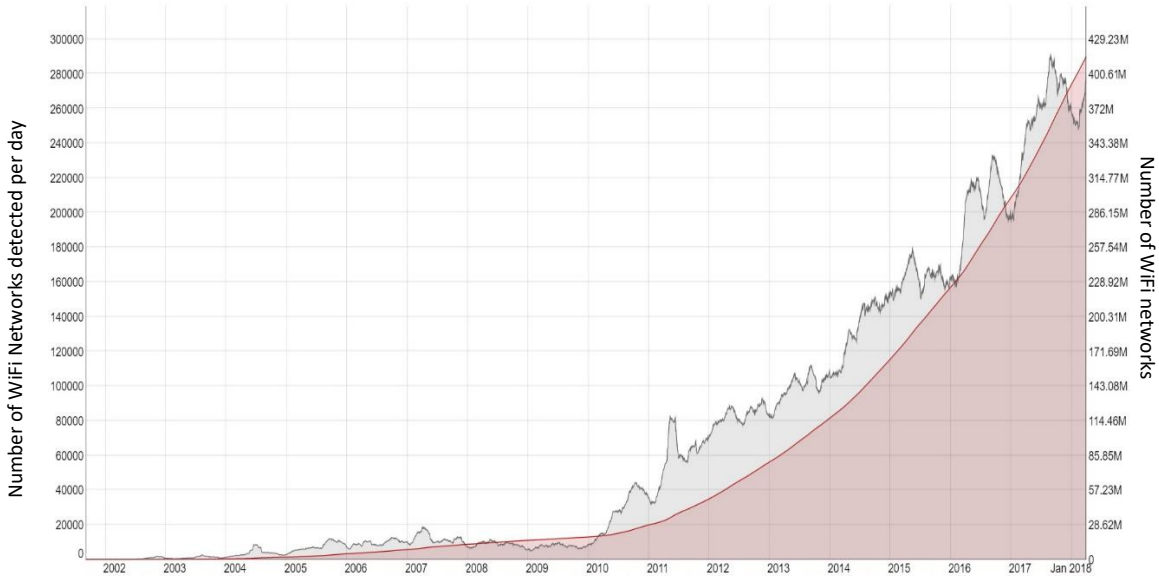

Figure 1.4 Plot of the growth of the number of WiFi networks worldwide [15]

1.4. RFEH applications

The number of communication devices used in applications such as smart devices and WSN, has grown rapidly during the last decades. Such an increase in wireless applications requires improved power sources to be developed. Many researchers are working on the improvement of the efficiency of the batteries [16], [17]. However, the last considerable improvement in this field was discovered 25 years ago, when Sony used the lithium cobalt oxide cathode, invented earlier by J. B. Goodenough [18], in combination with a carbon anode to discover the first rechargeable lithium-ion battery in the world [19]. Moreover, there is a discrepancy between the main requirements of autonomous systems and the limitations caused by battery's disadvantages such as: limited life, require constant recharging or replacement, and contain a variety of toxic chemicals. Ambient radio frequency energy harvesting may be considered as an emerging technology that enables wireless nodes to work for interrupted periods of time, which can be a very good alternative to conventional battery power.

A range of autonomous devices have already been powered successfully by energy delivery via microwave beams. This method was proposed for heavy wireless power applications, such as Solar Power Satellite (SPS) [20] and Unmanned Aerial Vehicle (UAV) [21]. Recently, with the rapid development of devices with low power requirements, this technology became commercially available. An example for a successful use of this method is Radio Frequency Identification (RFID) [22], [23]. All of these applications (see Figure 1.5) require specific source of EM energy to transmit for the purpose of RFEH.

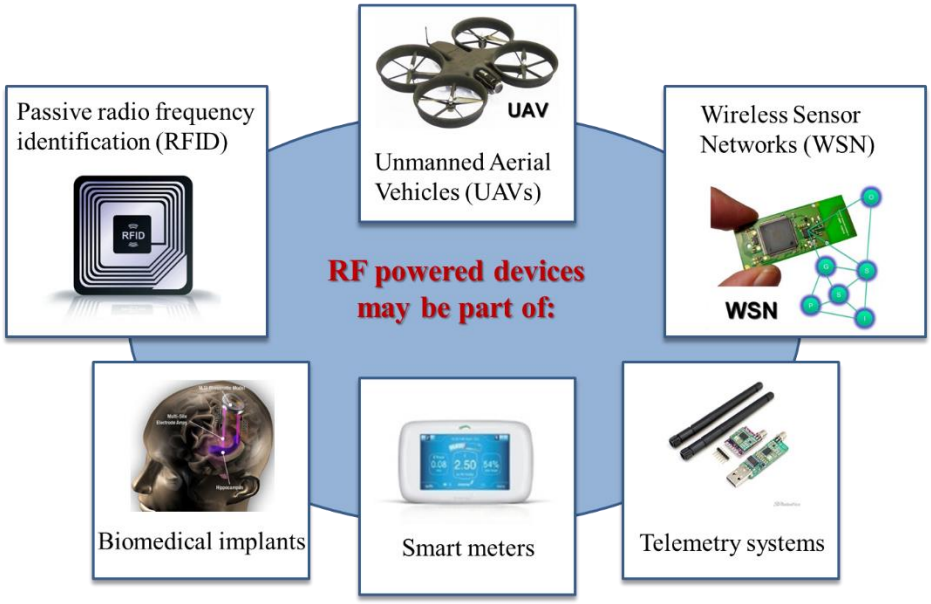

Figure 1.5 RF Energy Harvesting Applications

However, with the advancement of modern communications technologies a variety of ambient RF transmissions are available in urban environment. Moreover, the decreased power requirements of the sensor nodes used in the autonomous systems nowadays, are creating opportunities for new fields of application for harvesting ambient RF energy.

There are areas of applications for which such a type of energy is of extreme importance such as:

o ***Health monitoring***. Power supply for cardiac pacemakers, prostheses etc. where a high up-time is required and it is risky to install batteries or any other conventional power source;

o ***Smart sensors for environmental monitoring*** e.g. forest fire detection where it is difficult to approach the powered device for maintenance and no wired power source is available;

o ***Embedded sensors*** e.g. inside the asphalt of the bridges and other structures where it is impossible to install batteries or other conventional power sources and a high up-time is demanded.

Another application example is the concept of Solar Power Satellite (SPS) that would collect solar energy at geostationary Earth orbit, transfer it to high power RF energy, and re-transmit it to the Earth surface. The technology was first described in 1968 by P. Glaser of A. D. Little. Between 1976 and 1980, NASA supported an in-depth study of this concept, conducted by United States Department of Energy [24]. The research project was very well funded and resulted in a variety of useful research.

Many of the design parameters of such a system are defined by the node's power requirements. Examples of such nodes and approximate consumption are shown in Figure 1.6.

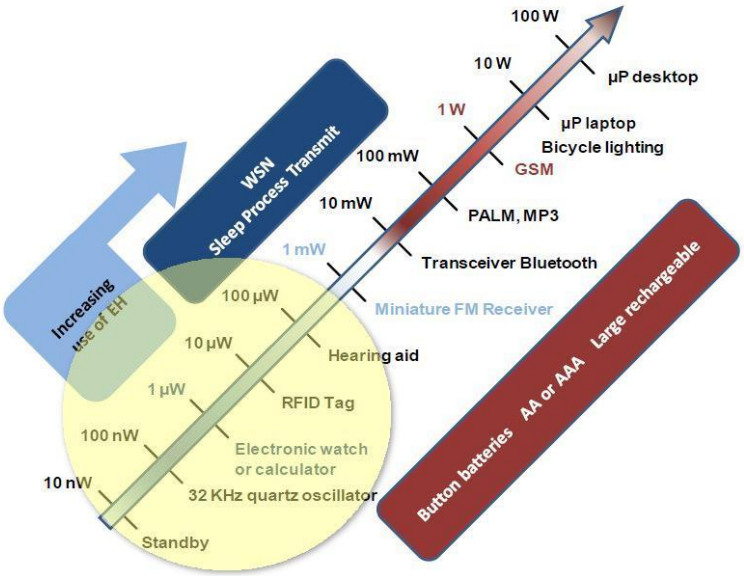

Figure 1.6 Power requirements of small electronic products

Selection of operating frequency band and type of rectenna for the RFEH system, based on the targeted application, may be crucial because of its effect on the overall efficiency of the autonomous system. As the state-of-the-arts shows,

the highlighted circle in Figure 1.6 covers the region where RFEH is currently applicable. In many cases this area can be extended depending on the energy source type. It also shows small electronic devices, such as WSN nodes, mobile phones, and the types of battery employed.

RFE harvesting may be considered as an urgent technology in application areas such as:

- Health monitoring. Power supply for cardiac pacemakers, prostheses sensors etc. where a high uptime is required and it is risky to install batteries or any other conventional power source;
- Smart sensors for environmental monitoring in difficult to access locations, e.g. forest fire detection where it is difficult to approach the powered device for maintenance and no wired power source is available;
- Embedded in structures e.g. inside the asphalt of the bridges and other structures where it is impossible to install batteries or other conventional power sources and a high uptime is demanded.

Therefore, the use of RF power harvesting systems as alternative power sources, capable of replacing the batteries and delivering an independent energy to decrease the maintenance and operational cost, will make it one of the most suitable candidates for alternative power of autonomous systems, and will attract attention for future research and development. However, its dependence on such low incident levels of RF power density, shows us that this technology still needs development.

1.5. RF power density of MW transmissions

In order to estimate how much RF energy can be harvested at a given distance from the transmitter we use different methods depending on the energy source. We also compare the estimated results with measurements in order to validate

them correctly. Calculating path loss levels for RF energy harvesting at low frequencies allows us to not take in account factors such as multipath, ionospheric reflection, tropospheric reflection, sky-wave interference, etc.

Using similar principles as those for measuring broadcasting transmitter ground wave coverage we can reduce all the complexity to a simple expression for the field strength (*E*) at distance *d* as it is shown in [25]:

$$E = Z_i \frac{I_0 \, h_e}{\lambda d} A \tag{2}$$

where h_e is the effective height of a vertical monopole with base current I_0 and *A* is the attenuation factor (dimensionless). An alternative expression for the electric field density at a distance *d* is given by Equation (3) when we use units of mV/m, kW and km.

$$E = \frac{FM\sqrt{P_t}}{d} A \tag{3}$$

where the term Figure of Merit (*FM*) is more suitable when calculating path loss at MW frequencies.

Note that in Equation (4) ε_r and ε_0 are describing some of the ground's specifications.

$$q = \frac{|J_c|}{|J_d|} = \sigma/(\omega \varepsilon_r \varepsilon_0) \tag{4}$$

If q is sufficiently smaller than 1, the ground is considered as a good dielectric. If its value is close to 1 the ground is a complex dielectric and more variables are needed for it to be explained.

There are more than 330 broadcast stations in the UK transmitting using Amplitude Modulation (AM) in the Medium Wave (MW) band (526.5 to 1606.5kHz for Europe) (see Figure 1.7). 140 of them are using power higher than 1000W. A

detailed list of MW AM broadcast radio stations, using power between 2kW and 500kW in the UK, is presented in APPENDIX E. Most of the broadcast antennas used currently on the MW frequencies are omnidirectional in the azimuth plane. The most conventional type of MW transmitting antenna used in the UK is the Monopole antenna. There are several monopole types – Base-fed, Shunt-fed, Folded Monopole, etc. [26]. The radiation pattern of all of them is omnidirectional in the azimuth plane, so, we will take it into account when estimating the path loss.

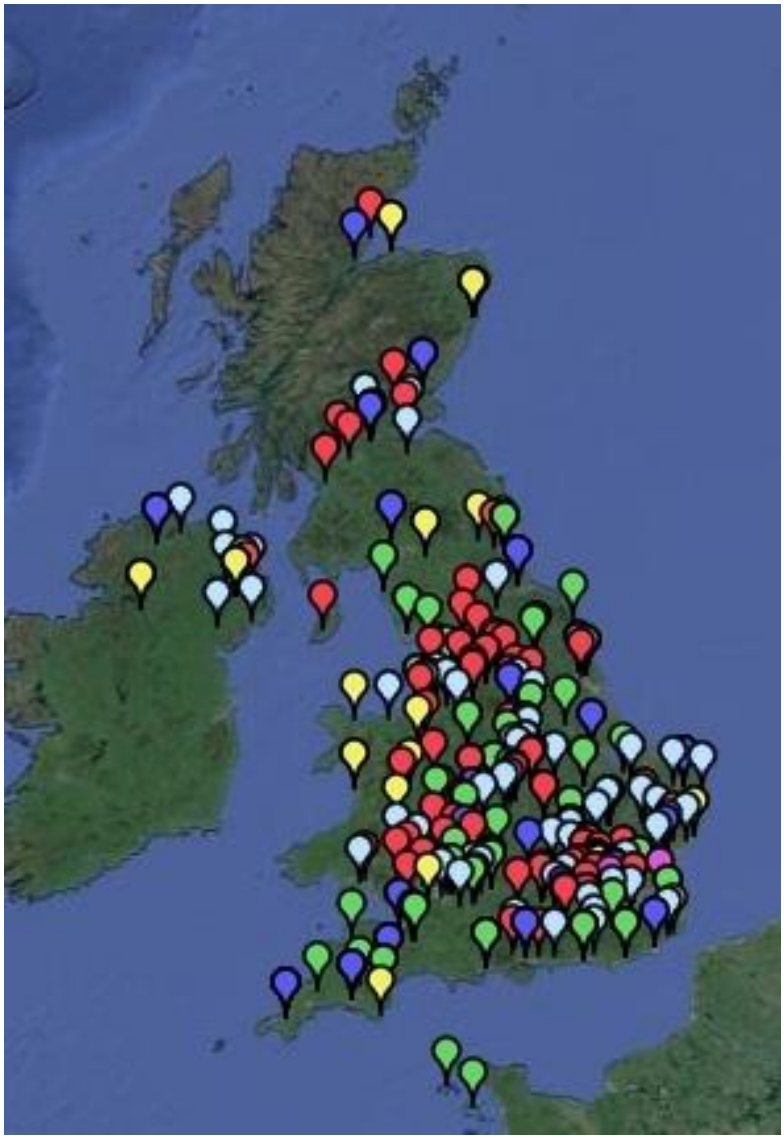

Figure 1.7 Density of AM broadcast stations transmitting on the MW in the UK [27]. In *light blue* colour – University and hospital radio stations; *Yellow*, *green* and *red* colour – BBC radio network; *Blue* colour – private commercial radio stations.

A review of the number of licensed broadcast stations in the USA over the last 17 years shows only 1% decrease in the number of AM stations (Figure 1.8). The Federal Communications Commission (FCC) of USA reports 4,685 licensed AM broadcast stations in the last quarter of year 2000 [28], compared to 4,639 in the last quarter of 2017 [29]. Also, the number of the FM broadcast stations in the USA has increased from 8,082 to 10,864 stations in 2017.

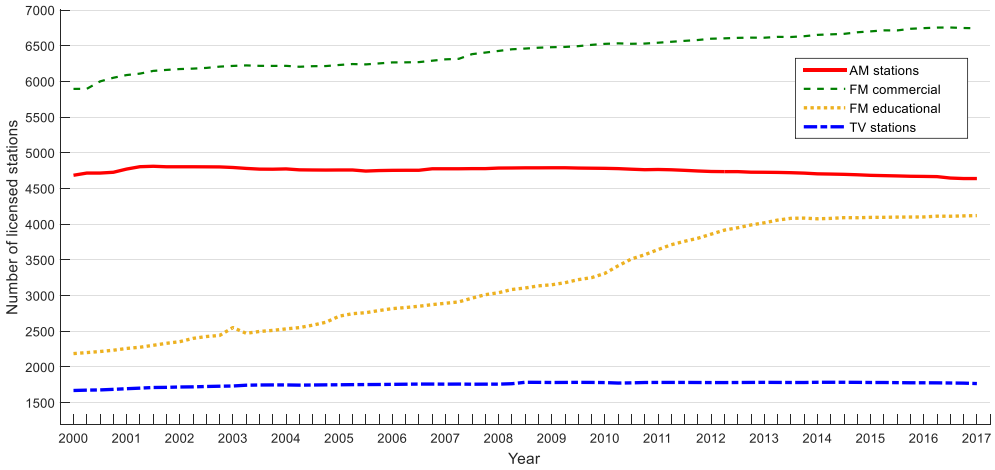

Figure 1.8 Plot of the number of AM, FM and TV broadcast stations licensed from 2000 to 2017 in the USA (source - FCC)

Since the very early 1900s', the first AM receiver, also well known as crystal radio [30] is a real RFEH system, since the earphone was directly driven by the energy harvested by the antenna. Moreover, AM broadcasting, is the earliest radio which has a worldwide coverage. However, few studies have noticed the potential in this type of transmission for energy harvesting applications [31], [32].

1.6. RF signal duty cycle

The transmitted signal's duty cycle may be defined as the percentage of time a signal is 'on' over an interval of time. It is an important signal feature because of its influence on the amount of energy available for energy harvesting. A comparison of 17 potential RFEH source signals was conducted experimentally, based on their duty cycles. The results are presented in Table I.

Table I Estimated and measured duty cycles for a range of RF transmissions.

Band Name	Frequency	TX Duty Cycle
MSF&DCF77 Time TX (LW)	60kHz, 77.5kHz	**Less than 85%**[1]
Broadcast (MW)	530-1600kHz	**More than 95%**[1]
Broadcast (VHF)	88-108MHz	**More than 99%**[1]
Air band	118-137MHz	**Less than 1%**[2]
Paging (VHF)	153MHz	**More than 92%**[2]
DVB VHF TV	174-230MHz	**More than 99%**[1]
DAB	211-230MHz	**More than 99%**[1]
DVB UHF TV	470-862MHz	**More than 99%**[1]
GSM900 Uplink	890-915MHz	**Less than 10%**[1]
GSM900 Downlink	933-960MHz	**More than 99%**[2]
Aircraft ADS-B	1090MHz	**More than 50%**[2]
GSM1800 Uplink	1710-1785MHz	**Less than 10%**[1]
GSM1800 Downlink	1805-1880MHz	**More than 99%**[2]
GSM 3G Uplink	1920-1980MHz	**Less than 10%**[1]
GSM 3G Downlink	2110-2170MHz	**More than 99%**[2]
Wi-Fi 802.11b/g/n	2400-2483MHz	**Less than 10%**[1]
Wi-Fi 802.11a/h/j/n	5150-5725MHz	**Less than 10%**[1]

[1] Calculated (based on specifications and statistics)
[2] Measured at 0.5MHz bandwidth

As demonstrated in Table I there are RF energy signals such as GSM uplink transmissions, with duty cycles of less than 10%. Calculating the path loss for such a transmission, we should include the duty cycle, e.g. a power level of 10W, transmitted just for 10% (duty cycle) of the time, should be calculated as average power of 1W. Similar estimations will apply to the WiFi signals calculations.

In the cases when the harvested RF energy originates from a signal generated for this purpose, it is obvious that we are in control of the source signal parameters, i.e., on/off time, power characteristics, frequency, phase etc. However, harvesting energy from electromagnetic signals, which are parts from communication systems such as mobile phone or Wi-Fi networks, requires a careful consideration of their duty cycles.

In order to investigate the AM broadcast signal's duty cycle at MW, we have conducted a continuous measurement for 30 days. A ferrite rod antenna and SDR receiver (SDRplay) were used for the measurements. An RF frequency mixer (Mini-Circuits) and a RF signal generator (Rohde&Schwarz) were used in a typical superheterodyne configuration. The monitored frequencies were scanned every 10 seconds and a log was automatically created. As a result, the continuity and stability of the received AM signal proved our expectations with a duty cycle of 100% at all the MW frequencies used for AM broadcast at Brookmans park transmitting site (909kHz, 1089kHz, 1215kHz, and 1458kHz). This experiment proved that the energy harvested from AM radio broadcast is more stable than solar, thermal and vibration energies. The RF signals at MW band are widespread, and they are not affected by the precipitation and atmospheric disturbance. Therefore, their reception will not be interfered by weather, light intensity or other environmental changes.

Another example of investigating a potentially useful RF energy source is analysing VHF paging transmissions in the 150MHz band (in the UK). In this case, measuring the TX duty cycle in the conventional way is not applicable for RF energy harvesting performance analyses. It is shown in Figure 1.9 that the bandwidth of

a paging transmission is much smaller than the actual RF energy harvester's bandwidth, so, several paging transmissions could be used in order to increase RF energy density. The latter measurement was conducted using Software Defined Radio (SDR) receiver (model SDRplay with SDR Sharp software) in a waterfall mode for easier monitoring of signals duty cycle.

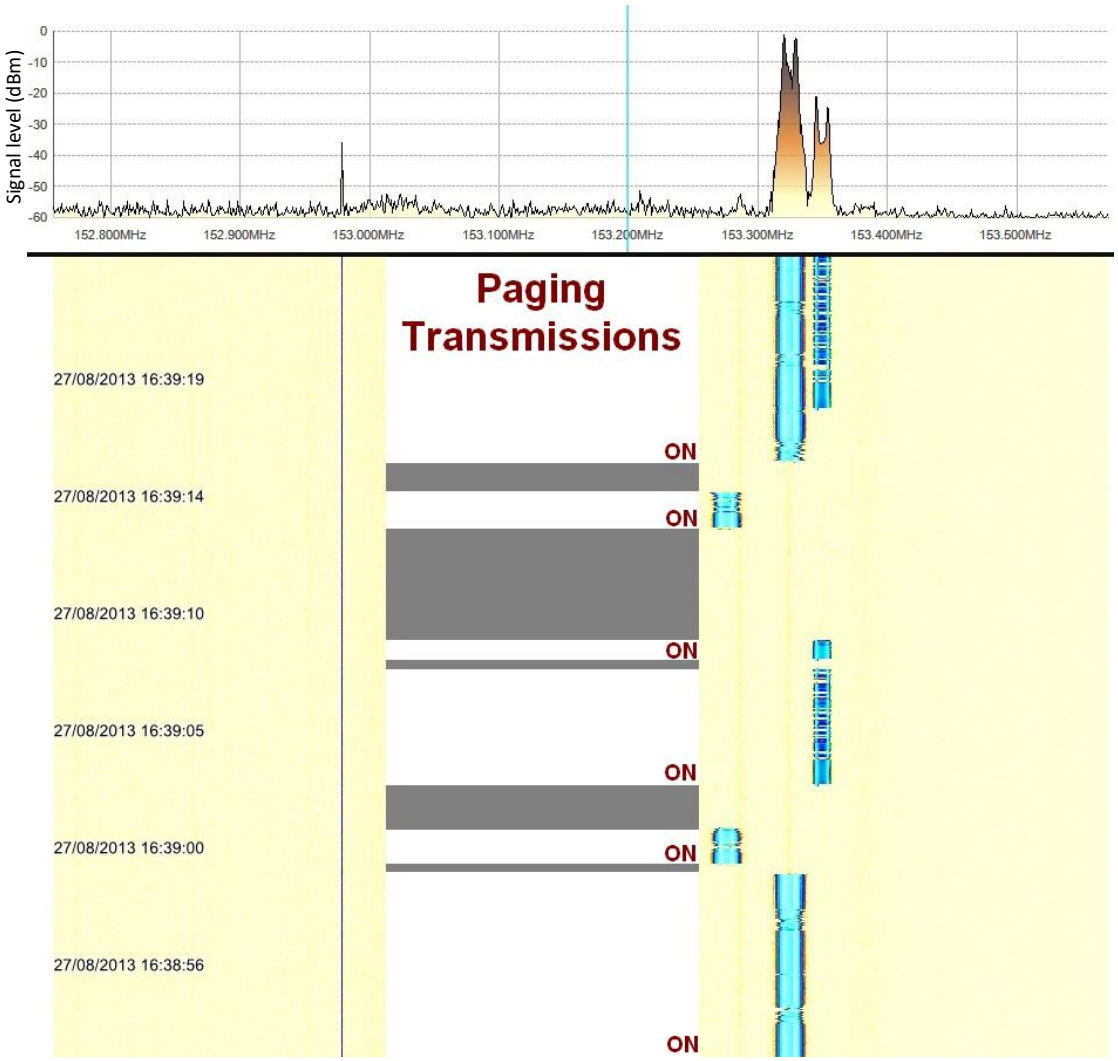

Figure 1.9 Spectrum and waterfall display of paging transmissions in the 153MHz band from Milton Keynes, UK

1.7. Structure of the thesis and contributions

This thesis is structured in six chapters, as follows:

Chapter 1 is an introduction to RF energy harvesting, with an analysis of the RF harvesting system, covering RF energy sources, rectenna designs, RF power density and applications. The system model of a RFEH system is presented in Section 1.2. A source signal duty cycle is discussed as an important factor of a RFEH system.

Chapter 2 is a systematic review of state-of-the-art in RFEH to date, covering RF power density measurements, rectenna designs and applications. This part will also review measurement techniques and measurements of how much RF energy is available for harvesting. The rectenna designs have been divided in those working from dedicated sources and those working from already available sources.

Detailed analyses of RFEH from MW energy signals are carried out in Chapter 3 together with descriptions of the parameters of ferrite rod antenna such as Q-factor, coil position along the rod, rod diameter to length ratio, etc. Two groups of experiments are presented in Section 3.6: the first series of trials are targeting RFEH of ambient RF energy from AM broadcast stations, and the second group experiments is demonstrating different aspects of RFEH from dedicated MW energy sources.

Chapter 4 describes single-band RF harvester that operate in a selected SHF band suitable for a particular application. It discusses and analyses the pros and cons of different antennas, rectifying circuits and rectifying devices, as well as their operation from ambient sources. This part concludes with a comparison between the proposed design and other energy harvesting rectenna designs and highlights the differences in the main specifications.

Chapter 5 discusses a systematic optimisation approach to the design of RF-DC conversion circuits along with multi-frequency waveform excitation. Diode

modelling for simulation purposes is explained and a variety of voltage multipliers are analysed. At the end of this chapter several optimisation methods are described with their drawbacks and advantages. A novel RF-DC conversion technique is proposed and a working prototype of a high efficiency rectenna is presented in order to demonstrate the concept advantages compared to the known conversion techniques.

Finally, in Chapter 6 , the important points of this work are summarised and possible future work on the topic is discussed.

The contributions to the field of RF energy harvesting are:

- Chapter 1
  - Novel analysis of the impact of signal's duty cycle on overall RFEH system efficiency
- Chapter 2
  - Comparison of ambient RF harvesters with other energy harvesting technologies and highlights the scenarios where RF harvesting could be an alternative for powering ultra-low power devices.
- Chapter 3
  - Discusses the theory behind MW power transfer systems and how to achieve efficient, lightweight and low cost coil designs;
  - Presents the details of how to characterise high Q-factor antennas as well as proposing rectenna optimisation techniques. Also, factors influencing the maximum possible Q-factor are considered;
  - Analyses the dependence of the antenna bandwidth, impedance and efficiency to the antenna size parameters, Q-factor, number of turns, permeability, and frequency;

- The methodology and results of the RF site-surveys around Brookmans park, demonstrating the feasibility of using MW source signals for RFEH of autonomous systems;
- Investigate the availability of MW radiated energy around Brookmans Park broadcast transmitter creating data-set to be used as a benchmark for future experiments;
- Derived variety of components of the equivalent circuit, such as conductor and core losses, capacitance and inductance, describing their importance for overall RFEH system performance;

- Chapter 4
  - Model and quantify the influence of substrate thickness of an non popular object (double glazing) on the antenna parameters, such as antenna gain, directivity, input impedance. Analysed the influence of the substrate combined permittivity on the overall antenna efficiency;
  - A novel balun is proposed for maximising the energy transfer efficiency of the rectenna;
  - Summarises the main parameters of different broadband rectenna solutions for the SHF bands, comparing them to the performance of the proposed rectenna;
- Chapter 5
  - A novel technique for using MW antenna array with a DC combining circuits optimised for different incident power levels. A working prototype was fabricated and tested.

Chapter 2 State-of-the-art in RF Energy Harvesting

2.1. History of RFEH

The idea of wirelessly transmitted electric energy appears for the first time in the Nikola Tesla's so called electric lighting system. He was mainly famous with his inventions in the area of alternating current systems, however, he was not well known for his contributions to the RF field, although he was dedicated to his ideas regarding wireless energy transfer for more than forty years of his life. The first publications about it appeared in 1891 [33] and a picture presenting his high frequency alternator is shown in Figure 2.1.

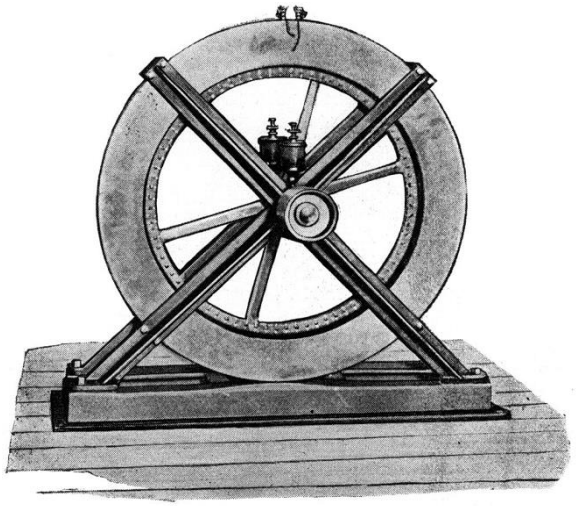

Figure 2.1 High frequency alternator presented in Tesla's paper in 1891 [33]

At this time only a few minor facts were known about the properties of radio waves. After Hertz published his famous research in 1888 [34] and [35], which provided evidence of the dynamic theory of the electromagnetic waves by J. Clerk Maxwell's [36], researchers became more convinced of the importance of the behaviour of the radio waves, i.e. that they are propagating like the sunlight, in straight directions. Although at the beginning this property was considered as a major drawback for the expected distance between the transmitter and receiver, this was soon disproved by Tesla's experiments with the antenna-earth system designed in 1892. He called his invention open 'resonant circuit' with one of the

plates above the earth level, and the other in the earth. The same configurations were used both at the receiving and the transmitting sides. Then Tesla predicted that one day devices powered by electrical energy will be easily using wireless energy instead. A really remotely powered device, is not only enabling extra mobility, but also allows designers to create very small devices neglecting the importance of batteries. Tesla's publications about wireless power transfer were not accepted well. Just over the past 20 years his name was cited in papers about extremely low frequencies [37], [9], [38].

Subsequently, Tesla presented his lecture at the IEE in London in 1892 where he shared his ideas about his future plans of researching in the area of HF currents. The same lecture was presented once again in London and in Paris. While he was demonstrating his 'single wires' during the lectures, he discovered by coincidence that some of the transmitted HF currents passed easily when the gases have lower pressure. That motivated him to go further with investigating the possibility to power electric devices at higher distance from the energy source. He fabricated a large coil in 1899 in his new laboratory in the United States in order to generate ten million volts in an open circuit. His target was to prove the concept of wireless power supply and he successfully powered several remotely positioned electric bulbs. Less than a year later, he had to cancel his research, because of financial difficulties, and focus on building his new lab at Long Island, USA, known as 'World Telegraphy'.

Another historical example of early usage of low level RF reception and rectification is the Crystal Radio Set which dates many years ago to the years of wireless communications (pre-World War I) [30]. A wide range of receiver circuit designs [39] and radio types have been discovered and developed over the years. The popularity of Crystal Radio was affected by the introduction other modern types of radio receivers. However, people's fascination by Crystal Radio as the simplest way of radio reception still remains strong nowadays.

Harvesting the surrounding or ambient energy is a well-known strategy of providing power for devices and processes. Most exploitable ambient energy sources can be found in physical motion and solar light, and they are already being collected by using photovoltaics [4] (calculators), thermoelectric [5] and kinetic energy harvesters [40] (pendulum-watches), respectively.

2.2. Literature review of RFEH

Today, RF energy signals are broadcast from millions of radio stations all around the world (WiFi, TV and radio broadcast, mobile phones, mobile radio communications, etc). Potential RFEH energy sources, such as handheld radios, mobile phones and their base stations, and radio and Digital Video Broadcast (DVB) stations, may be found everywhere around us. Harvesting RF energy from dedicated or ambient energy sources, enables uninterruptable powering of devices with low power consumption and will possibly completely remove the need for a battery. Both types of RF energy harvesters will increase the mobility of the powered devices in both states whilst either in use or charging.

RF energy harvesting has become an emerging research area clearly noticeable with its demanding requirements caused by the ultra-low power level RF environment (i.e. microwatts). A number of RFID applications were analysed, but only several in depth studies have been conducted that cover all the components of the RFEH for powering autonomous systems. Low power transceivers have been proposed that utilise RF power harvesting to directly power the system. These designs, which are often referred to as passive RFID tags, rely on a capacitor for energy storage and do not carry a battery. Therefore, they require enough input RF energy to be received in order to supply the instantaneous current demands of the transceiver. Facen and Boni [41] proposed a system that utilises a full wave rectifier and charge pump to power the transceiver from the 895.5 MHz received data signal. This system has a predicted operational range of only 5.3 m. Gregori et al. proposed an alternative design that

utilises a power-matched half wave rectifier circuit [42]. The proposed design requires 250 μW of energy to correctly function. These latter designs illustrate one of the disadvantages of passive RFIDs - they typically only operate at close range (<10 m) to strong power sources.

The Authors of [43] present a 64 element broad-band rectenna array optimised for the SHF band (2 to 18 GHz) for low-power RF-to-DC rectification (10^{-5}-10^{-1} mW/cm^2), arbitrarily polarised incidence signals. As shown in Figure 2.2, the rectifier in their proposal, is integrated in the antenna, so every antenna element is delivering RF energy to an individual diode. Using this technique, the RF power delivered independently by each of the antenna spirals, is added as a sum of DC currents and voltages.

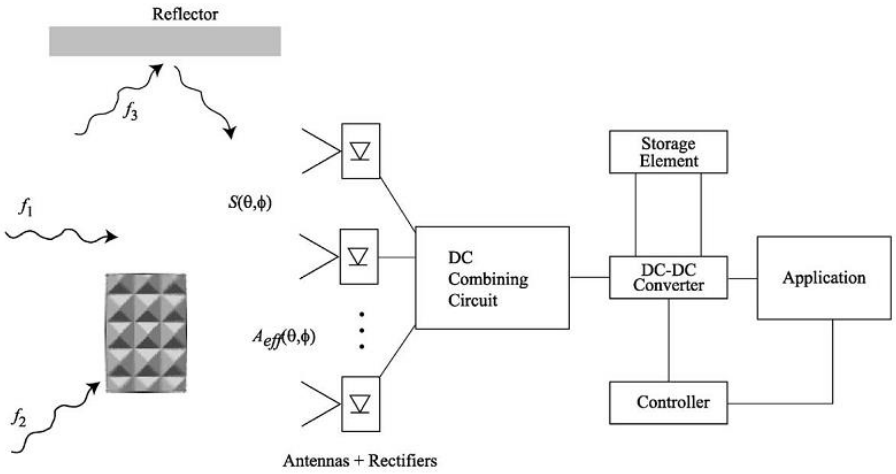

Figure 2.2 Block diagram of a rectenna array for ambient energy recycling, proposed by Helmbrecht, et al. [43].

In the proposed RFEH system [43] 10 μJ RF energy packets are transmitted, assuming that it is enough energy to power a 1 mW load for a very short time (10 μs). Although the size of the packets has been chosen arbitrarily, the idea is to be used for different type of applications, where basic data may be exchanged. The input power densities considered in their research are in the range of 250nW to 2.5mW for an antenna array with of 25cm^2. The output DC power achieved is

between 2nW and 450μW at frequencies from 2 to 18GHz, using DC-DC with efficiency of 90% and RF-DC with power conversion efficiencies of 1% to 20%.

According to authors of [44], there are two ways of preserving the harvested energy – micro-batteries and capacitors. Capacitive storage is used for particular applications where the states of charging and utilising the energy are changed frequently. This storage mode is using on-chip capacitors if the energy is less than tens of pico joules, or off-chip if it is up to tens of micro joules. If the application requires longer discharge periods, hence higher power densities are needed, micro-battery is used [45].

In [46] Kansal, et al. have analysed different techniques for managing the power harvested by RFEH by comparing them with similar methods in battery-power systems. The main advantages of this study are its practical aspect and its detailed analysis of the issues involved in managing the power resources in autonomous systems.

Mayaram, et al, in [47], conduct a study to investigate the importance of the rectification stage efficiency in RF-DC power conversion systems, where the input voltages are as low as -22.6 dBm (at UHF). They are describing a number of RF-DC conversion circuits for low incident power level as well as analysing some of the design challenges regarding such rectifiers. The authors have validated their concept by comparing two rectifier circuits using transistors instead of diodes on 0.25 μm CMOS base.

In [48] Sim, et al. present a particular RFEH application for powering up a sensor network for measuring soil parameters. Two types of low profile patch antennas have been proposed: the first one is a Folded Shorted Patch Antenna (FSPA), optimised for a wide impedance range, and the second one is an interesting FSPA design of four double slots sharing the same layer with the ground plane. The main advantages of the proposed antenna designs, in a RFEH aspect, are their low profile and fabrication simplicity. The Authors examine the performance of the proposed antenna both in free air and in the presence of four

types of soil (turf with short, dry grass; turf with short, wet grass; bare, dry sandy loam; and bare, wet sandy loam).

In [49] Penella-Lopez et al. present several in-depth analyses of some very efficient techniques for gathering the energy in autonomous systems. They provide an interesting approach by comparing the system performance with energy harvesting and primary batteries. A number of interesting tests are reported that concern both batteries and supercapacitors, and the design criteria for choosing their suitable values has been presented.

Zhi Wei Sim in [50] investigated the feasibility of using RFEH to power wireless sensor networks (WSNs), in which the sensor nodes are distributed across a field within the vicinity of domestic, agricultural or commercial buildings. The author presents the background on a range of energy harvesting methods, supplemented by a broad review of the state-of-the-art in energy harvesting, addressing the methods suitable for wireless sensors positioned at ground level. An important part of this research is where the author presents the design techniques and the measurement results of the antennas, including RF-DC power conversion circuits applicable in similar RFEH systems for powering up WSN.

Philipp et al. in [51] discuss energy harvesting for powering Wireless Sensor Networks (WSN) and their main target is not only to investigate a specific energy source, but a wide range of sources. They are describing the development of an inexpensive hardware, which is flexible to easily reconfigure its protocols and modules in order to improve the performance of a WSN working in severe environmental conditions. Their approach includes network traffic optimisation for increasing the efficiency of the proposed modular hardware. They also introduce several energy harvesting circuits for different outdoor conditions, such as, very hot weather, strong wind, etc.

The authors of [52] describe a simple RF energy harvesting circuit printed on a single FR4 substrate designed for 2.1 GHz. They are demonstrating a RFEH

system capable of providing a voltage of 2.7V_{DC} using a single diode rectifier and a dedicated RF energy source.

Table II Comparison of antenna type, frequency range and maximal levels achieved in selected RF energy harvesters.

Authors	-Antenna type -Frequency band	Strengths	Weaknesses
Helmbrecht, F.B., McCalpin, W.H., Zane, R., Popovic, Z.B. [43]	A dual-circularly-polarized spiral rectenna array SHF band (2-18GHz)	It is possible to collect RF energy in an indoor multipath propagation environment by rectifying two polarisations independently.	The losses in the antenna are interdependent to the gain achieved due to multi-polarisation.
Le, T., Mayaram, K., Fiez, T. [47]	Double loop PCB antenna USA ISM band (902–928MHz)	Feasibility of a multi-stage multiplier for low incident levels of less than 5.5 µW (-22.6 dBm) and a voltage gain of 6.5dB	Implementing a state-of-art rectifier is a useful feature, but it has its limits e.g. high price.
Z. W. Sim, R. Shuttleworth, M. J. Alexander, and B. D. Grieve [48]	Two Folded Shorted Patch Antennas (FSPAs) 860-960MHz&1.48-2GHz	Choosing and simulating a suitable rectenna design is one of the most important stages in designing an RFEH system. The height of the rectenna influences the overall efficiency.	The RF energy transmitted by a dedicated RF energy source is harvested only. It would be interesting to investigate how such a system would behave in a real world environment, capturing energy from an ambient source.
Maria Teresa Penella-Lopez and Manuel Gasulla-Forner [49]	A simple printed folded dipole ISM band (868MHz)	Useful in depth analysis of some very efficient techniques to manage RF and optical (solar) energy.	The simulations and experiments of rectifier efficiency are carried out on one frequency only.
Zhi Wei Sim [50]	Two air-substrate-based, folded, shorted patch antennas (FSPAs) USA ISM band (902–928MHz)	Good theoretical methods of designing RFEH systems are presented. The importance of the antenna's main parameters for overall efficiency of the system is proved.	Limitations of an RF harvesting design such as low efficiency and impedance matching losses are visible in such a detailed project.
Mikeka, C. and Arai, H. [52]	Circular Microstrip Patch Antenna(CMPA) SHF band (2.1GHz)	Specific application requirements influence the proposed design.	The proposed harvester is not designed to use ambient RF energy, and one generated for this purpose.
Georgiadis, A.; Andia, G. and Collado, A. [53]	Dual polarisation, square aperture-coupled patch antenna ISM band (2.43GHz)	The RF-DC power conversion efficiency of 38.2% with a 6.2k load is achieved for an input signal level of 1.5µW/cm2	The proposed design is optimised for one frequency band only. Their concept is based on simulated results only.
Ajmal, T., Jazani, D., Allen, B. and Ivanov, I. [54]	Compact ferrite antenna MW band (1MHz)	Useful in-depth analyses of MW broadcast transmissions as an RF energy harvesting source.	Compromises concerning efficiency are to be made because of the size.
Olgun, U., Chen, C.-C., Volakis, J.L. [55]	Koch-type patch antenna ISM band (2.45GHz)	Two different RF power harvesting configurations are discussed.	Nothing is mentioned about the polarization influence to the proposed design.

The application described in this study is a RFEH system integrated in a medical device, supplying power for its wireless sensors without the need of batteries. The level of the RF signal, transmitted at a very short distance to the rectenna, is carefully considered to not exceed the threshold level given by the requirements. They also discuss different techniques for increasing the rectifier's efficiency when used in a single stage configuration. The paper represents a very good example of one of the RF harvesting device's effective applications. The results achieved by previous researchers in developing their own systems were compared in Table II. The main motivation to classify the references in the table was to cover various publication types such as books, journals, conference papers, etc.

2.2.1. RFEH from dedicated energy sources

When dedicated RF energy sources are used, energy harvesting systems collect power from the RF energy transmitted by its own controlled transmissions. Recently, a number of different transmission methods for optimising the performance of networks using dedicated RF sources were studied in [56], [57], [58] and [59]. The researchers in [56] investigated a Simultaneous Wireless Information and Power Transfer (SWIPT) strategy in which both RF energy and data are transmitted at the same time on a Multiple-Input Multiple-Output (MIMO) system. An important conclusion, made in this reference is that modulating the RF energy source signal, broadcasted by purpose to improve the performance of the system and to increase its overall efficiency is a research challenge which is worthy of further investigating. According to the authors, an RFEH system may benefit from the presence of factors such as co-channel interference and receiver noise, regardless of the well-known theory that they have a negative impact on the performance of the traditional radio communication channel. Therefore, there are some important trade-offs in the optimisation of the radio channel interference in order to improve the balance between the energy transfer and the information.

A new strategy for splitting the power in an RFEH interference link was investigated in [57]. The authors formulated the minimum required energy with optimisation problem for both variable and constant beamforming weights at the energy sources. Analyses of algorithms for three standard multiple-input single-output (MISO) beamforming designs have been investigated: Maximum Ratio Transmission (MRT), Regularised Zero-Forcing (RZF), and Zero-Forcing (ZF). As a conclusion of their study, they recommend that for medium size systems with not more than 20 users, Semi-Definite Programming (SDP) is applicable, while for best balance between optimality and computational complexity, a hybrid scheme such as the combination between ZF and MRT is more suitable. They suggest that as a future work in that area, more practical experiments and simulations should be carried out with the proposed schemes for use-cases where the Channel State Information (CSI) is not perfect and whether SDP may be optimised for a bigger number of users.

Similar study is carried out in [58] where the authors characterise the trade-off between the harvested RF energy and the information flaw for different number of interference links. Two-user interference channel is analysed, in a configuration with two receivers, where the first one is used as RF energy harvesting device, and the second one is decoding the information stream. For the proposed technique of Simultaneous Wireless Information and Power Transfer (SWIPT) they are using Multiple-Input Single-Output (MISO) type Interference Channels (IFC) where every participating transmitter is sending energy or streaming data to a particular receiver.

Using the same principal of SWIPT, the authors of [59] analysed different beamforming and timing schemes in order to optimise a multi-user SWIPT system.

The authors investigated different options for improving the performance of wireless powered communication networks with imperfect and perfect CSI. A fast algorithm and a conservative approximation has been proposed to decrease the computational complexity with different beamforming schemes and perfect CSI.

2.2.2. RFEH from ambient energy sources

The main difference between the RFEH systems using dedicated energy sources and those using ambient RF transmissions as an energy source is that the systems using ambient energy do not have control over the parameters of the transmitter. The transmissions used for ambient RFEH may be static (TV and radio broadcast, GSM base stations, etc.) or dynamic RF energy sources (mobile radios, mobile phones, etc.) [60]. Examples for such RFEH systems are presented in [61], [62], and [63] where the authors are investigating different use cases and techniques for harvesting RF energy form ambient transmissions such as DTV broadcast, mobile devices, and WiFi networks.

The authors of [61] have combined all the components of a RFEH system in single RFEH unit (Figure 2.3) for harvesting ambient RF energy from WiFi signals.

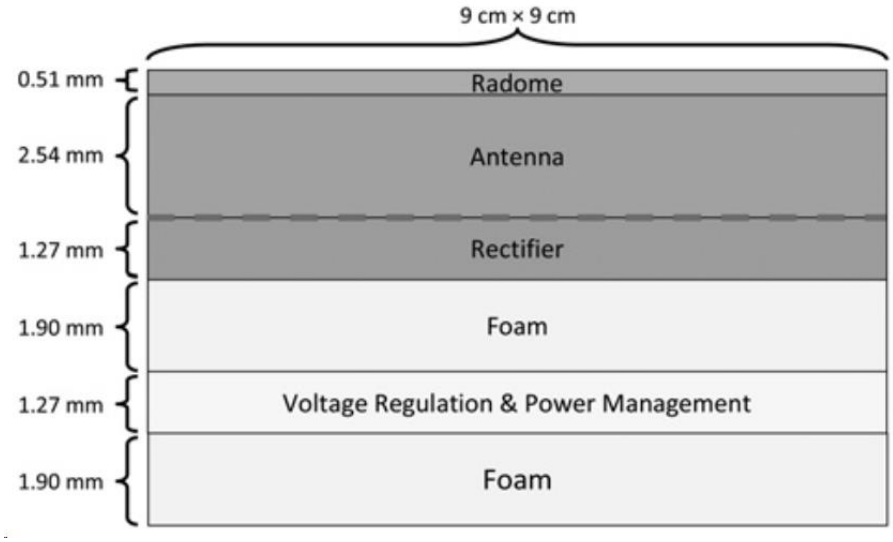

Figure 2.3 Ambient WiFi energy harvester stack [61]

The proposed design demonstrates an idea of integrating 3x3 planar array of Koch-type patch antennas with the rectifier and the power management circuitry. All the components of their energy harvester are embedded in a multi-layered prototype with dimensions of 90x90x10mm. In order to benchmark the sensitivity of the proposed RFEH device, the authors have used a simple whip antenna

connected to a spectrum analyser, measuring the incident power density level at a position very close to that of the RF harvester. They have demonstrated that their device can harvest enough power for charging a small battery, providing output voltage of 1.8 V at maximum of 50uA current. In this study, the minimum incident density level required by the proposed device to start converting the RF energy to DC voltage -40 dBm.

In [62] the results of a RF site survey at the GSM900 frequency band targeting mainly the underground stations in London was carried out. As a conclusion of their measurements, the authors state that the conditions at more than 50% of the stations are suitable for harvesting ambient RF energy using the proposed devices, which are both multiband and single frequency energy harvesters. They show that efficiencies of up to 40% may be achieved with their RF harvester, optimised for a single frequency band (GSM900), and a sensitivity to incident power density level of -25 dBm. The researchers also consider semi-urban environment as a suitable working condition for their harvester.

The authors of [63] proposed a new architecture for RF energy harvesting which uses different types of RF energy sources, although they focus their measurements on harvesting the energy transmitted by DTV broadcast stations. The study also propose a network protocol designed especially for the given application - RF energy Harvesting Sensor Networks (RF-HSN). Considering the duty cycle of the autonomous sensors in a particular scenario, the authors are optimising the RF harvesting distribution to fulfil their individual power requirements.

Analysing the results of their measurements, several research groups have used stochastic geometry tools to test the efficiency of ambient RFEH systems [64], [65] and [66]. They analysed mathematical models based on stochastic geometry with the aim of better understanding RF energy harvesting in communication networks to predict and control the performance of RF energy harvesting in such networks.

2.2.3. RFEH from an information-theoretic perspective

Although in the traditional battery-powered systems a deterministic model may be used for quantifying the energy, when analysing RFEH in wireless networking applications, the available energy must be considered as both charging and discharging cycles, including the external factors which have influence on this procedure. If there is not enough energy in the battery, the system will stop functioning. However, if the available energy is more than needed for a particular operation, the additional energy may be stored for later usage. The model shown in Figure 2.4 represents the two queues of such a transmission method. The data queue stores the data arrivals (B_i is the number of bits in the i^{th} arriving data packet), while the energy queue stores the energy harvested from the environment (E_i denotes the amount of energy in the i^{th} energy arrival).

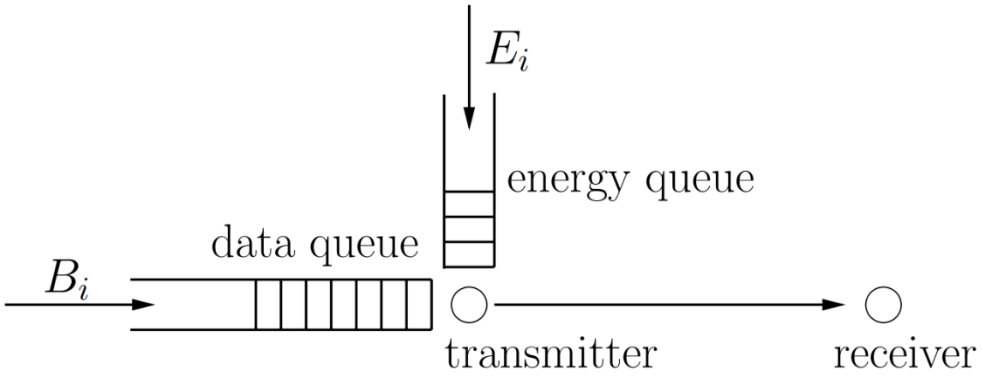

Figure 2.4 An energy harvesting communication system model

One of the pioneering works in the area of energy harvesting communications was the study of the information capacity of an two-user RFEH communication system in [67]. The authors derived the capacity of a point-to-point radio communication link with Additive White Gaussian Noise (AWGN) and a RFEH transmitter. It is shown that the potential of an AWGN channel with random RF energy packets (packets with carrying no data) is similar to the potential of a

traditional (non-energy harvesting) AWGN channel with average power restrictions similar to the average recharge rate of the RFEH transmitter. As briefly explained previously, there are two main configurations in such systems: save and then directly transmit, and save and transmit when possible. The basic intuition behind these capacity achieving schemes is the fact that if the transmitter remains idle for a long enough period, using a battery to store the energy in this period will help eliminate the randomness of the energy arrivals. In this paper, the authors showed that the prior information about the stochastic energy packets will not increase the capacity of the AWGN channel as long as the battery capacity of the EH transmitter is unlimited. RF energy may be a desired complementation for existing energy harvesting and reusing resources such as solar energy and wind energy.

The optimal packet scheduling problem for a two-user communication system with a RFEH transmitter is studied in [68]. The transceiver receives data packets and energy packets randomly during the transmission. The aim is to minimise the delivery time of the received data to the destination. This is achieved by adaptive control of the transmission rate, according to the available data packets and the amount of power present in the battery of the RFEH transmitter. This work considers an offline setting, i.e., it uses preliminary knowledge of the energy and data packet reception. It is shown that the transmission power must remain constant between data packet or energy packet arrivals. It is also proven that in the optimal power allocation scheme, transmit power levels form a non-decreasing sequence over time. Using these structural properties, the optimal policy is obtained using a geometric framework similar to that introduced in [69].

In [70], the challenge of maximising the information transfer is demonstrated for a point-to-point communication system. The study examines the problem in the online setting. In order to optimise the transmission policy, the authors of [70] have presented the procedure as Markov Decision Process (MDP). It is also shown that the optimal transmission policy is a non-decreasing function of the battery level and the fading channel state. Another investigation for throughput

maximisation in a single link RFEH wireless communication system is carried out in [71]. In this publication, the goal is to find the optimal power available for transmission as a function of the available energy in the battery at each time instance. In this study, it is assumed that the energy harvesting process is a compound Poisson process and the channel is static, based on the compound Poisson dam model described in [72]. These assumptions lead to a compound Poisson model for the energy storage unit. Using a calculus-of-variations approach, the authors obtain a necessary condition for optimality of the online energy consumption policies. This condition is used to derive the connection between transmission power and the battery content. This work is extended to the case with a time variant fading channel in [73], where the fading channel is modelled as a continuous-time finite-state Markov chain. An upper-bound to the ergodic channel throughput is also analysed in [73]. In [74], a similar approach to [71] is used to find the optimal transmission policy for sum-rate maximization in a multiple access EH communication system.

2.3. RF power density measurements

Power densities may vary up to four orders of magnitude at the same distance (see Figure 2.5). This is caused by the different transmitted power levels from mobile phone base stations, spatial conditions, and environmental conditions at the time of the measurement. These variations have to be taken into account when designing and testing the RF harvesting capabilities of rectennas [75]. As seen in this figure, the maximum power densities were measured outdoors and the minimum levels were measured indoors. However, it is obvious that there is great variation in the strength of measured signals, even at similar distances from the antennas. There does not appear to be any obvious trend for the signal strength to increase at distances closer to the antennas as the measurement locations would have been outside the main beam.

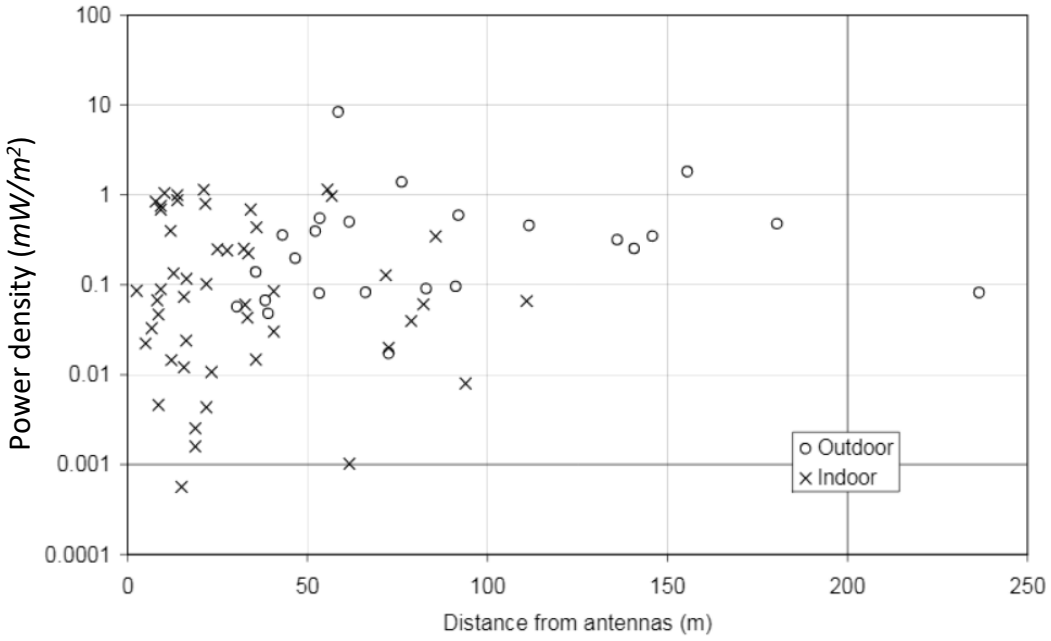

Figure 2.5 Total power densities due to all environmental radio signals measured at 73 locations vs. distance from transmitter [75]

Similar measurements have been taken at distances of 50 to 200 m and a height of 1.5m above ground level in five Australian cities, where the maximum measurement of 0.86μW/cm^2 is received from a GSM tower at a distance of 25m from the transmitter [76]. In another study, a similar variation of measurements at the same distance from the transmitter has been recorded using a NARDA SRM-3000 spectrum analyser [77]. A comparison between the measurements from GSM and UMTS signals is showing that in 85% of the measurements, GSM power is higher than that of UMTS. Median values for GSM power densities are 0.063 and 0.05μW/cm^2 for UMTS and a power density of 0.016 μW/cm^2 has been measured at a distance of 1km from a UMTS base station [77].

Another study is comparing the measurements undertaken with a spectrum analyser and with a personal exposimeter. Average values from GSM900 and GSM1800 at a distance of 100 to 200 m were 0.025μW/cm^2 outdoors and 0.013μW/cm^2 indoors. Since similar variations as discussed in the previous paragraphs were recorded, the use of a personal exposimeter was proposed to

record field or power density variations versus time. In the personal exposimeter survey, power received from a GSM downlink while travelling was the highest, with 0.2μW/cm^2, while office and home environments were 0.04μW/cm^2 and 0.032μW/cm^2, respectively [78].

Due to the limitations defined in the IEEE Standard for Safety Levels with Respect to Human Exposure to Radio Frequency Electromagnetic Fields (3 kHz to 300 GHz) from 2006 [79] for the frequencies between 0.1 GHz and 10 GHz, the recommended RF power density levels in controlled environment are 10 mW/m^2 -100 mW/m^2 (1mW/cm^2 - 10 mW/cm^2). The regulations for the same frequency range in urban environment are limiting the safety power density levels between 1 mW/m^2 and 10 mW/m^2 (0.1 mW/cm^2 - 1mW/cm^2).

2.4. Voltage rectification and multiplication

Independently of the type of the energy used, the RF-DC power conversion circuit, depends on the diode, which enables different modes of power conversion [17], [80], [81]. The diode (known as 'rectifier') is an important semiconductor which reacts differently based on the properties of the applied voltage. A large number of studies in the literature address energy-conversion efficiency of RFEH circuits based on diode and circuit parameters. The micrometre spark resonator was first used by Heinrich R. Hertz to detect RF as described in Section 1.1. Although it has had a very limited sensitivity, hence the received signal had to be very strong, it is considered as an important research in the area of wireless power transfer [82].

Due to high practical demand, significant research attention has been focused recently on low-voltage rectifying circuits which address two main challenges: first, how to improve the voltage converter's efficiency when low voltage energy is harvested [83], [84], and secondly, how to amplify the low voltage level in order to charge a battery [85], [86]. The authors of [87] have proposed different compensation methods for multi-stage rectifiers based on P-type metal-oxide-

semiconductor (PMOS) and N-type metal-oxide-semiconductor (NMOS) transistors to be used as high efficiency RF-DC conversion circuits. Their measured results confirm that the proposed circuit operates successfully at incident levels as low as -21.6 dBm (6.9 μW), delivering DC voltage of 1 V with a calculated conversion efficiency of 22.6% at a 1 MΩ load. The second RF-DC voltage multiplier is optimised to deliver a higher DC voltage from very low incident power densities. DC voltage value of 2.8 V is achieved with a maximum of 170 mV (rms) AC input voltage for the same load resistance.

The authors of [88] discuss a novel technique for reducing the internal loss by decreasing the level of impedance mismatch. Their second target is to optimise it for a wide range of incident power densities by using differential Resistance Compression Networks (RCNs), which are a special class of matching network that provide reduced impedance variation at the RF input as compared with the rectifier inputs. The study presents a theoretical analysis of the proposed RCN and test results with wide range of incident densities. The authors conclude that the proposed differential RCN has a better power conversion efficiency (by just over 12%) for a wide incident power density range, compared to a voltage rectifier without RCN. The researchers are also investigating different techniques for minimising the influence of the load on the power conversion efficiency.

A comparison between all the RF-DC conversion circuits discussed in this Section, shows a need for development of rectifiers with improved power conversion efficiencies capable of delivering high levels of output power at very low levels of incident power densities.

2.5. Energy storage technologies

Selecting a suitable recharging method and an energy storage element for a RFEH system in a particular application may have a great impact on the overall performance of the system. The specifications of the storage element and the way

it has been charged must be optimised considering the parameters of the RF-DC conversion circuit and the requirements of the application.

There are several known technologies for rechargeable batteries: Nickel Cadmium (NiCd), Sealed Lead Acid (SLA), Lithium Ion (Li-ion), and Nickel Metal Hydride (NiMH). The characteristics of these recharging technologies are:

- *charge-discharge efficiency* – ratio between the energy applied to the battery and the power preserved into it;
- *power density* – the amount of extractable energy stored in a system per unit volume or mass;
- *number of recharge cycles* – the number of complete recharge cycles that the battery is able to support before its capacity falls under 80% of its original capacity;
- *self-discharge rate* – indicates how the power density of a battery is reduced with no load connected to its electrodes. It is caused by internal chemical reactions.

Some of the electrical and physical parameters typical for the rechargeable batteries are shown in Table III, including their nominal voltages which are 1.2 V for NiCd and NiMH batteries, 6 V for SLA and 3.7 V for Li-ion batteries. The Lithium ion batteries are known with their highest power density and number of recharging cycles, as well as their very low self-discharge rate compared to the other technologies. NiMH batteries, on the other hand, have better power density than NiCd batteries. As manufactured with a less effective technology, SLA batteries have the lowest power density and number of recharging cycles.

Compared to all of the existing technologies for rechargeable batteries, super capacitors (or sometimes called 'Goldcap'®) have much higher charge-discharge efficiency (in the range of 97−98%) and no 'memory' effect which is typical for the NiCd and NiMH batteries. However, the super-capacitors have a very low of weight to energy ratio (5Wh/kg) compared to NiMH batteries (100Wh/kg). Considering the conditions of a particular application, the super capacitors may be used

instead of rechargeable batteries, however, their parameters must be carefully analysed. One of the important specifications is their high self-discharge rate which can reach values of 5.9% per day [89]. Furthermore, super-capacitors have unlimited recharge cycles [90], which may be a very important feature for RFEH applications.

Table III Different types of energy storage elements used for EH power systems [89].

Type	Lead Acid	NiCd	NiMH	Li-ion	Li-polymer	Supercap
Make	Panasonic	Sanyo	Energizer	Ultralife	Ultralife	Maxwell
Model	LC-R061R3P	KR-1100AAU	NH15-2500	UBP053048	UBC433475	BCAP0350
Characteristics of a single storage element						
Nominal voltage	6.0V	1.2V	1.2V	3.7V	3.7V	2.5V
Capacity	1300 mAh	1100 mAh	2500 mAh	740 mAh	930 mAh	350 mAh
Energy	7.8 Wh	1.32 Wh	3.0 Wh	2.8 Wh	3.4 Wh	0.0304 Wh
Weight energy density	26 Wh/Kg	42 Wh/Kg	100 Wh/Kg	165 Wh/Kg	156 Wh/Kg	5.06 Wh/Kg
Volume energy density	67 Wh/L	102 Wh/L	282 Wh/L	389 Wh/L	296 Wh/L	5.73 Wh/L
Weight	300 g	24 g	30 g	17 g	22 g	60 g
Volume	116.4 cm^3	8.1 cm^3	8.3 cm^3	9.3 cm^3	12.8 cm^3	53.0 cm^3
Self-discharge (per month)	3% - 20%	10%	30%	< 10%	< 10%	5.9% / day
Charge-discharge efficiency	70% - 92%	70% - 90%	66%	99.9%	99.8%	97% - 98%
Memory effect	No	Yes	No	No	No	No
Charging method	trickle	trickle/pulse	trickle/pulse	pulse	pulse	trickle

According to the authors of [49], there are two options for power supplies in an energy harvesting system as shown in the block diagram in Figure 2.6. The first one is if no battery is used and the energy passes through the Energy Transducer, Energy Conditioning and Energy Storage blocks. In the second option a Primary Battery has been used. However, using similar powering options for RFEH applications requires a different approach, mainly because of the low incident levels compared to the levels available with the methods described by the authors.

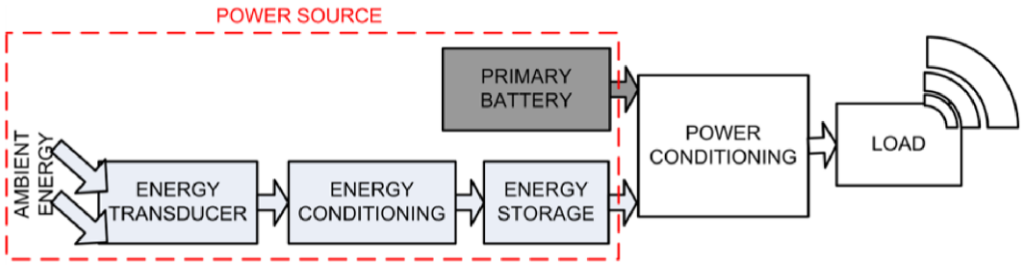

Figure 2.6 Block diagram of the power supply of an autonomous sensor

The same study [49] suggests that the amount of energy (E_{bat}) required for a given lifetime period of operation (T_{op}) may be calculated by:

$$E_{bat} = P_{c,av}.P_{L,av}.T_{op} \quad (5)$$

where the power required from the energy source ($P_{c,av}$) is also including the power losses in the components of the system ($P_{L,av}$). The duty cycle of the autonomous sensor is considered by the authors in order to improve the accuracy of the proposed calculations. Estimating the power required by the sensor, only its active periods are included (P_{active}). Also, they suggest that if a suitable capacitor is connected in parallel, a low power battery should be added because of its contribution during the active time period [91].

Chapter 3 Antennas for RF Energy Harvesting from MW Transmissions

3.1. Introduction

In far-field RFEH systems, the RF power energy density level is extremely low, compared to the power transmitted by the source transmitter. The propagation energy level is decreased rapidly with the increment of distance from the source of energy [92]. The loss shows logarithmic behaviour with respect to the distance. Moreover, the minimum energy required at the RF-to-DC convertor's input is relatively high compared to the levels extracted directly from the air. To minimise this problem, especially if a power-threshold is defined, the RFEH system requires a significantly more efficient antenna than that for many communication systems.

The aim of this chapter is to introduce for the first time the importance of the Q-factor of a MW antenna, optimised for RFEH usage. Novel ways of optimising the parameters which has direct influence on performance are described.

This chapter is organised as follows. In Section 3.2, a background of state-of-the-art in antennas for RFEH is presented along with a description of the antenna's efficiency influence on the overall harvester's efficiency. Also, the need for a different design approach is explained, compared to the approaches used for microwave frequencies and based on the requirements of the application. An in-depth analysis of a ferrite rod loop antenna for EH for the MW band, as well as novel techniques for design optimisation, are presented in Section 3.3. The analysis includes the derivation of Q-factor and efficiency of the electrically small loop antenna using a spheroidal core, by applying quasistatic electromagnetic theory. The spheroidal coordinate system has been used because of its capability to represent some of the antenna properties that are in good agreement with the specifications calculated with an FEM analysis for cylindrical-core antennas of equal core volume and aspect ratio. Factors of the equivalent circuit, such as wire conductor losses influenced by the core losses, coper quality of the coil wire, coil position over the ferrite rod, coil diameter to rod length ratio, rod diameter to coil internal diameter ratio, are derived. The practical experiments and field trials

conducted to validate the proposed optimisation methods, are described in Section 3.6. Finally, conclusions are drawn in Section 3.7.

3.2. RFEH antenna types and design

There are several different types of antennas proposed for RFEH in the state-of-the-art. Some of the most researched antenna designs are types such as: Dipoles [93]–[95], fractal antennas [55], circularly polarised antennas [96], dual-band antennas [97]–[99]. However, all of those designs require short distances (less than 50m) to the RF sources in order to provide voltage levels high enough for the RF-to-DC convertors to work efficiently. Antennas with much better directivity are needed for RFEH systems. In order to increase the antenna efficiency, some researchers design antenna arrays [55], [100]. Nevertheless, there is always a trade-off between the antenna size and its performance.

The average size of a receiving antenna for MW frequency band is tens of metres, because of its wavelength (>200m). For the sake of the specific energy harvesting requirements, we have chosen to investigate the ferrite rod antenna. They have been used for receiving Low Frequency (LF) and MW for many years [101]. The main reason for their popularity is their compact size. They are much smaller compared to the wavelength of the radiated electromagnetic signal in the MW broadcasting frequency band. This feature is mainly due to the permeability of the ferrite rod introduced in the coil. In this configuration, the ferrite rod antenna may be presented as a coil antenna with an enhanced effective area.

The antennas designed for RFEH have specific requirements for their parameters. They will be expected to work under extreme conditions, such as arbitrary polarisation, ultra-low power (micro or nano-power) densities and varying incident power levels. All the antenna designs investigated in this research were analysed as an integral part of the RFEH system. Using such an approach

allows us to optimise the antenna parameters for specific requirements and therefore achieve better overall performance.

A flow chart is proposed to be used to model, simulate, configure and optimise RFEH systems (Figure 3.1). The process starts with initial design specification, such as available RF energy source (MW, DAB, DVB, GSM, etc.), RF energy density, device size, minimum voltage power output. A key block in that model is the question 'Best performance achieved?'. An answer should be given after all the known structures have been tried, therefore, the quality of the result depends directly on the number of structures we are familiar with.

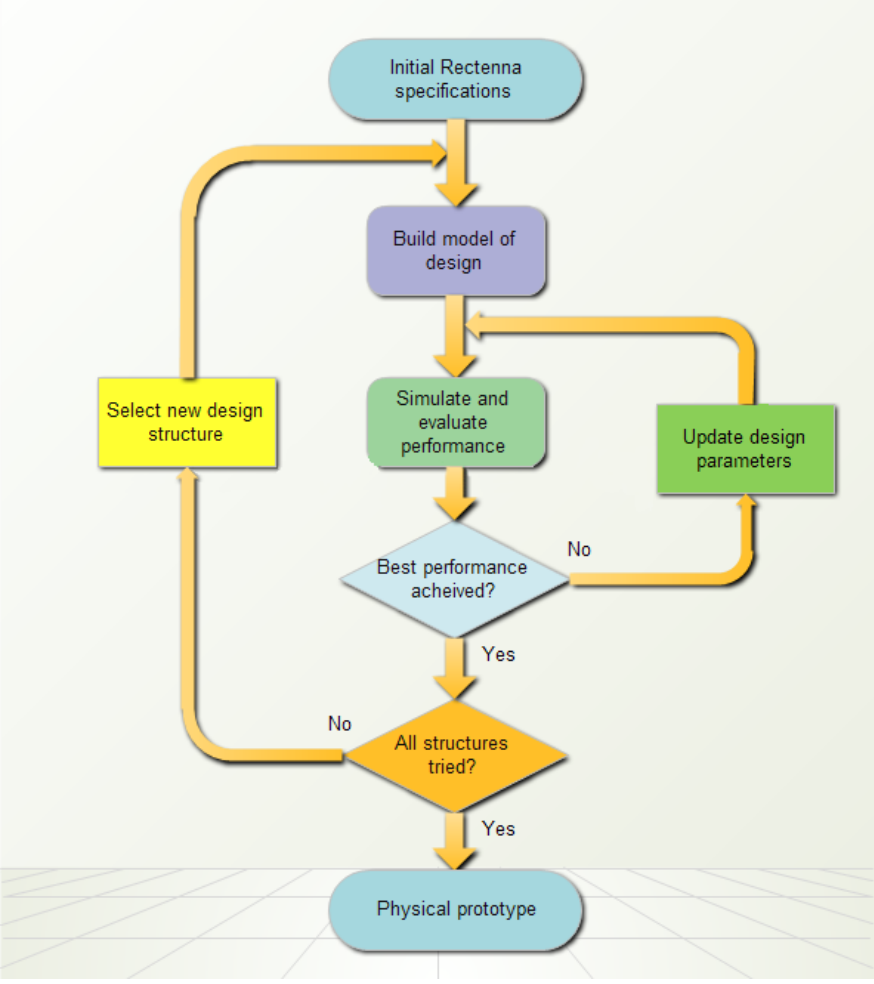

Figure 3.1 Flow chart of RF Energy Harvesting rectenna design

The choice of electrically small antennas for MW is very limited because of the long wavelength (1000 to 100m). Even a small loop antenna is too big (more than 1m in diameter) to be considered as a useful EH antenna for powering very low rank autonomous systems. The only type of MW antenna found to be suitable for small size RFEH applications is the tuned ferrite rod antenna.

3.3. Quality factor of ferrite rod antennas

There are two reasons for why Q-factor of a ferrite rod antenna is an important factor when it is used in the traditional MW receivers. The first reason is that the receiver's selectivity depends on the antenna's bandwidth, thus the higher the antenna's Q-factor is, the lower the out-of-band signals are. In the cases when the Q-factor is too high it would become a disadvantage as a traditional AM receiver should cover the entire MW frequency band. Secondly, the noise performance of the receiver relies on the antenna's Q-factor. In RFEH Designing a ferrite rod antenna for energy harvesting applications is a different challenge, which requires a different approach, because of the specific requirements of a RFEH system.

The antenna gain (*G*) is a very important characteristic when it comes to antenna optimisation for higher frequencies (VHF, UHF, SHF, etc.). It is sometimes discussed as a function of angle since directivity is closely related to gain, but when a single number is quoted the gain is its peak value over all directions and it is related to directivity (D) by [101]:

$$G = DE_R \tag{6}$$

By definition, the only requirement for E_R (radiation efficiency factor) in (6) is $0 \leq E_R \leq 1$. If it is less than 1 indicates energy dissipation in the antenna itself. The gain of a SHF antenna can be as high as 30-40dBi for large parabolic antennas.

However, the peak gain of a ferrite rod antenna can be relatively low because it is electrically very small compared to an isotropic radiator or to a dipole antenna at MW frequencies. It can be quite insufficient for some applications, where the antenna gain is lower than -30dBi (although not accounting any impedance mismatch loss). Therefore, the Q-factor is the most important efficiency indicator for a ferrite rod antenna for RF energy harvesting and is more suitable than comparing it to a half or even to a quarter wavelength antenna.

The quality factor of an antenna represents the ratio of energy stored to the energy lost per cycle and in [101] it is given for a ferrite rod antenna by:

$$Q = \frac{2\pi f_0 L_{coil} + L_p}{R_r + R_{DC} + R_f} \tag{7}$$

where f_0 is centre frequency in Hz; $(R_r + R_{DC} + R_f)$ is total resistance of the ferrite antenna; L_{coil} is inductance of the coil; L_p is the parasitic inductance. By knowing R_r (radiation resistance), R_{DC} (ohmic or loss resistance), R_f (loss resistance due to the ferrite) we can calculate the Q-factor for a given frequency. The radiation resistance can be presented as given in [101]:

$$R_r = 31200\ \mu_{er}^2 n^2 \left(\frac{A}{\lambda^2}\right)^2 = 197 \mu_{er}^2 n^2 c_\lambda^4 \tag{8}$$

and

$$R_f = 2\pi f \mu_{er} \frac{\mu_r''}{\mu_r'}\ \mu_0 n^2 \frac{a}{L} \tag{9}$$

where *f* is frequency in Hz, μ_{er} is effective relative permeability of the ferrite rod, μ_r' , is the real part of the relative permeability of the ferrite material, μ_r'' is imaginary part of the ferrite material, μ_0 is $4\pi\ 10^{-7}\ H\ m^{-1}$, n is number of turns, a is ferrite rod cross-sectional area in square meters, and L is length of ferrite rod in meters as shown in Figure 3.2.

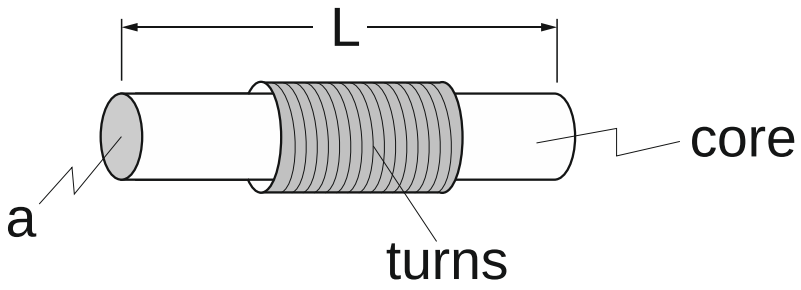

Figure 3.2 Dimensions of the ferrite rod antenna

Ohmic or loss resistance can be presented as:

$$R_{DC} = \frac{L}{\sigma \pi d \delta} = \frac{L}{d}\sqrt{\frac{f\mu_0}{\sigma\pi}} \tag{10}$$

where R_{DC} is in Ohms (Ω), L is wire length in meters, d is the coil diameter in meters, σ is conductivity of medium in $\mho$ m^{-1}. The current density associated with a wave travelling along a conductor is greatest close to the surface, because of the so-called skin effect. The quantity δ is referred to as the depth of penetration. It follows that the RF resistance of a round wire is equivalent to the DC resistance of a hollow of the same material of wall thickness δ. It is assumed that the wire diameter is much larger than δ.

As a conclusion, several parameters of the ferrite rod antenna (described in details in Sections 3.5.1. , 3.5.2. , 3.5.3. , 3.5.4. , and 3.5.5.) are found to increase the overall efficiency which was verified by measuring the Q-factor describing as:

$$Q = \frac{f_0}{\Delta f_{HP}} \tag{11}$$

where Δf_{HP} is bandwidth at half power in *Hz*.

3.4. Maximum acceptable Q-factor value

When a ferrite antenna is designed for MW broadcast reception of amplitude modulated signals it is not required for its Q-factor to be limited in any way. Moreover, it is preferable for such a type of antenna to have as high as possible Q in order to maximise the ratio of signal voltage to noise voltage at the input of the amplifier stage of the receiver (*S/N*).

As described in Section 3.3 using a ferrite rod antenna for harvesting energy from AM broadcast frequencies requires a different approach. The reason for defining maximum acceptable limit of the Q-factor is that in some cases the frequency bandwidth of the source signal may be larger than the antenna's bandwidth.

It can be described by presenting a ferrite rod antenna as a parallel RLC circuit (Figure 3.3). The bandwidth (BW) of the antenna is presented as:

$$BW = \Delta f = \frac{f_0}{Q} \tag{12}$$

The connection between the antenna's bandwidth and its Q-factor can be presented as:

$$Q = \frac{f_0}{BW} \tag{13}$$

If the half power bandwidth of the ferrite rod antenna (Equation (12)) is much narrower than the bandwidth of the modulated signal, a large proportion of the RF energy may be lost as an out-of-band signal.

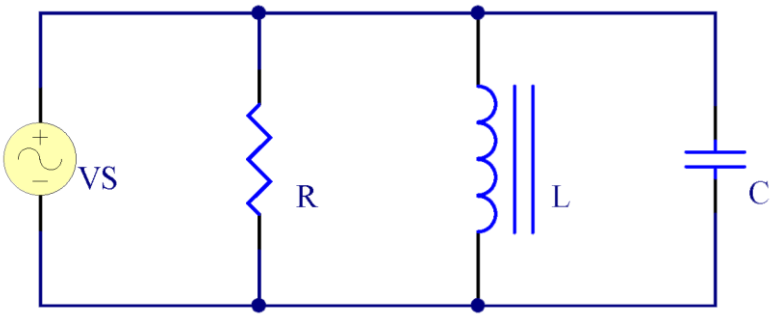

Figure 3.3 A ferrite rod antenna presented as a parallel resonance circuit

In Figure 3.4, f_0 is the central frequency of the ferrite antenna, and $BW = f_2 - f_1$ is typically determined by measuring a characteristic such as Voltage Standing Wave Ratio of 2:1 (VSWR 2:1) or Return loss, L_R, of -3dB.

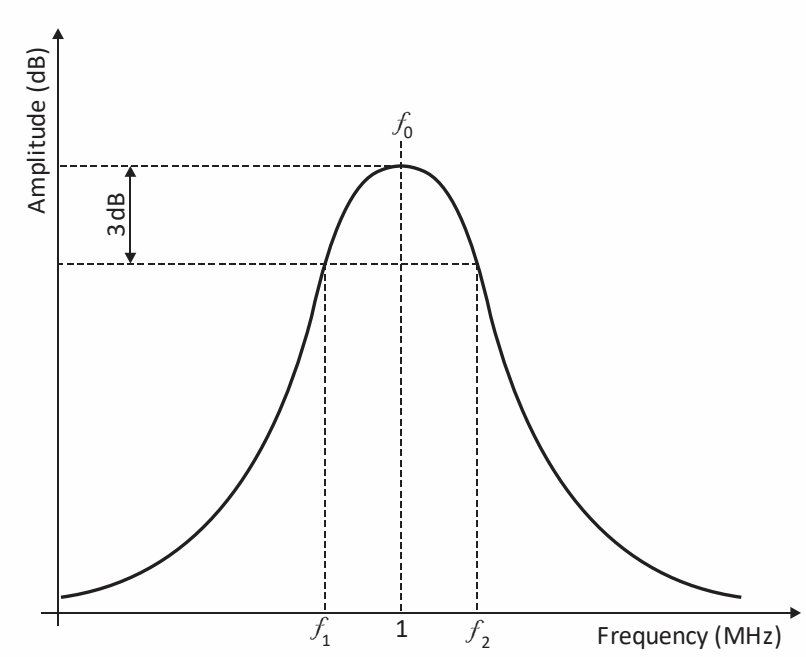

Figure 3.4 Frequency bandwidth of a ferrite rod antenna

The main modulation mode used for MW broadcast transmissions currently is Amplitude Modulation (AM). As shown in Figure 3.5, the bandwidth of a frequency modulated (FM) broadcast signal would not be suitable for RFEH using a high-Q ferrite rod antenna.

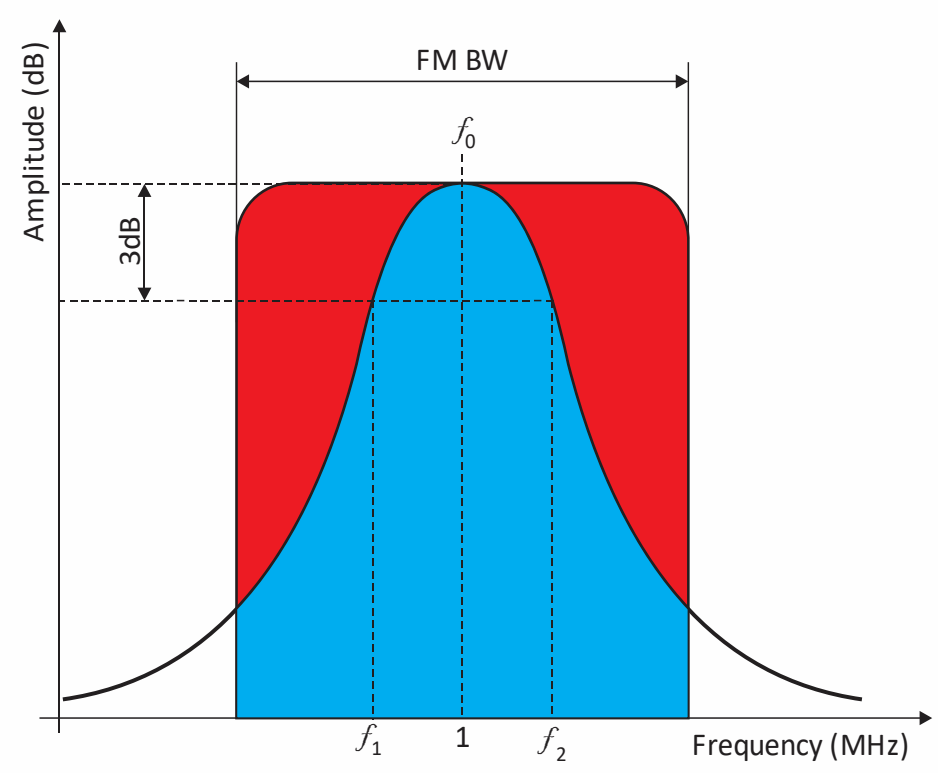

Figure 3.5 FM signal received with a ferrite rod antenna if FM bandwidth (in red) is bigger than (f_2-f_1)

The power levels of the AM components were analysed and a range of signal losses were simulated for ferrite rod antennas with the maximum Q-factor of 1020, achieved during the practical experiments described in Section 3.6.1.

In order to calculate the AM energy levels, it was assumed that that the signal is dissipated in a load of R ohms, R_L (Figure 3.3). The total power dissipated will be the sum of the powers in all of the components of the signal (carrier frequency and two sideband frequencies). Figure 3.6 shows that the carrier power of AM represents two-thirds of the total transmitted power, or 66.7%.

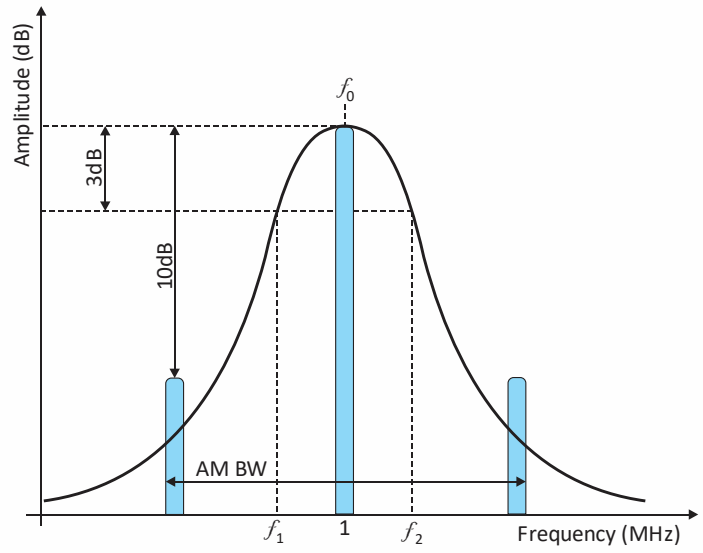

Figure 3.6 AM signal received with a ferrite rod antenna if AM bandwidth is bigger than (f_2-f_1)

The sideband power is 33.3% of all the signal, therefore, the actual energy losses will be insignificantly small (Figure 3.7) and they will not be considered for calculations of ferrite rod antennas with $Q < 1000$.

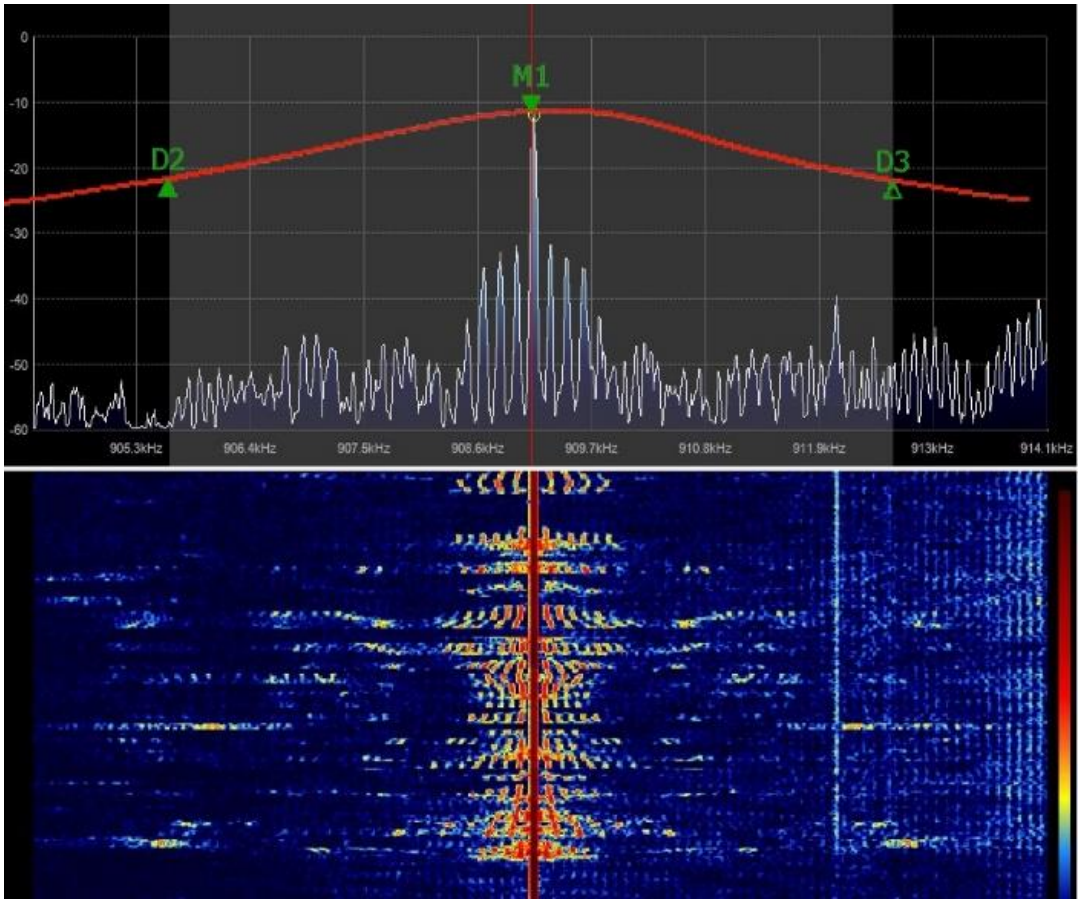

Figure 3.7 Spectrum and waterfall display of AM transmissions at 909kHz with simulated overlay of a Q-factor curve

3.5. Ferrite rod antenna optimisation

The open-circuit voltage at the output of the small loop antenna can be increased by inserting a high permeability core material inside the coil, such as ferrite. It is concentrating the magnetic flux through the central axis of the loop, valid for a cylindrical core placed inside an uniform solenoidal coil (Figure 3.8).

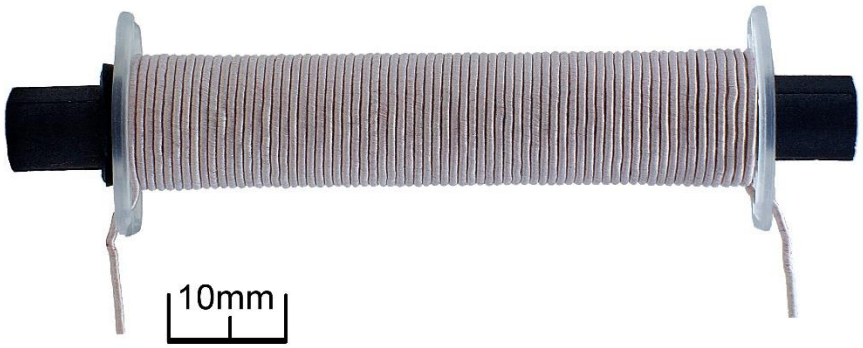

Figure 3.8 A ferrite rod antenna prototype used in the experiments

The ferrites are typically made from two types of material – Nickel-Zinc (NiZn) and Manganese-Zinc (MnZn). NiZn ferrites are known for their higher resistivity compared to that of MnZn hence they are more preferred for frequencies higher than 1 MHz. They are characterised by a complex relative initial permeability $\mu_r = \mu/\mu_0 = \mu_r' - j\mu_r''$ and a relative permittivity of $\varepsilon_r = \varepsilon/\varepsilon_0$. It is very difficult to measure their relative permeability, so manufacturers usually quote the permeability which they have measured using a toroid of the same material. In Table IV are listed several ferrites with their specifications provided by the manufacturer [102]. Because of its open geometry (as contrasted to a closed core or ring) a ferrite rod with a relative permeability μ_r will have a smaller effective relative permeability μ_{er} due to the demagnetisation effect [101].

Table IV The nominal properties of some ferrites provided by the manufacturer

Material	μ_r at 25 ° C	B_{sat} (mT) at 25°C	Tc(°C)	p (Ωm)	Ferrite type
4B1	250	≈ 360	≥ 250	≈ 105	NiZn
4S2	850	≈ 340	≥ 150	≈ 105	NiZn
4S3	250	≈ 360	≥ 250	≈ 105	NiZn
4S60	2000	≈ 260	≥ 100	≈ 105	NiZn
3C11	4300	≈ 390	≥ 125	≈ 1	MnZn
3E65	5200	≈ 480	≥ 165	≈ 0.5	MnZn
3E26	7000	≈ 430	≥ 155	≈ 0.5	MnZn
3E5	10000	≈ 380	≥ 125	≈ 0.5	MnZn
3E6	12000	≈ 390	≥ 130	≈ 0.1	MnZn

For an electrically small loop it is assumed that the axial current distribution is uniform; that is, the current value I_0 is equal to the value of the current at any point of the conductor. The measurements in [101] show that for multi- and single-turn loops which are using single-layer solenoidal coils, the latter assumption is valid if the total length of the wire conductor (N × circumference) is much smaller the wavelength of the frequency, typically $\leq 0.1\lambda$, and ratio between the coil length and its diameter is higher than 3. Such a loop antenna (electrically small) is analysed as radiating inductor when the current along the conductor is uniform.

If such loop is used as a receiving antenna, the voltage measured at its terminals V_{OC} is estimated by using its proportionality to the part of the magnetic flux density, normal to the plane of the loop B_z^i:

$$V_{OC} = j\omega\mu_r NAB_z^i \tag{14}$$

where it is assumed that the incident field value is uniform along the area of the loop. Equation (14) describes the connection between V_{OC} and B_z^i , hence may be used for measuring the magnetic flux density.

3.5.1. Copper quality characteristics of the coil wire

As shown in Equation (7) the value of total resistance $R_r + R_{DC} + R_f$ of the ferrite antenna affects its performance. Designing a multi-turn loop antenna inevitably leads to an increased ohmic loss value. If we compare the skin depth, which is approximately 0.07mm at 1MHz in copper, we can conclude that its value is negligible to the other dimension values of the loop. Hence, the conductor loss can be calculated by using the values of resistance and the surface current.

The accuracy of ferrite rod antenna analysis was limited by manual computation methods until Simpson and Zhu [103] presented a new technique of analysing circular loops on prolate spheroidal core. To model it accurately, we need to present the ferrite rod as a hollow spheroidal core shown in Figure 3.9 (a=1, b=0.2, and ξ=1.033) with semiaxes a and b centred on a hollow spheroidal coordinate system and its coordinates are (ξ, η, ϕ) where the two foci are positioned at $\pm c$ of its z-axis [104][105][106].

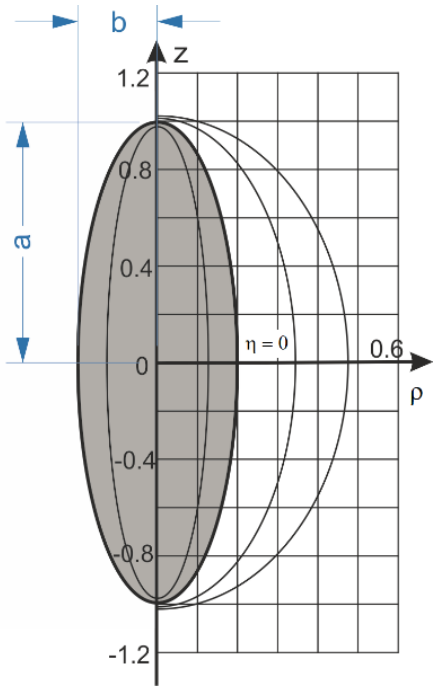

Figure 3.9 Hollow spheroidal core

In order to convert the spheroidal coordinates to cylindrical coordinates we use:

$$\rho = c\sqrt{(\xi^2 - 1)(1 - \eta^2)} \tag{15}$$

and

$$z = c\xi\eta \tag{16}$$

A confocal system of orthogonal hyperboloid surfaces η is constant and it is presented by:

$$\frac{z^2}{c^2\eta^2} - \frac{\rho^2}{c^2(1 - \eta^2)} = 1 \tag{17}$$

The metric coefficients are given by

$$h_\xi = c\sqrt{(\xi^2 - \eta^2)/(\xi^2 - 1)}, \tag{18}$$

$$h_\eta = c\sqrt{(\xi^2 - \eta^2)/(1 - \eta^2)}, \tag{19}$$

and

$$h_\emptyset = \rho. \tag{20}$$

If we assume that the surface current is continuous (K_ϕ), the dissipation density ($R_S K_\phi^2/2$) may be used to present its integral as conductor loss. If it is wound over a spheroidal shape $\xi = \xi_0 = a/c$, where the surface resistance is $R_S = 1/(\sigma\delta)$, the conductivity is σ, and the skin depth is δ.

In Equations (15), (16), (18), (19) and (20), the variable element on the spheroid surface is $dS = h_\eta h_\emptyset d\eta d\emptyset$. Therefore, the result for a coil on a spheroidal core, may be presented as an integral for its power loss:

$$P_{pr} = \frac{1}{2} R_s \left(\frac{NI}{2}\right) \sqrt{\xi_0^2 - 1} \int_{-1}^{1} \frac{1 - \eta^2}{\sqrt{\xi_0^2 - \eta^2}} d\eta d\emptyset. \tag{21}$$

If the closed form of the integral in Equation (21) is assigned to a lumped resistance value, R_{pr}, where $P_{pr} = I^2 R_{pr}/2$, then:

$$R_{pr} = \frac{\pi}{2} R_s N^2 \sqrt{\xi_0^2 - 1} \left\{ \left(2 - \xi_0^2\right) \sin^{-1} \frac{1}{\xi_0} + \sqrt{\xi_0^2 - 1} \right\} \tag{22}$$

All of the Equations (15) to (22) are valid for a prolate-spheroidal core, where *a>b* (Figure 3.9). In the case where a<b (oblate-spheroidal core), Simpson et al [107] have analysed the conductor loss for different scale factors. However, the cases where the ferrite rod (core) is a sphere (a=b) or an oblate-spheroid (a<b) are beyond the scope of this research and will not be further analysed.

Several ways of minimising the ohmic loss value were proposed. During the experiments five different types of wire were used for winding the coils of the antennas. The first two types were solid copper wires with different diameters – 38SWG and 23SWG. Both coils produced similar results.

Litz wire was used as a low resistance alternative of the solid copper wire in order to reduce the impact of the skin effect. It is a stranded wire with individually insulated conductors (Figure 3.10). Every individual conductor is very thin, so a single strand does not suffer a substantial skin effect loss. However, this wire type may be assumed as a single wire, because all the thin wires are individually insulated in order to prevent them from shorting together. An important feature of this type of wire is to present a very low resistance at high frequencies, because of its strand's uniform impedances. In this way the individual strand currents are also equally distributed.

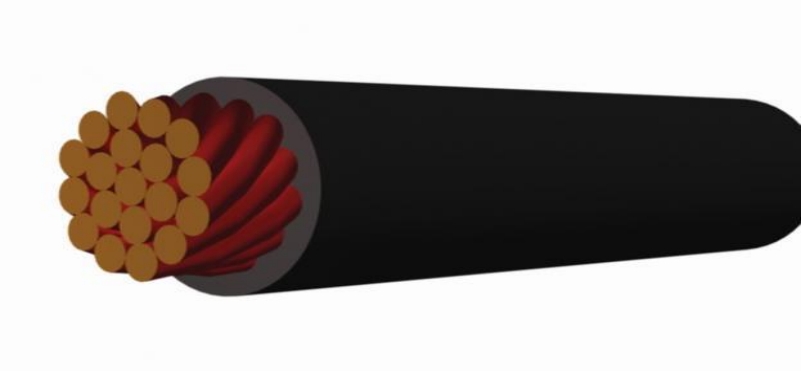

Figure 3.10 Cross-section of Litz wire

Three different Litz wire types were used: 66/46, 220/46 and 660/46. The first number shows the number of the strands and the second is the individual wire diameter in British Standard Wire Gauge (SWG). In the experiments described in Chapter 3 ,the wire used for the high Q-factor ferrite rod antenna is Litz wire, type 660/46, which means 660 strands of 46SWG diameter.

The same ferrite core was used for all the coils under test in order to minimise the effect of the other parameters such as ferrite permeability, rod length, etc. The results showed a clear advantage for the antennas made using Litz wire. Moreover, the one designed with 660/46 type wire (see Chapter 3) achieved a Q-factor of 820 which is four times more than the one measured with the antenna using 38SWG solid wire.

3.5.2. Capacitor's type influence on RFEH performance

Both conductor and capacitor used in the ferrite rod antenna, are reactive components, therefore their losses may be ignored only if we assume that they are ideal reactive components. Since any real component also has loss due to its resistivity, in reality the losses in the capacitor affect overall efficiency and bandwidth, therefore the Q-factor of the antenna. Connecting a non-variable capacitor in parallel with a lower value variable capacitor decreases the overall Q-factor by approximately 8% compared to the same design with a variable capacitor

only. However, adjusting a high Q resonant circuit on MW with one capacitor was found to be a difficult task and the losses could be high because of an inaccurate adjustment and frequency drift. Several types of capacitors were chosen and practical tests were conducted with the shortlisted candidates, and as a conclusion I would recommend polystyrene capacitor for the non-variable one and a PTF film or a piston type for the variable one as they are known to be low loss capacitors for even higher frequencies. For higher frequencies, the ceramic multi- layer capacitors are a good choice, because of their compact construction and absence of leads.

3.5.3. Coil position along the ferrite rod

Figure 3.11 shows the relationship between Q-factor and position of the coil along the ferrite rod. If the coil is placed centrally it is marked as 0.5 at the horizontal axis, whilst 0 and 1 correspond to it being at either end.

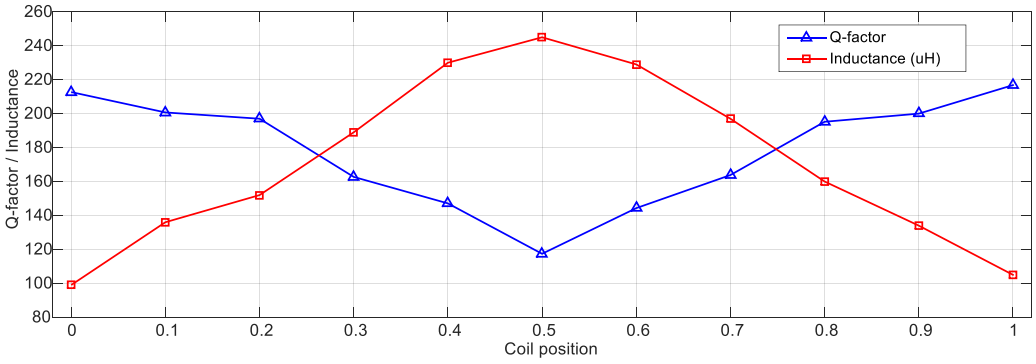

Figure 3.11 Measured inductance and Q-factor as functions of coil positions.

Changing the position of the coil on the rod influences inductance and Q-factor values differently. In Equations (7) and (10), Q and L are given as functions of different parameters, hence the experiments confirm the expected result. Aiming a higher Q-factor we should position the coil at one of the ends of the ferrite rod.

3.5.4. Coil diameter to rod length ratio

One of the main physical parameters of the ferrite rod antenna is the effective area as it has direct influence on the effective permeability and therefore on the overall efficiency of the antenna (Equation (9)). The ferrite rod permeability can be presented as in [108]:

$$\mu_{rod} = \frac{\mu_r}{1 + (\mu_r + 1)(D/L)^2}(\ln(L/D)\{0.5 + 0.7[1 - exp(-\mu_r x 10^{-3})]\}) \quad (23)$$

where the rod permeability rises with *L/D* ratio and reaches its maximum at *L/D* = 20 regardless of the rod diameter. Equation (25) is valid only for rods with 2<(L/D)<100.

The L/D ratio would increase the Q-factor as shown with Equation (10), nevertheless, the only available ferrite rods on the market are with ratios between 10 and 15, so there is no practical significance to investigate it further.

3.5.5. Rod diameter to coil internal diameter

In order to decrease the physical size of a ferrite rod antenna we are trying to take advantage of the main property of the ferrite to 'squeeze' the electromagnetic waves.

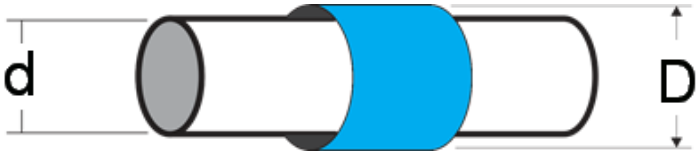

Figure 3.12 Rod and coil diameters of a ferrite rod antenna

At the same time the loss resistance (R_f) is increased due to the ferrite's loss influence as shown in Equation (9). By moving the coil away of the ferrite, this

effect can be optimised by choosing a compromise position where the Q-factor is at its maximum. As the shown in Figure 3.13 the highest Q-factor was achieved using D/d ratio of 1.3.

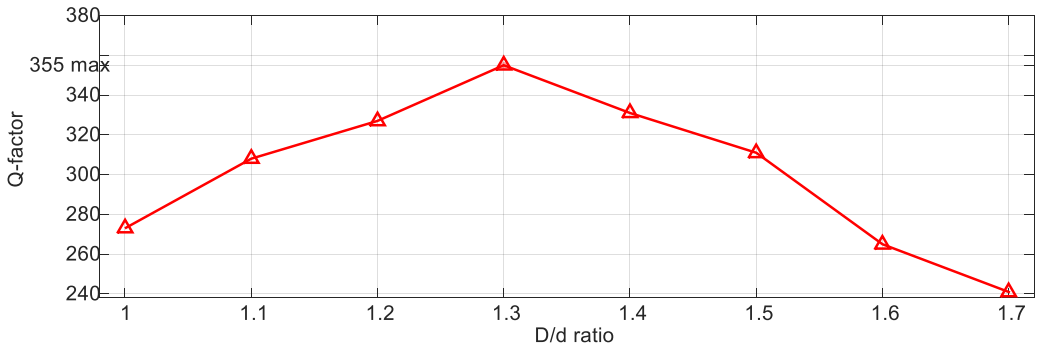

Figure 3.13 Q-factor vs. D/d ratio (rod to coil diameter).

3.6. MW experiments

Factors such as polarisation, multipath propagation, modulation, physical environment, response time, dynamic range, and the capability of sensing near-field and far-field signals will have to be taken into account before selecting the best device, or designing your own RFEH rectenna. Two groups of experiments were conducted, in order to investigate the impact of practical factors on the efficiency of RFEH. The first set of measurements were organised as *outdoor* trials for measuring the power available on MW using an AM broadcast transmitter as an energy source. The second part was a set of *indoor* experiments using dedicated RF energy source.

3.6.1. Site surveys for harvesting ambient RF energy

Aims of the trials:

- Create a dataset which may be used as a benchmark for future RFEH experiments on MW bands.
- Verify main antenna specifications and compare different antenna types.
- Proof of concept of long distance ambient RFEH for powering a typical wireless sensor.
- Define a coverage area for RFEH on MW from AM broadcast transmitters fulfilling the minimum requirements for autonomous sensors.
- To validate the effectiveness of the optimisation methods proposed earlier and their impact on different antenna design parameters. To use the results as a design optimisation tool for extending the range RFEH devices

The equipment used for the first set of trials is listed in Table V.

All the prototypes were designed and manufactured in the engineering laboratory of University of Bedfordshire, University Campus of Milton Keynes (UCMK).

Table V Measuring equipment.

Equipment	Description	Function
Thermal µPower Sensor	R&S® NRP-Z51 -35 dBm to +20 dBm DC to 18 GHz	Accurate power measurements
Spectrum Analyser	R&S® FSL 9kHz-6GHz	Field density measurements and frequency adjustments
Digital Voltmeter	M-3650D	Voltage Data Logger
RF-to-DC Converter #1	1-stage SMS7621	Voltage multipliers
RF-to-DC Converter #2	2-stage 1N6263	Voltage multipliers
RF-to-DC Converter #3	4-stage SMS7621	Voltage multipliers
GPS Tracker	Garmin eTrex 20	GPS logging
Antenna#1	Low-gain, single rod	Field density measurements
Antenna#2	Medium-gain 7-rod	Field density measurements and LCD digital clock
Antenna#3	High-gain 15-rod	Field density measurements
Tripod	Spectra-Physics	Rectenna support

Brookmans park transmitter site was chosen for the trials because of its variety of MW broadcast frequencies and antennas. There are currently four AM broadcast radio stations transmitting at this location in the MW band as shown in Table VI. All the rectenna prototypes were set for 909 kHz - BBC Radio 5 Live. This radio station was chosen for the measurements mainly because its signal is transmitted uniformly in all directions. The antenna is a guyed steel lattice mast, insulated against ground, 152m above the ground level (AGL) high.

Table VI MW AM broadcast radio stations at Brookmans park site.

Frequency	kW	Service	Information
909 kHz	150	BBC Radio 5	Omnidirectional antenna
1089 kHz	400	Talksport London	Directional antenna (South)
1215 kHz	125	Absolute Radio	Omnidirectional antenna
1458 kHz	125	Lyca Radio	Since 04.02.2014

Figure 3.14 and Figure 3.15 illustrate the ferrite rod antenna assembly and the measurement system. A spectrum analyser and a tripod-mounted receiving ferrite antenna were used to measure throughout a suburban environment.

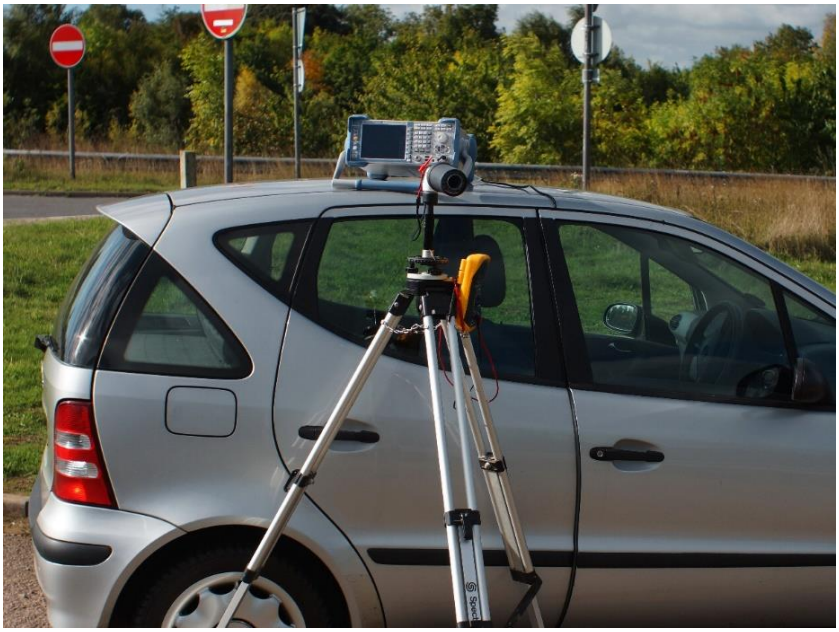

Figure 3.14 Antenna#3 setup used for the first set of MW trials.

Figure 3.15 Antenna#2 setup used for the first set of MW trials.

Three types of ferrite rod antenna were used for the measurements in order to compare their performance, as well as to demonstrate the effectiveness of the proposed optimisation methods by using different antenna designs:

- ***Low gain single-rod antenna.***

A coil of 68 turns was wound onto a low loss ferrite core with Litz wire of 220 strands/46SWG diameter (see Figure 3.16). The ferrite core is MnZn material with relative permeability of 2000 and dimensions of 10mm diameter, 100m in length. The coil is placed at the end of the ferrite rod in order to improve the Q-factor as described in Section 3.5.3. and shown in Figure 3.11. The inductance of the coil is 147μH. A diameter of 13mm was chosen for the coil base as the best *D/d* ratio recommended in Section 3.5.5. and demonstrated in Figure 3.13. is 1.3. An air type capacitor was used for setting the centre frequency. After the centre frequency was adjusted to 909kHz, a loaded Q-factor of 190 was measured.

Figure 3.16 Low gain ferrite rod antenna prototype

- ***Medium gain 7-rod antenna.***

A coil of 35 turns was wound onto a low loss 7-rod ferrite core with Litz wire of 440 strands/46SWG diameter (see Figure 3.17). The ferrite rod material is MnZn with relative permeability of 2000 and dimensions - 30mm diameter, 100m in length. The coil is placed at the end of the ferrite rod to improve the Q-factor as described in Section 3.5.3. and shown in Figure 3.11. The inductance of the coil is 180μH. A diameter of 40mm was chosen for the coil base in order to achieve *D/d* ratio as close as possible to the one recommended in Section 3.5.5. and demonstrated in Figure 3.13. An air type capacitor was used to set the centre frequency. After the centre frequency was adjusted to 909kHz, a Q-factor of 435 was measured.

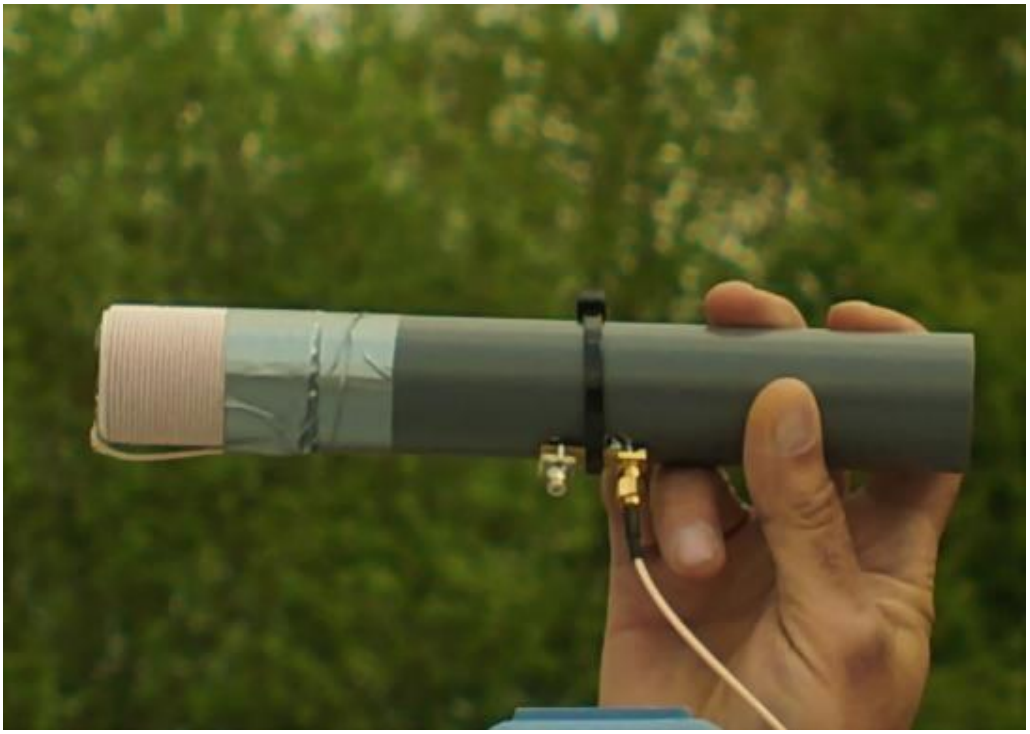

Figure 3.17 Medium gain ferrite rod antenna prototype

- ***15-rod antenna***

A coil of 45 turns was wound onto a low loss 15-rod ferrite core with Litz wire of 660 strands/46SWG diameter (see Figure 3.18). The ferrite rod material is MnZn with relative permeability of 3000 and dimensions - 70mm diameter, 100m in length. The coil is fixed at the end of the ferrite rod in order to improve the Q-factor as described in Section 3.5.3. and shown in Figure 3.11. The inductance of the coil is 220μH. An air type capacitor was used to set the centre frequency.

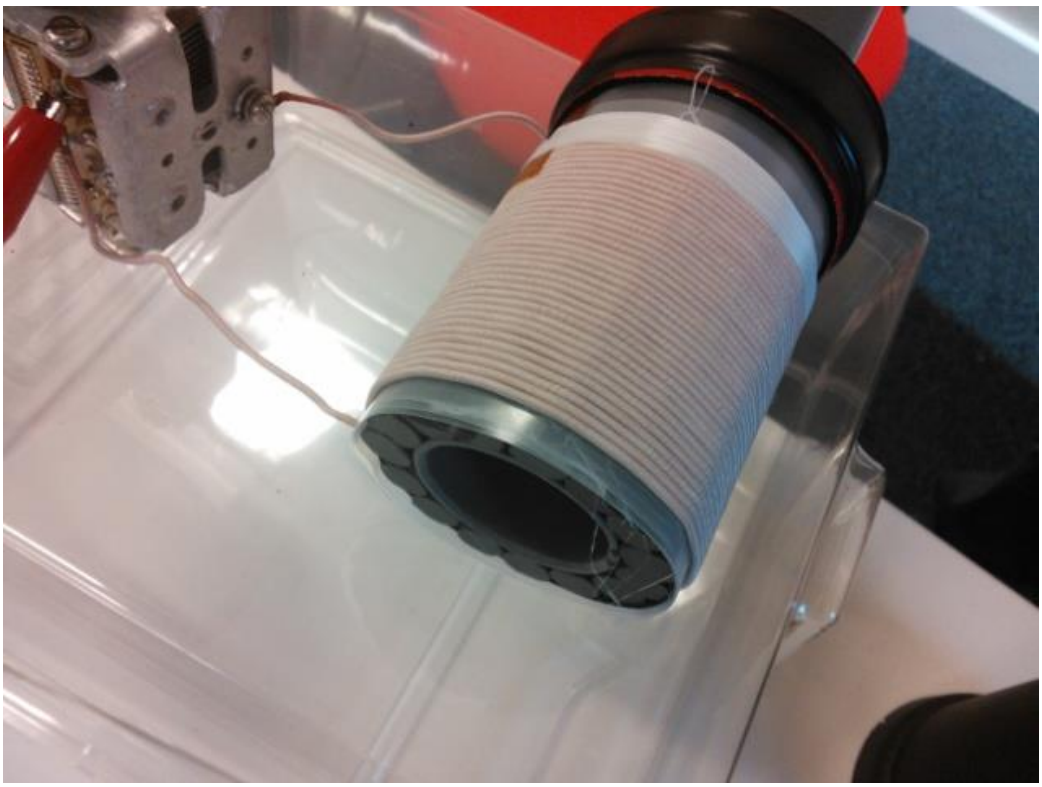

Figure 3.18 High-gain ferrite rod antenna prototype 15 rods

After the centre frequency was adjusted to 909kHz, a Q-factor of 710 was measured at the centre frequency. The highest Q-factor of 1024.9 was measured at 609.6kHz (see Figure 3.19).

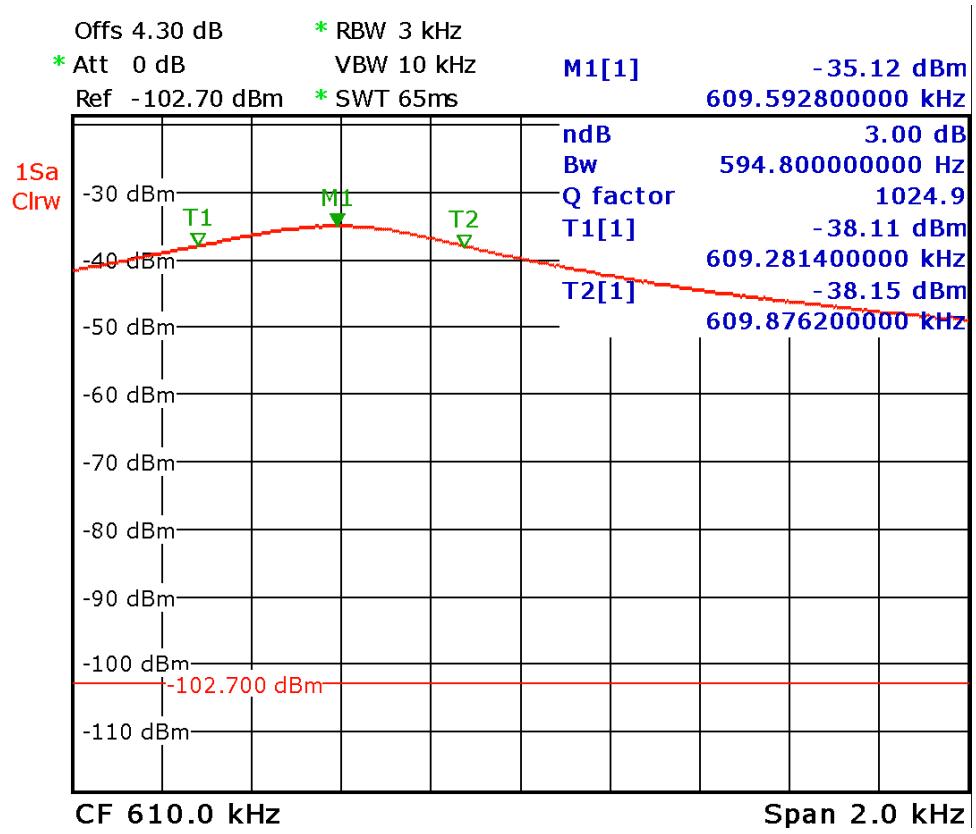

Figure 3.19 The highest Q-factor measured with 15-rod antenna.

The geographical coordinates of the measuring locations were recorded in order to be able to compare the results in future trials (Figure 3.20). Longitude and latitude values were converted to distances to the transmitter. The results were summed for each of the measurements and the average values were used for each of the test spots.

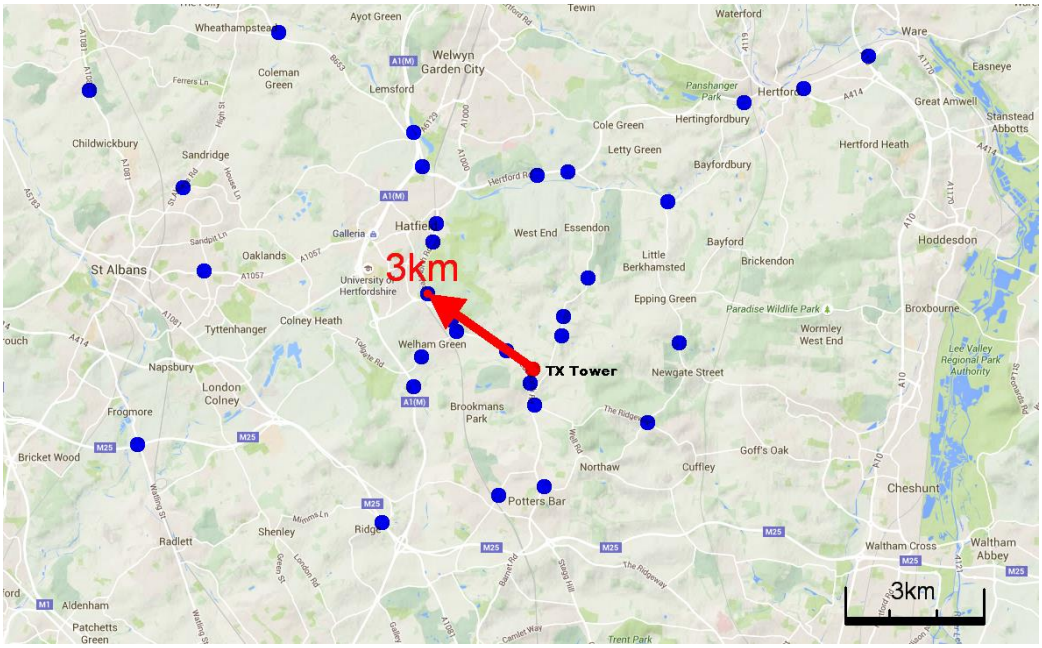

Figure 3.20 Map with the measuring points around Brookmans park.

At a distance of 3.1km, which corresponds to 11mi^2 area around the transmitter, I managed to harvest enough energy to power a digital LCD clock (see Figure 3.21). The clock's start-up voltage is 1.1V.

In order to compare the power available to the power required by a typical wireless sensor, we simulated several types of transmission behaviour of an MSP430 board with an IEEE 802.15.4-compatible CC-2420 radio chip. Instant Contiki was used as a simulation environment, together with Cooja. Contiki is an open source operating system for the Internet of Things (IoT) and Cooja is a network simulator for Contiki. For duty cycles in the range of 0.5% to 1% the minimum power needed was 100-120μW. Assuming that the power required by such a wireless sensor is twice lower than the value harvested at this distance, the estimated useful range can be easily extended. However, more than 4,000 people are living in the area of 11 mi^2 around the transmitting tower in Brookmans park according to the Office of National Statistics [109].

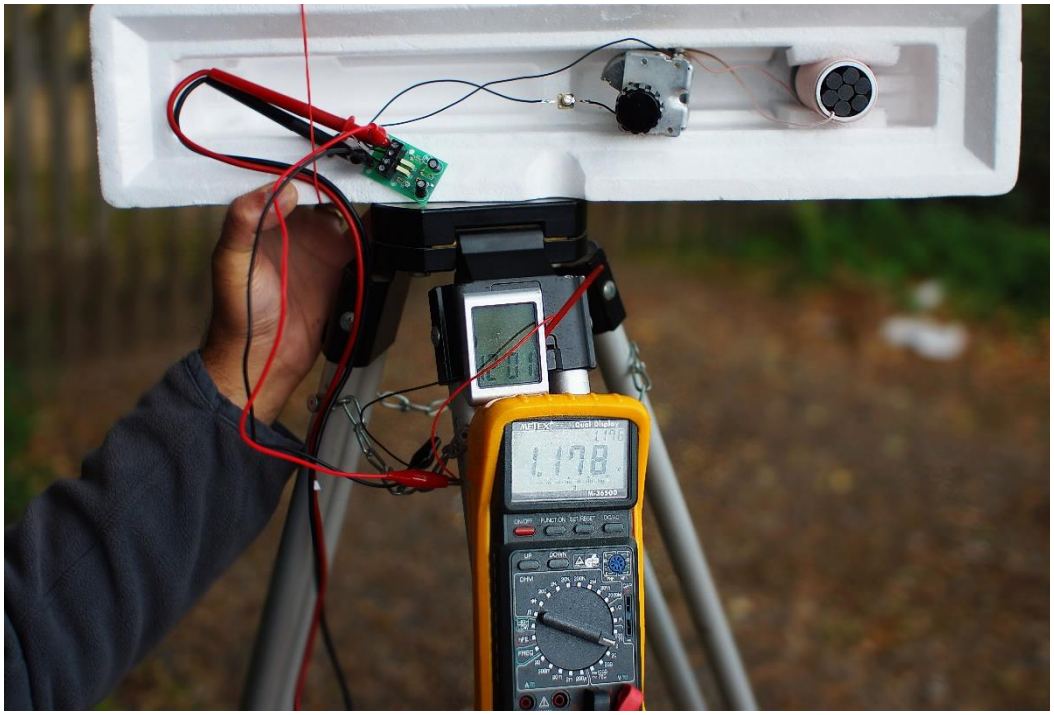

Figure 3.21 An LCD digital clock powered by one of the rectenna prototypes, 3km away of the transmitter.

The Friis transmission equation (26) was used to calculate the power level expected to be received at the antenna output.

$$P_R = \frac{P_T\ G_T G_R \lambda^2}{(4\pi D)^2} \tag{24}$$

Where P_R is the power received at the antenna; P_T is the power delivered to the transmit antenna; G_T is the transmit antenna gain in the direction of the receive antenna; G_R is the receive antenna gain; λ is the wavelength and D is the distance to the transmit antenna. The path loss and received power are computed for an outdoor channel in free-space similar to the way it has been done in [110] and [54]. The simulated results were then compared to the measured values collected during all the site surveys conducted earlier.

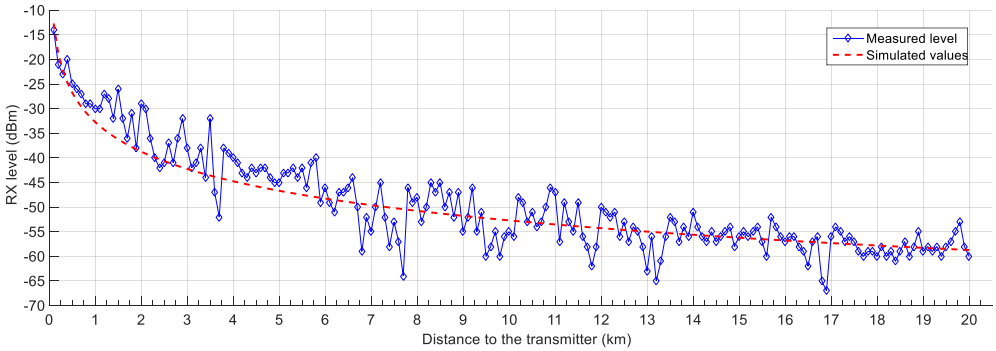

Figure 3.22 Power densities of AM broadcast radio signals measured and simulated at 262 locations vs. distances from transmitter ranging from 100m to 20km

It is obvious that less power is available by positioning the device further away of the transmitter until we reach a distance of around 20 km where the harvested RF signal becomes unusable with the current equipment. The agreement between the simulated and the measured levels was achieved by choosing an average theoretical gain of -42 dB for the ferrite rod antennas which was the only unknown value during the simulations.

3.6.2. Experiments for RFEH from dedicated energy sources

The aim of this part of experiments is to present to what extent the RF energy harvester could prolong the battery lifetime of an autonomous sensor using a dedicated RF energy source. Most of the experiments described in this section were part of a Heritage Retrofit project [111] (Small Business Research Initiative), funded by Cardiff Council, with support from Welsh Government, Technology Strategy Board, Cadw and Low Carbon Research Institute. The goal of this project was to develop innovative measures that will improve the energy performance of traditional & historic buildings in Cardiff.

Using remote temperature monitoring and control is a well investigated research area, however, in some cases wireless powering and control may be considered as a huge advantage compared to the conventional wired or battery

systems. We started with power consumptions analysis of variety of off-the-shelf electronic heater control valves (see Figure 3.23).

Figure 3.23 Off the shelf electronic valves.

The preliminary measurements (see Figure 3.24) showed that the current and duty cycle required are difficult to be achieved with the suggested harvester to suit the off-the-shelf control valves. All of the tested devices were using 3V battery power.

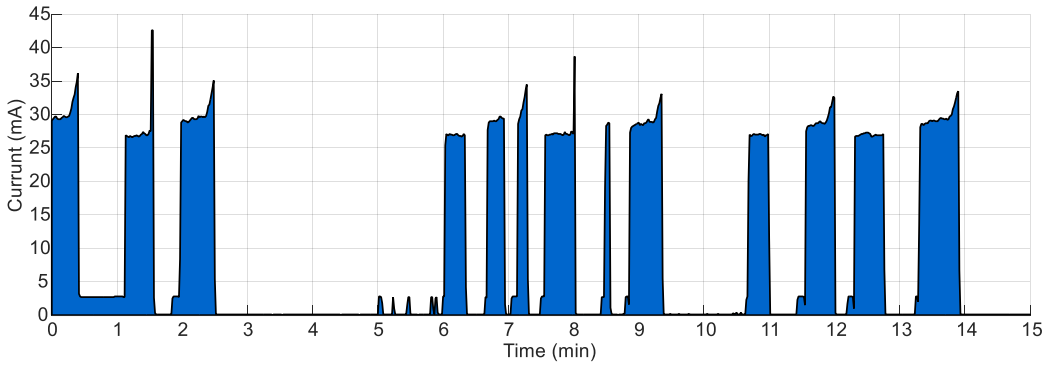

Figure 3.24 Valve's current (mA) recorded for 15 minutes with temperature variations of ±3°C.

With a duty cycle in the range of 35% to 40%, measured with temperature variations of ±3°C, the power required for a normal work of such a type of valve would be more than 50mW which exceeds the capabilities of any RFEH rectenna known in state-of-the-art. The main reason for this high consumption is that the devices we have chosen are not designed to be powered by alternative power supplies. As there aren't such optimised devices available currently on the market,

we decided to continue our research with contributing to the other part of the control system – remote temperature sensing.

As shown in Figure 3.25, at the transmitting part of the diagram, MW signal generated by the Signal Generator (SG) is amplified by 20dB to a power of 5W (PA) and applied to a Loop Antenna (LA) through a impedance Matching Network (MN). At the receiving part, the signal received at the Ferrite Rod Antenna (FRA) is multiplied and rectified by the RF-to-DC convertor (RF-DC) and applied to an embedded DC-DC convertor (DC-DC).

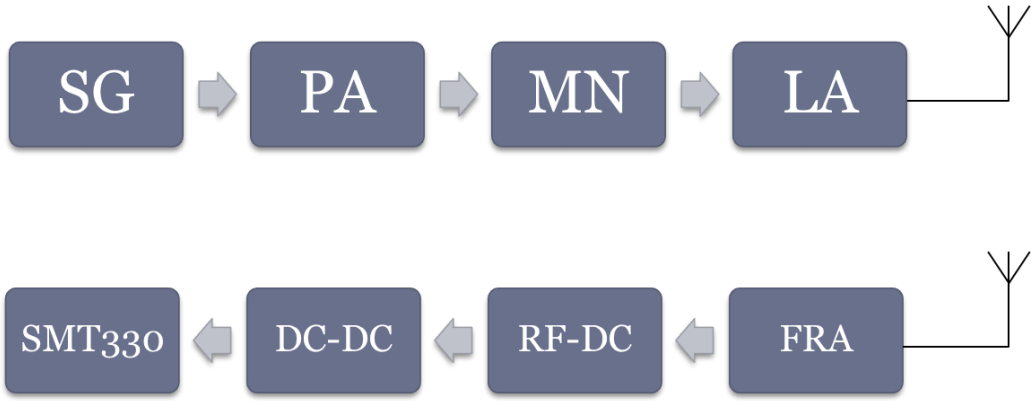

Figure 3.25 Block diagram of the experiment.

The equipment used for the first set of trials, and their descriptions, are listed in Table VII.

Table VII Equipment used in the trial.

Equipment	Description	Function
Spectrum Analyser	R&S® FSL 9kHz-6GHz	Q-factor measurements and frequency adjustments
Signal Generator	R&S® SMC100A	MW dedicated signal transmission
Power Amplifier	MOSFET 5W (20db) MW @1071kHz	Amplifies signal from SG
Digital Voltmeter	M-3650D	Voltage & Current Data Logger
RF-to-DC Converter #1	2-stage 1N6263	Voltage multipliers
RF-to-DC Converter #2	4-stage SMS7621	Voltage multipliers
TX Loop Antenna	Wire loop antenna prototype	MW transmitting antenna
Antenna	Low-gain, single rod	Provides power for the sensor
Temperature sensor	EnOcean STM330	Senses and transmits temperature
Heater control valves	Off-the-shelf valves	Control the temperature

After a simple site survey was conducted, the frequency of 1071kHz was approved and used for the experiment. A licence was issued by Ofcom (see APPENDIX A). The experiment was conducted indoors, at the UCMK laboratories.

The main elements of the transmitting part of the RFEH system are shown in Figure 3.26. During the first transmissions only the output power was measured which made it very difficult to minimise the return loss of the loop antenna. Moreover, the amplifier was not working properly with VSWR values higher than 1.3. The S11 parameter between the output of the matching network and the input of the antenna was measured and the antenna was well matched to the amplifiers output impedance. Figure 3.27 shows S11 graph of the antenna

measurement at 909kHz as originally set to demonstrate its receiving capability (BBC Radio 5 Live). The antenna was easily adjusted from 600kHz to 1.5MHz.

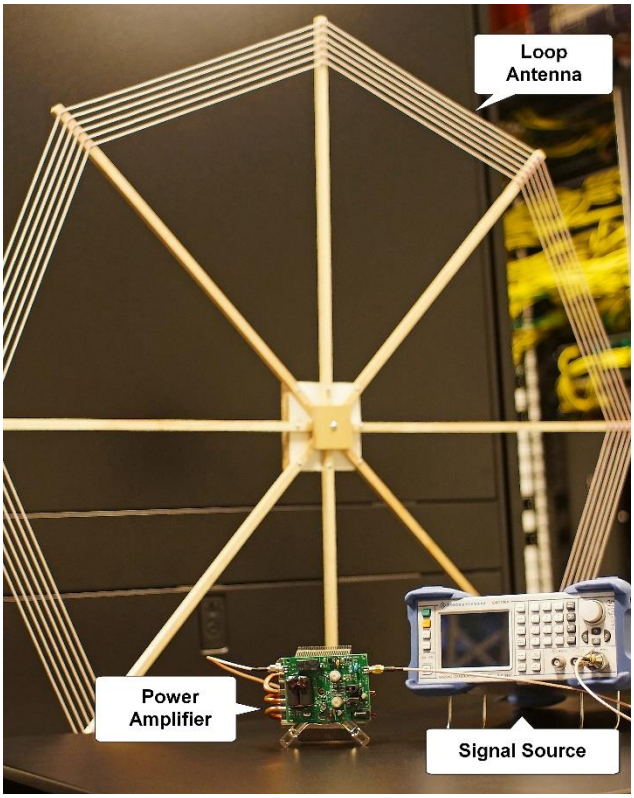

Figure 3.26 The transmitting part of the RFEH system.

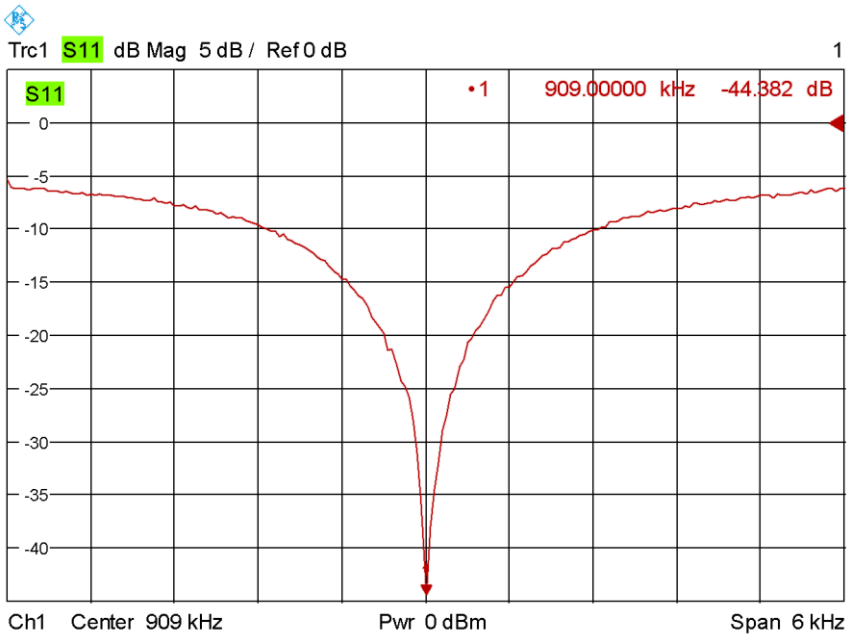

Figure 3.27 TX loop antenna's S11 measured at 909kHz.

As shown in the S11 graph, the useful frequency bandwidth of the matching network with a threshold VSWR requirement of less than 1.3 (S11 of -17.7dB) is less than 1kHz. It was wide enough for this experiment, however, the matching network may not be suitable for mobile or outdoor tests.

The main elements of the harvesting part of the RFEH system are shown in Figure 3.28. A 45mm long ferrite rod antenna with a diameter of 10mm was used for this experiment. The ferrite's relative permeability according to its specifications was 1200 which fulfils the requirement for this frequency. The maximum loaded Q-factor achieved with this antenna was 144 which is a very good result considering the ferrite size limitations and the type of the wire used. The Litz wire used for the coil was 44 strands of 56SWG. The original solar panel was removed from the sensor's PCB and a 4-stage SMD RF-DC convertor was mounted at its place.

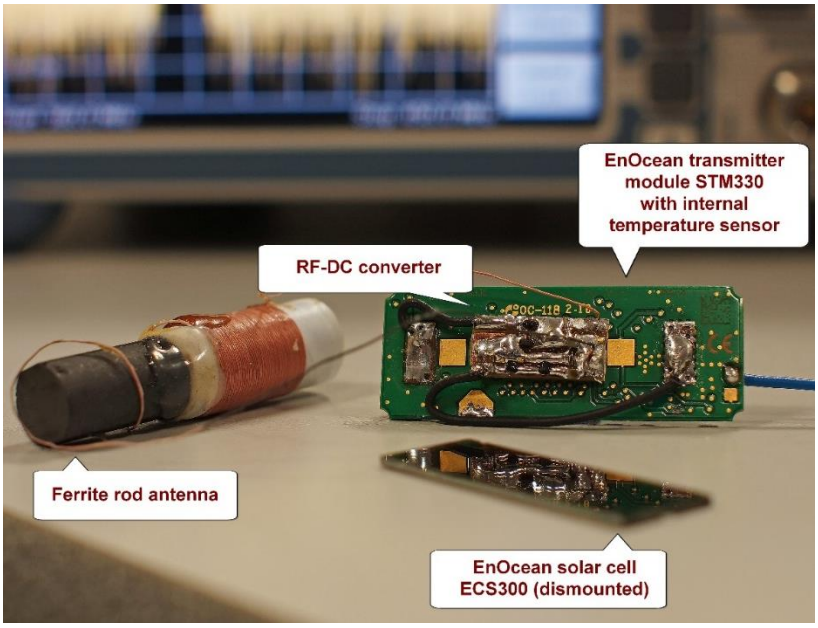

Figure 3.28 Wireless temperature sensor STM330 powered by a MW energy harvester.

The minimum voltage required for the proper functioning of the sensor was found to be 3V (in red), which according to Table VIII corresponds to a value of 1.06V of input voltage. Hence, the value used as minimum harvested voltage was 1.06V.

Table VIII The relation between the input to output voltages of the embedded DC-DC convertor.

Input voltage (V)	Charging Voltage (V)
1.2	**3.14**
1.06	**3.0**
0.9	**2.5**
0.7	**2.0**
0.5	**1.35**

The results of the simulations are illustrated in Figure 3.29 for three values of the harvested voltage simulated with Friis transmission equation.

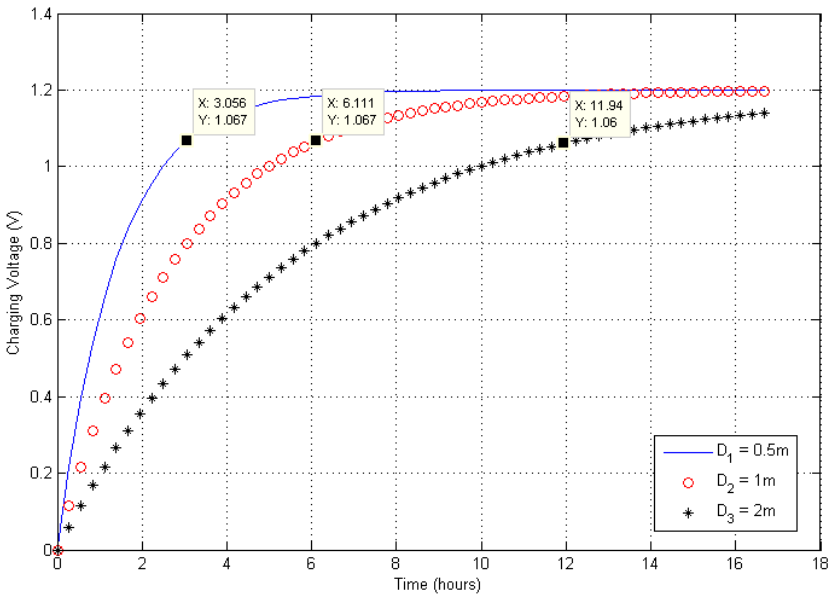

Figure 3.29 Charging time of modified STM 330 at three distances with TX power of 17dBm.

The results of the measurements are summarised in Table IX. The expected charging times, simulated previously in Matlab fully agree with the measured times and voltage levels demonstrated in Figure 3.30.

Table IX Timing statistics of EnOcean's Scavenger Transmitter STM 330

Event	from	to	Notes
1st charge	10pm (July 15th)	5pm (July 16th)	
TX on	10am (July 16th)		12 hrs after the 1st charge
2nd charge	9pm (July 19th)	9am (July 20th)	
3rd charge	10pm (July 23rd)	10am (July 24th)	
TX off		2pm (July 29th)	5 days after the last charge

The signal graph shown in Figure 3.30 represents graphically the results in Table IX. The experiment was conducted using TX power of 17dBm and the distance between transmitter antenna and the rectenna was fixed to 2m.

Figure 3.30 Signal strength of EnOcean's Scavenger Transmitter Module STM 330 powered wirelessly at 2m distance.

3.7. Summary

In some UHF/SHF power transmission schemes, directional antennas were suggested on the RF energy harvesting side to reduce the effect of increased distance but this technique is limiting the mobility of the devices, because of the size of the rectenna. Also, the portable rectennas do not have a fixed location or orientation. As it was demonstrated in this thesis, by using a MW RFEH system, the latter can easily be neglected firstly because the small size of the ferrite rod antenna, and secondly because of its uniform directivity. During the experiments conducted in a suburban environment, we had the opportunity to observe rectenna robustness to variety of electromagnetic disturbances and we haven't found anything to be worth it to be further investigated. Factors such as altitude were neglected during the trials, although the altitude information was part of the collected dataset. The maximum detected deviation in the altitude value was 125m between different measuring spots situated at the same distance from the transmitter, however, no influence to the RF density levels was detected.

Chapter 4 RF Energy Harvesting Antennas for SHF Operation

4.1. Introduction

The fast increase in the number of mobile devices and wireless communications nowadays, is influencing current requirements towards the size of the data exchanged wirelessly. In order to fulfil these challenges researchers are developing new spectrum and energy management solutions in the SHF bands. RFEH and spectrum sharing in the frequencies between 700 and 3000 MHz has become a favourite topic for researchers to solve the problems with the growing number of data users. The demand of low-profile directional antennas is not only justified by the growing number of such wireless networks, moreover, such antennas may be easily embedded in different structures, therefore improving the portability and mobility of a wide range of devices. Using wideband directional antennas for RFEH at microwave frequencies implies higher requirements towards their design parameters, such as high Front-to-Back (FB) ratio, unbalanced output, high efficiency, etc. Furthermore, achieving higher antenna gain, compared to the omnidirectional antennas, unidirectional antennas are delivering much higher incident power levels to the RF-DC conversion circuit, hence increasing its power conversion efficiency.

4.2. Printed microstrip antenna for harvesting energy from mobile phone base stations

Several antenna designs and their advantages and disadvantages have been investigated considering wideband directional antennas [112], [113]. Controlling the radiation pattern of such antennas may be achieved by changing the position of a dipole above a ground plane [114]. This gives the antenna designers flexibility to optimise particular parameters required by a RFEH application.

The concept of the Yagi-Uda antenna [115] is extensively used for designing end-fire antennas. Microstrip Yagi-Uda, or Quasi-Yagi structures have been

studied during the last three decades as a more suitable alternative for the microwave bands. Most of the known designs use coplanar configuration, i.e., the most of the elements of the antenna are printed on a single plane, except the reflector which is considered as a ground plane for the balun and impedance transformer [116] and [117].

In this Section, a novel multilayer design with a directivity vector perpendicular to the substrate plane was proposed [118]. The idea was presented at the 10th European Conference on Antennas and Propagation (EuCAP 2016). As shown from Figure 4.1, all the planes of the antenna are mounted around a double glazing window. A series of power density measurements were conducted in indoor environment, in order to investigate the availability of ambient RF energy in closed spaces such as offices and leaving rooms. The RF power density measured at the GSM bands around the windows, was proved to be much higher (in some cases >20dB) than anywhere else in the room and therefore the most suitable spot for an energy harvesting rectenna.

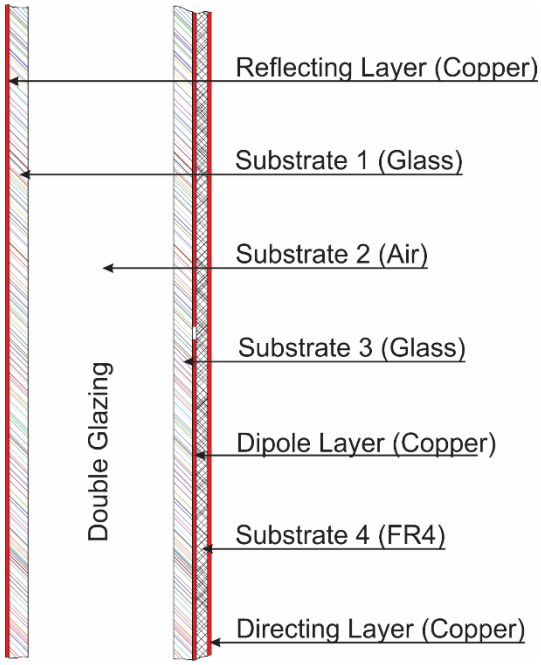

Figure 4.1 Cross-section of stacked microstrip antenna mounted on a window.

Microstrip dipoles have low radiation resistance and narrow bandwidth when used on thin substrates, compared to the patch antenna which becomes non-resonant on thick substrates [119]. However, the resonant element in the proposed antenna is mounted on a thick substrate i.e. double glazing, therefore the input resistance is no longer a limitation, and the achieved bandwidth would be sufficient for the requirements of a typical RFEH system.

4.3. Rectenna elements

Due to the complex structure of the proposed antenna, it is important to consider the relative permittivity (ε_r) of each layer. There are three different materials used as substrates in this antenna (Figure 4.1): substrates 1 and 3 are inner and outer glass of the double glazing with a permittivity of 5; substrate 2 is the air inside the window; substrate 4 is FR4 epoxy with ε_r of 4.4.

The initial parameters of this design were defined, firstly by the specific application, i.e. RF energy harvesting, and secondly, by the physical conditions of the medium, i.e. double glazing thickness, glass permittivity etc.

A copper layer of 35 μm thickness is employed on both sides of an FR4 epoxy board with 1.6 mm thickness (ε_r=4.4 and loss tan δ=0.0023). The top copper layer forms the first parasitic element (director) which is placed parallel to the driven element, and the ground which is covering only the balun, the microstrip impedance transformer (MIT), and the rectifier tracks (Figure 4.2).

The bottom copper layer consists of a driven half-wavelength dipole, coplanar stripline (CPS), balun, microstrip impedance transformer, and voltage multiplier. The third copper layer is placed on the inner glass and consists of a second parasitic element which acts as a reflector for the antenna.

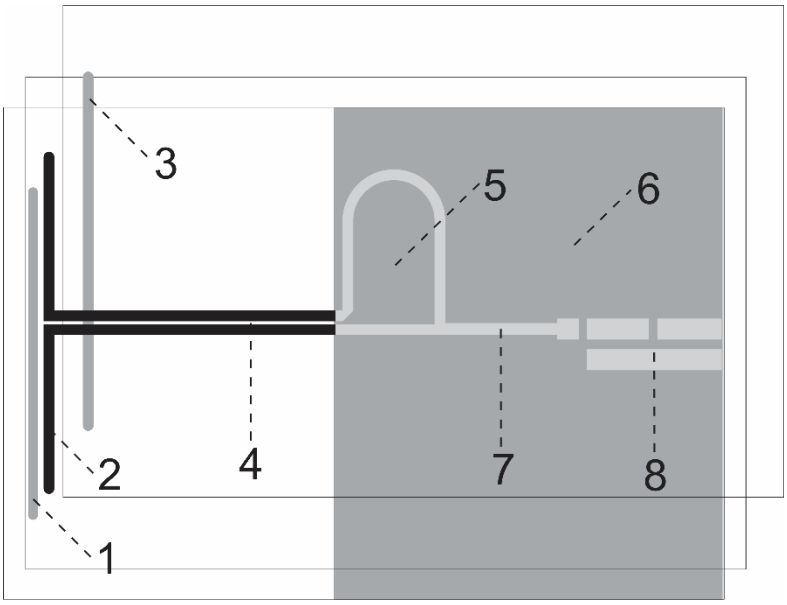

Figure 4.2 Antenna components:

1) director; 2) driven element; 3) reflector; 4) CPS; 5) balun; 6) ground plane (in grey); 7) λ/4 impedance transformer; 8) voltage multiplier tracks

The initial dimensions for the design were calculated based on [120] and [121]. As a result of further optimisation with HFSS, the design parameters are director element length (l_d), the director microstrip width (w_d), the dipole overall length (l), the dipole microstrip width (w), the reflector length (l_r), the reflector microstrip width (w_r), the separation (s), and the double glazing thickness (H_a). The dimensions are shown in Table X.

Table X Antenna dimensions (mm)

l_d	w_d	l	w	l_r	w_r	s	H_a	l_{CPS}	W_{CPS}
128	5	129.4	5	141	5	1	20	114	4

4.4. Transmission line

The transmission line of the proposed design consists of coplanar stripline (CPS), a microstrip-to-CPS transition (balun), and a quarter-wavelength impedance transformer.

4.4.1. Coplanar stripline

A λ/2 CPS structure was used as a parallel feed line. The effective permittivity was calculated as described in [122]:

$$\varepsilon_{eff} = 1 + \frac{\varepsilon_r - 1}{2} \frac{K(k')K(k_1)}{K(k)K(k_1')} \tag{25}$$

$$\mathrm{k} = \frac{s}{b} \tag{26}$$

where, K is the complete elliptic integral of the first kind, s is the distance between the strips, b is the CPS width, and

$$k' = \sqrt{1 - k^2} \tag{27}$$

$$k_1' = \sqrt{1 - k_1^2} \tag{28}$$

$$k_1 = \frac{sinh\left(\frac{\pi\, s}{4\, h}\right)}{sinh\left(\frac{\pi\, b}{4\, h}\right)} \tag{29}$$

For the half-wavelength CPS,

$$l = \frac{\lambda_g}{2} \tag{30}$$

where,

$$\lambda_g = \frac{\lambda_0}{\sqrt{\varepsilon_{eff}}} \tag{31}$$

The optimised CPS length (l_{cps}), and microstrip width (w_{cps}) are shown in Table X.

4.4.2. Balun

In order to connect a balanced source (dipole) to an unbalanced load (RF-DC convertor) and in this way to obtain maximum power transfer between the dipole and microstrip feed line, a transition from balanced line to unbalanced line is required (balun).

Several balun configurations were considered as suitable for the chosen frequency: tapered microstrip balun [123] , Marchand balun [124], and microstrip balun [116]. A microstrip-type balun is proposed as shown in Figure 4.3, because it has simple configuration and can be easily manufactured.

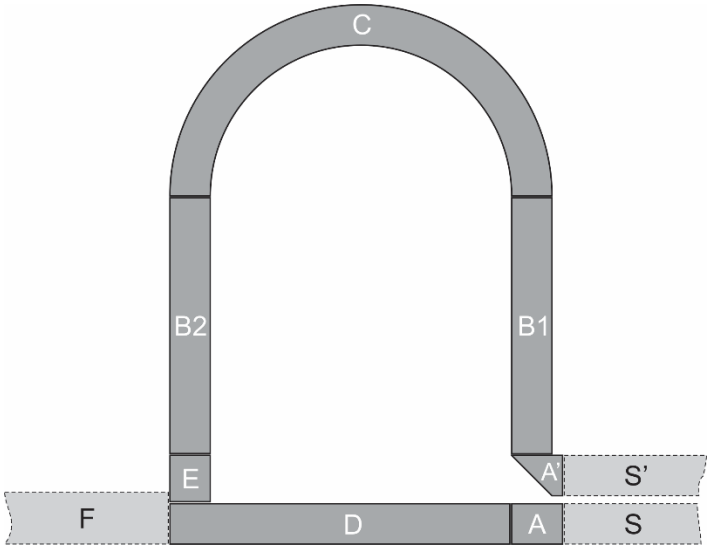

Figure 4.3 Balun diagram presenting its functional components

All the physical lengths of the balun parts are calculated using the length (L_D=44.3mm) and width (W_D=2.1) of sector D. These dimensions are calculated using (33) for a resistance of 62Ω. The rest of the dimensions are shown in Table XI, where L_A is the length of parts *A* and *A'*, L_B is the length of parts B_1 and B_2, L_C is the length of sector C with a diameter of L_D, L_E is the length of part *E*, and *s* is the gap given in Table X.

Table XI Physical dimensions of the balun components.

L_A	L_B	L_C	L_E
W_D*1.5	L_D*0.7146	$\pi L_D/2$	W_D+s

The results illustrated in Figure 4.4 and Figure 4.5, show good fulfilment of the initial requirement.

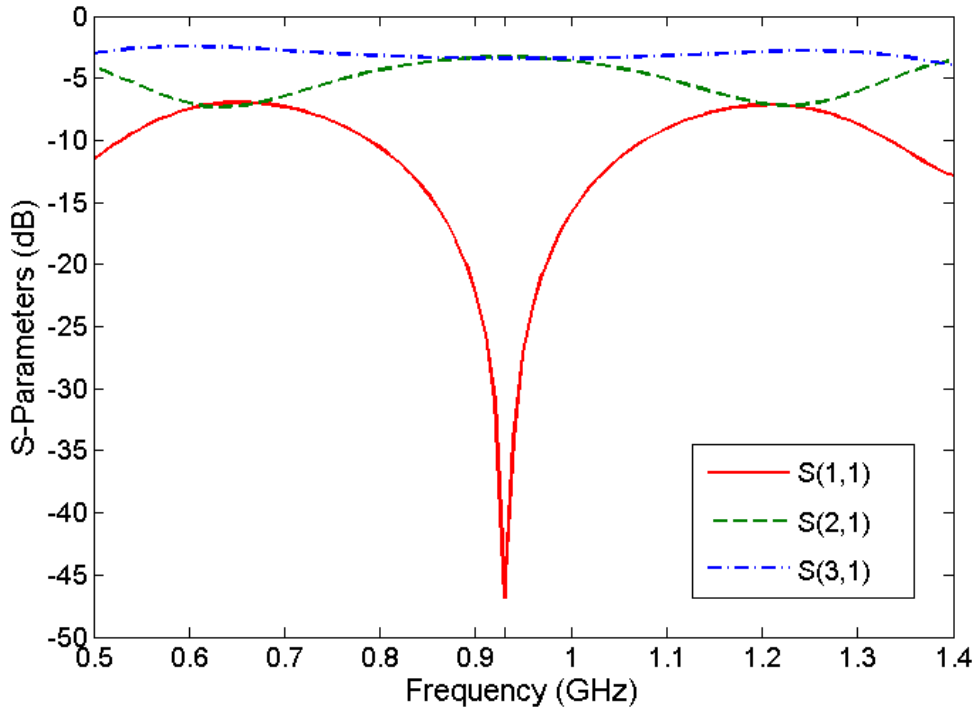

Figure 4.4 The main parameters of the balun, simulated using three ports configuration

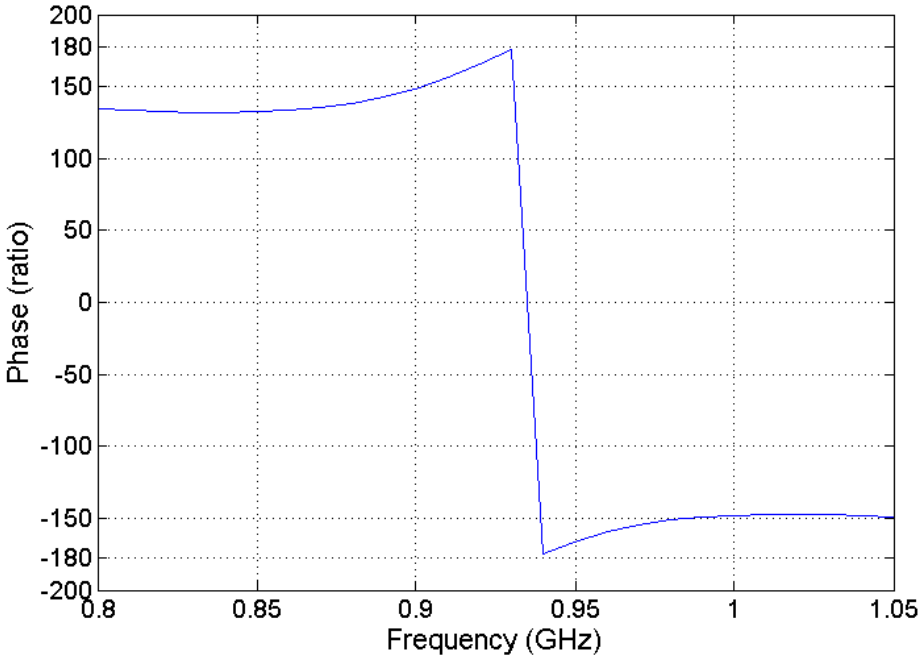

Figure 4.5 Balun phase ratio, simulated by using S_{11} parameter.

This balun can be used as an impedance transformer if the characteristic impedance (Z_C) is calculated to be different than the input impedance (Z_0) and output impedance (Z_L).

$$Z_C = \sqrt{Z_0 * Z_L} \quad ,\Omega \tag{32}$$

4.4.3. Impedance transformer

A quarter-wavelength impedance transformer is used as an additional impedance transition in order to maximise the power transfer between RF-DC conversion circuit and antenna. In this way voltage multipliers with a different input impedance may be used. An initial value of 50Ω for output resistance (Z_L) was chosen for easy measurement, however, the impedance (32) can be converted to a different value by calculating new dimensions for the λ/4 impedance transformer (33) used as an optional part of the feeding line [122]

$$Z_0 = \frac{120\pi}{\sqrt{\varepsilon_{eff}}\left[\frac{W}{H} + 1.393 + \frac{2}{3}\ln\left(\frac{W}{H} + 1.444\right)\right]} \quad (33)$$

where, *W* is the effective width of the microstrip line, and H is the effective height of the substrate, calculated with:

$$W = w + \frac{t}{\pi}\left[\ln\left(\frac{2h}{t}\right) + 1\right] \quad (34)$$

$$H = h - 2t \quad (35)$$

where, *w* is the physical microstrip width, *t* is the physical microstrip thickness, and *h* is the physical substrate height (thickness).

The effective permittivity ε_{eff} for $\frac{W}{H} \geq 1$ calculated with:

$$\varepsilon_{eff} = \frac{\varepsilon_r + 1}{2} + \frac{\varepsilon_r - 1}{2\sqrt{1 + 12\frac{H}{W}}} \quad (36)$$

The proposed antenna could be used in an array configuration by combining several antennas and choosing suitable impedance for the microstrip transformer. This would have the advantages of obtaining a higher gain without adding extra impedance transformers, and therefore higher array efficiency.

As shown in Figure 4.6, the usable frequency range of the proposed antenna is between 908.5 to 942.5MHz for VSWR<2 which fully satisfies the requirements of a RFEH system.

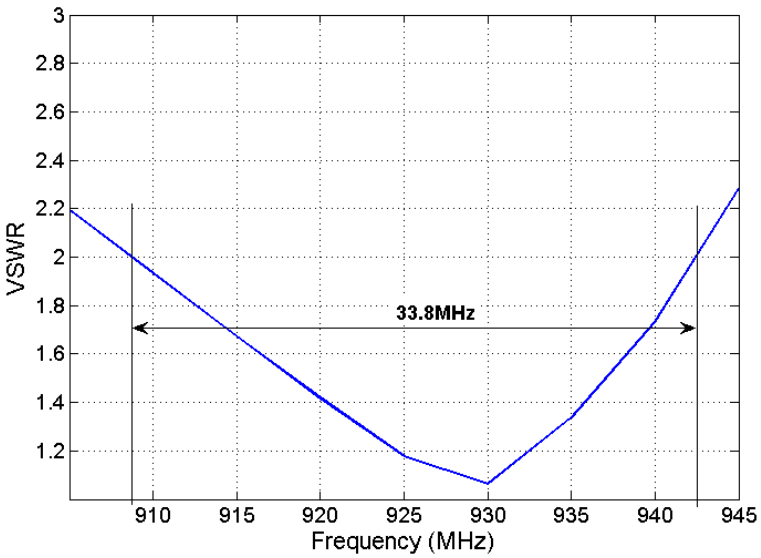

Figure 4.6 Simulated bandwidth of the antenna for VSWR less than 2:1.

In the H-plane, a radiation angle of more than 100° was achieved as shown in Figure 4.7, Figure 4.8. It is an important advantage for an energy harvesting antenna, used at locations where the direction to the source signal is not known and the antenna direction cannot be changed. If a higher gain is required, several vertically positioned antennas could be grouped in an array. In such configuration the radiation angle in the H-plane will not be affected.

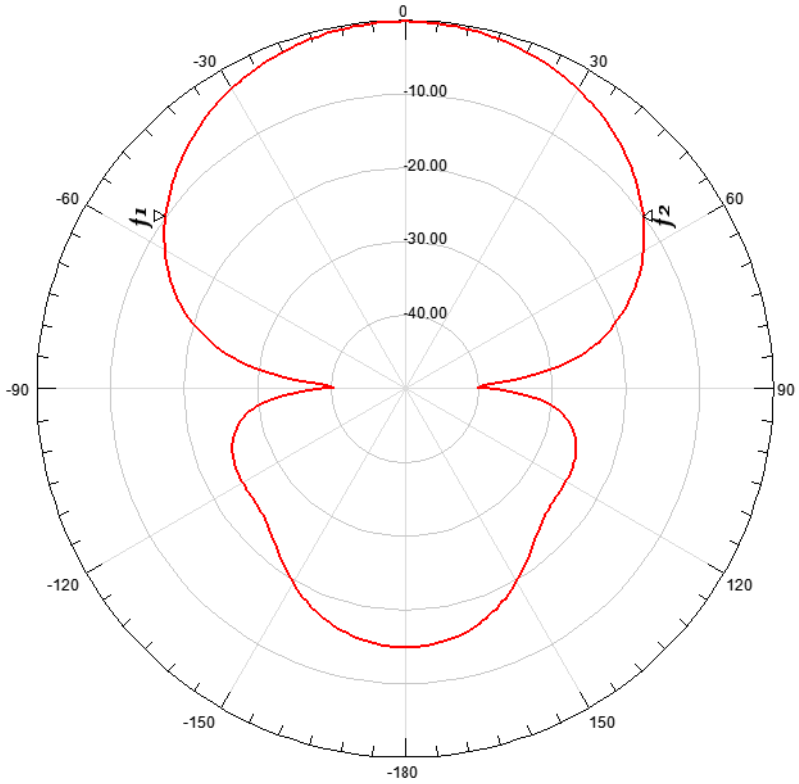

Figure 4.7 Simulated H-plane co-polarisation radiation pattern of the printed microstrip antenna at 930MHz.

Further improvements of the PMA can be made, such as, using transparent conductive foil for the antenna elements, calculating the same design parameters for other frequencies e.g. GSM1800 (1805-1880MHz), GSM 3G (2110-2170MHz), etc.

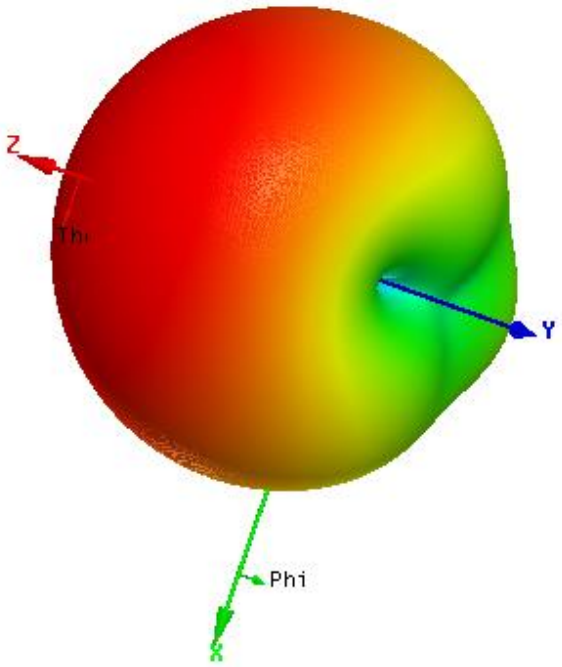

Figure 4.8 Simulated 3D radiation pattern of the PMA at 930MHz.

4.5. Summary

The analysis in this chapter exposed a variety of techniques deemed to be vital in providing maximum efficiency of proposed antenna designs for RFEH applications at SHF bands. It was the aim to analyse different design specific issues in order the most suitable design approaches to be proposed, towards a real life design example for an SHF frequency band.

In order to test the performance of the proposed antenna, several RF-DC configurations were measured and the results are shown in Table XII. All the multipliers used Schottky diode - SMS7621. A DC-DC voltage step-up converter (LTC3108) was used as a load. In this way we minimised the influence of the load parameters on the multiplier input impedance. In such configuration the complex impedance depends only on the frequency and input power level (discussed in details in Section 5.7). A voltage quadrupler was used for this experiment, because

of the higher voltage provided, compared to a single doubler. As shown in Table XII, the complex impedance for the anticipated incident power levels, i.e. -20dBm is 20+j4.3. The impedance mismatch would be minimised by choosing suitable characteristic impedance (Z_0) for the quarter-wavelength impedance transformer using (32).

Table XII Input impedances of voltage multipliers measured for three power levels at 930 Mhz

RF-DC type	Input Power (dBm)	Input Impedance (Ω)	
		Resistance (R_a)	***Reactance (X_a)***
Voltage doubler	-20	9.5	-j14
	-10	30	-j17
	-3	59	-j26
Voltage quadrupler	-20	20	j4.3
	-10	41.5	-j6.7
	-3	65	-j27

Table XIII summarises the main parameters of different broadband rectenna solutions for the SHF bands, comparing them to the performance of the proposed rectenna.

Table XIII Comparison of similar RF rectenna

Reference	Frequency (MHz)	Input Power (dBm)	Antenna Gain (dBi)	Dimensions (mm)	Efficiency (%)
[125]	1800-2500	-30 to -10	4	70 x 70 x 13.2	57
[126]	2200-2600	10 to 18	10	135 x 93 x 22	72.5
[61]	2300-2500	-20 to -10	4.5	90 x 90 x 10	50
[127]	850-1940	2.7 to 7.2	2	130 x 130 x 1.5	60.4
This work	908-943	-17 to 7	8.3	210 x 141 x 22	65

During the simulations, a Bow-tie antenna was found to be a good candidate for similar rectenna design. Moreover, compared to the dipole used as driven element for the proposed rectenna, a Bow-tie type driven element would have a wider frequency bandwidth, hence easier practical implementation.

Chapter 5 RF-to-DC Conversion and Impedance Matching

5.1. Introduction

RF-DC conversion, has long been investigated for low frequency operation (AC-DC). In its simplest form, a series diode may be used to deliver the half of the alternating current to Resistance-Capacitance (RC) circuit where only the DC component appears across the load terminals, and the alternating content is filtered. Such a half-wave rectifying circuit is limited to 50% AC-to-DC power conversion for an ideal diode. At microwave frequencies, the rectifier circuit must be looked at as a resonant circuit, containing a nonlinear element which traps modes of the fundamental frequency and its harmonics. If the circuit is matched at each frequency, the rectifier acts as a full-wave rectifier.

Figure 5.1 RF Energy Harvester system block diagram

The diode (presented as a nonlinear device) is creating dc bias, in addition to harmonics in the resonant circuit. This can be extracted without any impact on the resonant circuit's RF characteristics. The relationship between the time varying current and voltage at the diode's physical point in the resonant circuit defines the overall RF-DC efficiency. In theory, if the cavity is high-Q for the main frequency and harmonics, the RF-DC efficiency can approach 100%. If the RF circuit is well designed, the losses can be limited to the forward voltage, reverse breakdown voltage, and series resistance of the diode.

The main goal of this chapter is to assess a number of rectification modes considering their high and/or optimal RF-DC power conversion efficiency for variety of diodes at different frequencies.

5.3. Rectifier efficiency

A diode connected to the antenna output is a popular solution for RF-DC power conversion for RFEH. To rectify the most of the incident power received by the antenna, high RF-DC power conversion efficiency rectifying circuitry is needed. There are several factors which may have a high impact on the efficiency, such as load resistance selection, diode type, ability to suppress harmonics, and junction frequency characteristics. A diode that achieves its highest efficiency at relatively high input power levels does not have the same properties at lower power levels, e.g. -20dBm.

The RF-DC power conversion efficiency for a Villard voltage multiplier (explained in Section 5.6.1.) versus the input power was measured with two different diodes and the result is shown in Figure 5.2.

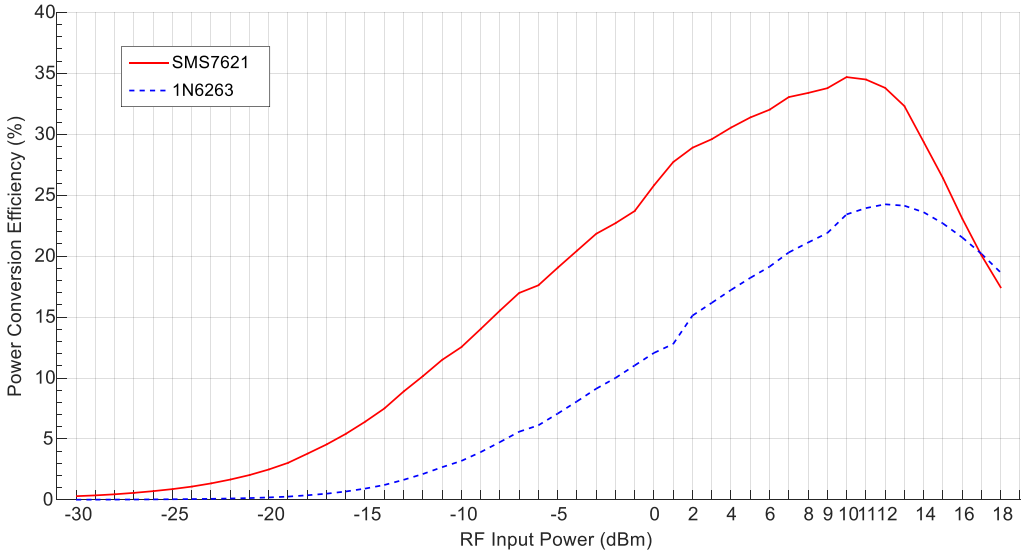

Figure 5.2 Measured power conversion efficiency for two types of diodes as a function of RF input power at 1MHz

In order to achieve the maximum possible power conversion efficiency of a RFEH system, it requires the load impedance to be matched to the source impedance of the RF-DC conversion circuit [128]. A rectifier may be considered as

a resistive and capacitive circuit (RC). The diodes' aspect ratio and the number of stages will have impact on its impedance. Although high output voltage will be achieved when used with a higher load resistance value, it does not mean that maximum power cannot be reached when smaller load is used.

The RF-DC conversion efficiency may be defined as relation of total input power to the total DC output power delivered to a load, R_L:

$$\eta_{RF-DC} = \frac{P_{RF(in)}}{V_{DC}^2/R_L} \tag{37}$$

where, η_{RF-DC} is RF-DC power conversion efficiency, $P_{RF(in)}$ is the input RF power, and the DC power dissipated in a DC load R_L is $P_{DC(out)} = V_{DC}^2/R_L$. This calculation should be conducted for each frequency in the chosen range for a particular RFEH system. However, the values of DC power level obtained in this way cannot be summed in order to calculate multi-frequency efficiency, because such a process is nonlinear. Therefore, if multi-frequency or broadband modes are required, the same characterisation needs to be conducted but in this case the actual power density of all the spectrum and the incident power levels should be included.

There are three main sources of loss in a rectifier: reflected power at the fundamental, I^2/R dissipation in the diode and power lost in the harmonics generated by the diode. If conversion efficiency is calculated without taking into account, the reflected power of the fundamental, the result will not show the efficiency of the entire circuit, and only the diode efficiency:

$$\eta_{RF-DC} = \frac{P_{RF(in)} - P_{RF(refl)}}{P_{DC(out)}} \tag{38}$$

where, η_{RF-DC} is RF-DC conversion efficiency, $P_{RF(refl)}$ is the reflected power, and $P_{DC(out)}$ is the total DC output power delivered to a load.

5.4. Diode modelling

The diode is the most important component of the rectifying circuit. The diode is generating harmonic signals, because of its nonlinear characteristics, which can drastically reduce the conversion efficiency of the RFEH system [129]. Furthermore, such signals could affect the working mode of the load.

The classical diode used in low frequency applications, usually has a relatively high value of junction capacitance, which limits its applications for high frequencies. Figure 5.3 demonstrates the effect of the diode on the conversion efficiency, when used at 0.9MHz, 2MHz, and 100MHz.

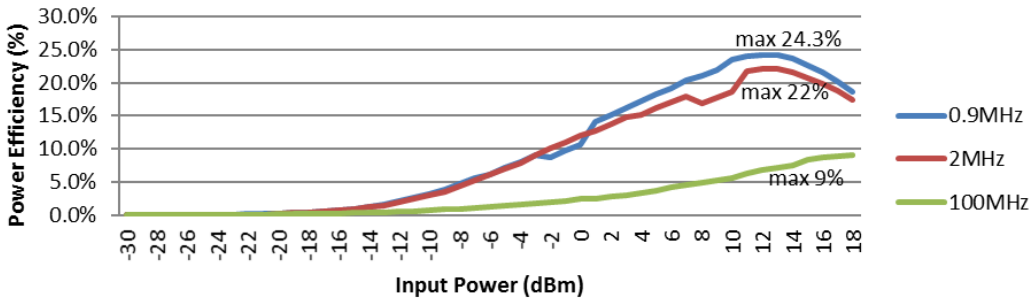

Figure 5.3 Power efficiency of a voltage multiplier with 1N6263 measured for P_{in} -30 to 18dBm at three different frequencies.

The Schottky type diode, however, has a much lower value of junction capacitance, because of its semiconductor-metal type of junction. This feature makes it the most suitable choice for high frequency rectification applications.

The most attractive features of the Schottky barrier diode are very fast switching and low substrate losses. The model of the Schottky diode (Figure 5.4) consists of several parts: junction capacitance C_J, substrate resistance R_S, assuming that they have a linear voltage-current relation, and a junction resistance R_J, with nonlinear characteristics. The has a voltage-current characteristic is defined by [129]:

$$i_D = I_S(e^{\alpha \upsilon_D} - 1) \tag{39}$$

where, i_D is the current through the nonlinear diode, υ_D is the voltage over the nonlinear diode, I_S is the saturation current and α is s the reciprocal of the thermal voltage, given by:

$$\alpha = q/nkT \tag{40}$$

where, n is the diode ideality factor, T is the temperature in Kelvin, and q is the charge of an electron.

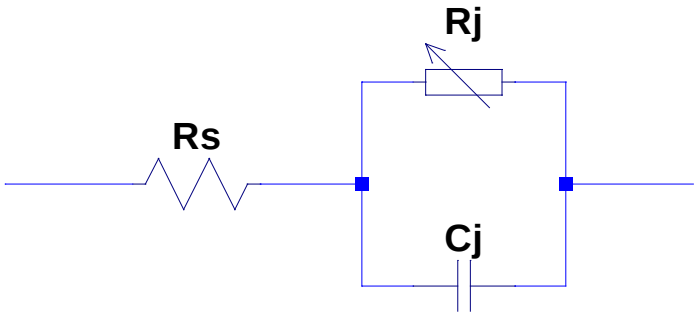

Figure 5.4 Linear circuit model of the Schottky diode

The admittance Y_z of the linear model shown in Figure 5.4, can be presented as:

$$Y_z = Y_{C_j} + Y_{R_j} \tag{41}$$

Considering the working frequency Y_z, it may be given as:

$$Y_z = j\omega C_j + \frac{1}{R_j} = \frac{j\omega C_j R_j + 1}{R_j} = \tag{42}$$

The linear model has an impedance Z which is:

$$Z = \frac{R_j}{1 + j\omega C_j R_j} \tag{43}$$

Therefore, the total impedance Z_T is:

$$Z_T = R_s + \frac{R_j}{1 + j\omega C_j R_j} \tag{44}$$

Where, R_j is the junction resistance, described with (39) and In (44), and R_s is the series resistance of the circuit, R_j and C_j are constants and the working frequency (ω) is the only variable parameter. As the frequency increases, the Z_T value will become much lower compared to the diode's series resistance R_s. Therefore, it is operating independently of its working frequency. However, diodes with lower values of and R_S and C_j should always have advantages when selected for high frequency energy harvesting applications. Relatively high values of C_j, e.g. around 1 pF, reduce the diode Z_T together with its switching speed. Moreover, R_S consumes ohmic power, hence diodes with low series resistance should be considered. The main reason for their low power conversion efficiency at lower incident levels (lower than -10dBm) compared to their good sensitivity at higher voltages, is the low impedance value Z_T. At lower input power levels, the diode voltage losses V_j are increased, because of the increased higher current values through the diode.

The modelling parameters for Schottky diodes are described by the diode manufacturers in their data sheets. When using simulation software such as Multisim, LT Spice, ADS etc., these parameters are used for modelling purposes. The modelling is a process of converting the diode into an equivalent circuit using passive elements defined by the SPICE model parameters. Examples for Spice parameters are shown in Table XIV for three types of Schottky diodes – SMS7621, SMS7630 and HSMS-285x.

Table XIV SPICE parameters of three types of Schottky diodes

Parameter	Units	SMS7621 Series	SMS7630 Series	HSMS-285x
I_S	A	$4E^{-7}$	$5E^{-5}$	$3E^{-6}$
R_S	Ohm	12.00	20.00	25
N	-	1.1	1.1	1.06
C_{j0}	PF	0.1	0.1	0.18
M	-	0.4	0.4	0.5
E_G	eV	0.7	0.7	0.69
XTI	-	2.00	2.00	2
B_V	V	3.00	2.00	3.8
I_{BV}	A	$3E^{-5}$	$3E^{-4}$	$3E^{-4}$
V_J	V	0.5	0.3	0.35

By simulation in LT Spice the performance of a few selected Schottky diodes (HSMS-2850, HSMS-2860, 1N6263, and SMS7630) were compared. Also, the efficiency of 1N6362 and SMS7630 Schottky diodes was measured at three different frequencies (0.9, 2, and 100MHz). An example with 1N6263 is shown in Figure 5.3. A conclusion was made that the impact of the Schottky diode's junction bias resistance (R_j) and junction capacitance (C_j) and on the RF-DC power conversion efficiency is negligible on the MW frequencies. Nevertheless, at UHF and SHF bands, different approaches for rectifying circuit loading and suppressing the Schottky diode's harmonics should be investigated for achieving the maximum efficiency available.

5.5. Special modes of RF-to-DC conversion

Class-E behaviour was first introduced by Sokal et al. in 1975 [130]. The idea was presented in an amplifier context. The theory was later on modified [131] for rectifiers to be used in high-efficiency DC-DC converters. The frequency of operation, in both cases, was around 1 MHz. In 1995, Mader et al. [132] developed a new theory for class E transmission line amplifier at microwave frequencies, together with equations estimating the approximate power and efficiency for class-E amplifiers.

5.5.1. Class-E rectification

The development of the Class-E rectifier theory begins with the assumptions that 100% RF-to-DC efficiency can be achieved with an ideal switch in parallel with a linear capacitance, C_s. This corresponds to the nonlinear resistor, R_j , and the junction capacitance, C_j , in the diode (Figure 5.4). The AC voltage that controls the switch is assumed to generate a 50% duty cycle. During the open cycle of the switch, C_s stores energy which is partially dissipated in the switch during the closed cycle if there is any resistance in the closed switch (Figure 5.5). The output impedance of the switch is then set to present impedances at the fundamental and harmonics that will force C_s to dissipate all its stored energy before the switch closes.

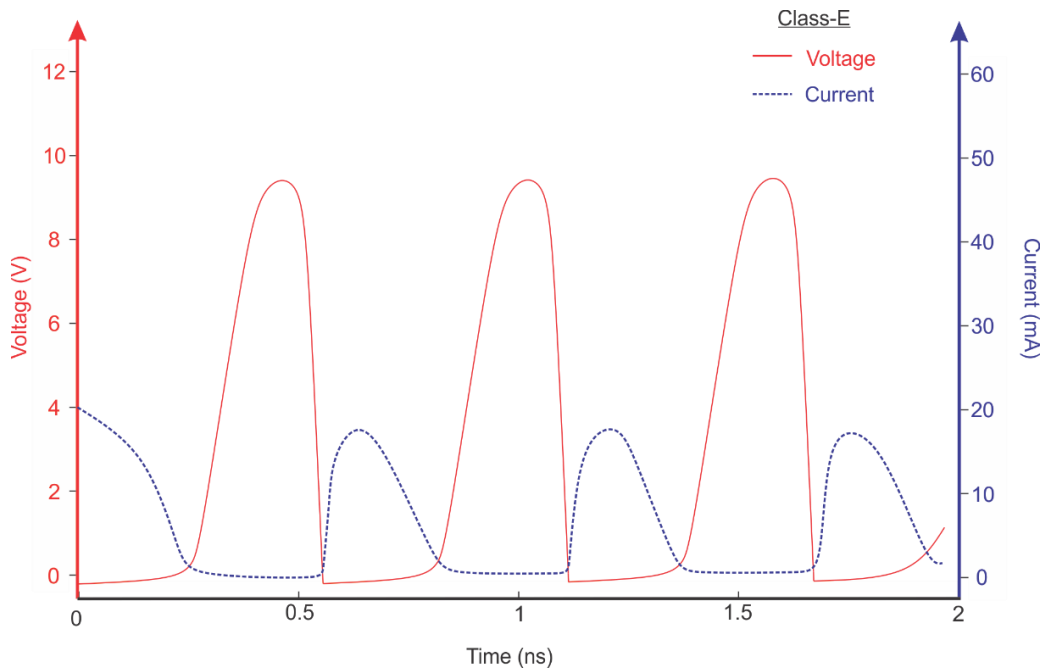

Figure 5.5 Class-E waveforms appearing at across the idealised exponential switch

Additional assumptions about the instantaneous switch voltage and slope of the voltage at the moments of switching serve as initial conditions for the circuit equations which determine the following impedances to be seen by the diode:

DC $$R_L = \frac{V_s}{I_s} = \frac{1}{\pi \omega_s C_s} \quad (45)$$

f_{fund} $$Z_{net} = \frac{\upsilon_s}{i_s} = \frac{0.28}{\omega_s C_s} e^{j49^\circ} \quad (46)$$

f_{harm} $$Z_{harm} = \frac{\upsilon_s}{0} = \infty \quad (47)$$

The way of implementing the Class-E impedance at the fundamental is to transform the source impedance to this value. The harmonic impedances are created by using open circuited transmission lines of appropriate length and distance from the diode. In practice, only the second and third harmonic are terminated with an open circuit. The limitations of using a finite number of harmonics in Class-E has been addressed in [133]. The DC load resistance is RF-decoupled from the circuit using a bias network.

Equation (47) must be solved for using $V_{DC} I_{DC} = P_{in}$ for 100% efficiency, in order to find V_{DC}, I_{DC} $\upsilon(t)_{max}$ and $i(t)_{max}$. This first order approximation of the Class-E impedances will have limitations for large signal operation and alternative design methods are discussed and proposed later in this chapter.

5.5.2. Class-F rectification

Class-F theory has been developed in a less extensive manner than Class-E for RF transmission line circuits. The main aspect of Class-F behaviour is the wave-shaping accomplished by the harmonic terminations. Even harmonics are

terminated with an open circuit, odd harmonics with a short circuit such that the switch voltage achieves a square wave form. The determination of the fundamental impedance is designed for maximal power transfer to the load in an amplifier aspect. It has been shown that a real impedance equal to $2V_{ds}/I_{dss}$ can be used for the fundamental impedance. However, like the Class-E impedances, the optimal fundamental impedance for Class-F will be better found using nonlinear simulation techniques rather than first order approximations.

5.6. Voltage multipliers

Considering the efficiency η as defined in (37), where the output DC power $P_{DC(out)}$ is presented as V_{DC}^2/R_L and $P_{RF(in)}$ is the incident RF power, then γ (voltage sensitivity) may be presented by (48), where V_{DC} is the DC voltage present at the output terminals.

$$\gamma = \frac{V_{DC}}{P_{RF(in)}} \tag{48}$$

The current requirement of the low power sensors towards their DC voltage supplies is less than 1V and about 10 µA of DC current. Therefore, there is a need for different requirements to be defined for the output voltage and current, rather than using the overall DC output power value, if RF energy harvesters are considered for low power sensors and autonomous systems [134]. The incident RF power $P_{RF(in)}$ from the RFEH antenna is converted to at least the minimum voltage needed to provide enough power to the sensor. A RFEH can be capable of delivering output DC power higher than what is needed by the remote sensor, however, it may be unable to energise the sensor due to its specific voltage and/or current requirements. Therefore, in some cases the voltage sensitivity of a RFEH system may be preferred instead of maximising the output efficiency when

powering up autonomous systems from ambient RF power. In the current state-of-the-art in the RFEH for low power autonomous systems there are various voltage multiplier circuit topologies.

5.6.1. Villard voltage doubler

The voltage doubler circuit is essentially composed of two sections. The first section is a voltage peak detector circuit composed of C_1 and D_2 as shown in Figure 5.6. Assuming ideal diodes, when this circuit is excited by a sinusoid of amplitude V_p, it provides a voltage waveform similar to the input but shifted up by V_p across diode D_2. While the negative peaks are clamped to 0 V, the positive peaks reach 2Vp. The second section is a peak rectifier circuit that is formed by *D1* and *C2*. In response to the voltage across the first diode, this circuit provides a DC voltage of magnitude $2V_p$ across capacitor C_2. Since in the ideal case the output voltage is double the input voltage amplitude, the circuit is called voltage doubler [135].

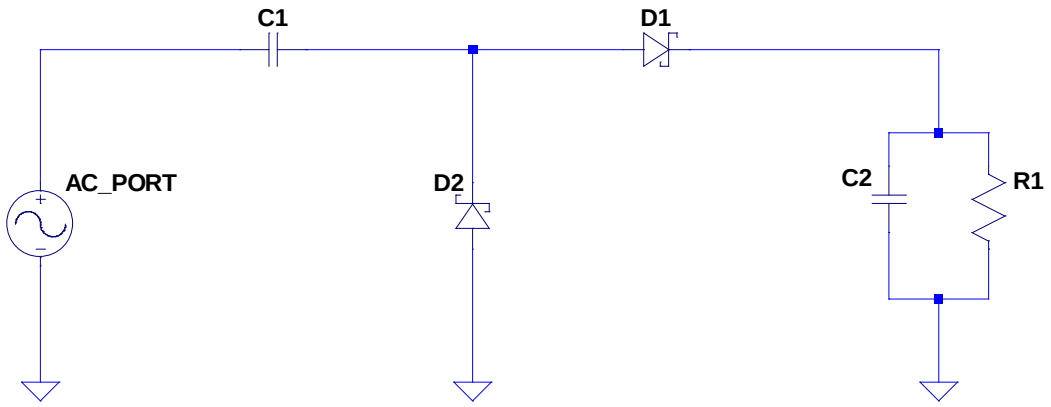

Figure 5.6 Basic configuration of a voltage doubler circuit.

In the ideal operation, during the negative half cycle of the input voltage V_p, diode D_2 will be forward biased, while diode D_1 is off. Thus all the voltage drops across capacitor C_1 and charges it up to the peak amplitude of the input signal. During the positive half cycles D_1 is forward biased while D_2 is reverse biased and

therefore will not conduct current. Hence both the source voltage and the voltage stored on C_1 drop across C_2 charging it up to a DC value equal to two times the input signal amplitude [136].

In order to provide higher output voltages, multiple stages of the basic doubler circuit can be cascaded. As shown in Figure 5.7, the output of each stage provides the DC input of the next stage, while the direct coupling from the source provides the AC input for each stage. Despite achieving higher output voltage, the increase in number of stages degrades conversion efficiency due to increase in power dissipation. The trade-offs involved in cascading voltage doubler stages have been previously studied in [47] and [137].

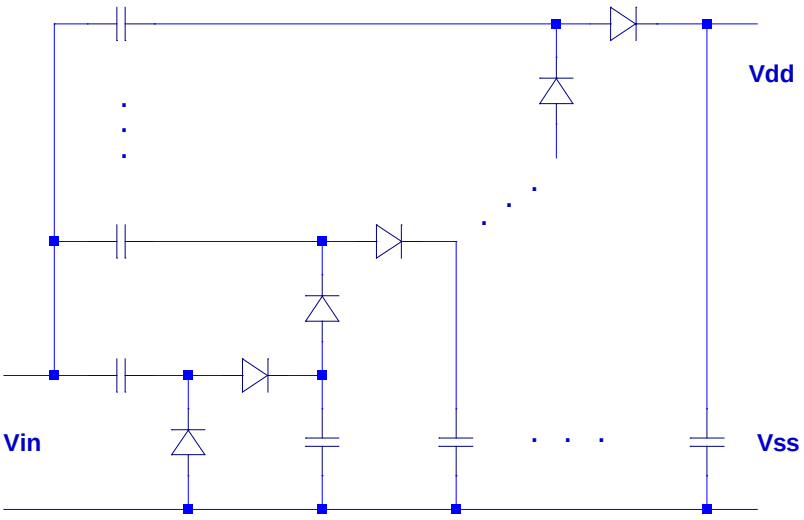

Figure 5.7 N-stage voltage multiplier

Output voltage and RF-DC power conversion efficiency are the two primary performance parameters of an RF energy harvesting conversion circuit. A straightforward DC steady-state analysis of the doubler circuit with real identical diodes yields the following expression for the output voltage [138], [139]:

$$V_{out} = 2n(V_{in} - V_d) \tag{49}$$

where V_{in} is the amplitude of the input RF signal, n is the number of stages, and V_d is the voltage drop across each rectifying element. For the case of ideal diodes with no threshold voltage, (49) simplifies to $V_{out} = 2nV_{in}$ as expected.

In addition to the number of stages, other parameters such as effectiveness of power matching, the width of the diode-connected transistors, and load impedance, have impact on the power conversion efficiency in an RF harvester.

5.6.2. Single-stage voltage multiplier

In Figure 5.8 the input voltage is a sinusoidal signal $V_{in}(t)$ with amplitude $\overline{V}_{in}$ and angular frequency ω_0. Denoting the current through diode D_1 by $i_1(t)$ and the current through $D2$ by $i_2(t)$, time domain analysis based on conservation of charge yields their relation to the output DC current I_{out}.

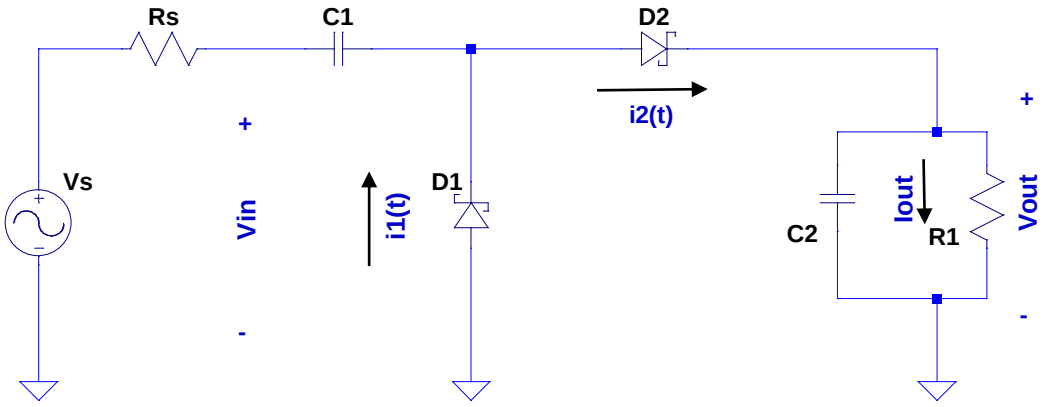

Figure 5.8 Single stage voltage doubler circuit indicating the current flows

Assuming that the ideal diodes conduct only during half the input voltage cycle when forward biased, then:

$$\int_0^{T/2} i_2(t)dt = \int_0^{T/2} i_{C_2}(t)dt + \int_0^{T/2} I_{out}dt \tag{50}$$

$$\int_{T/2}^{T} i_2(t)dt = \int_{T/2}^{T} i_{C_2}(t)dt + \int_{T/2}^{T} I_{out}dt = 0 \tag{51}$$

In the steady state the amount of charge drawn off by the load from the capacitor during negative half cycles is compensated by the equal amount of charge provided from diode D_2 during positive half cycles, the total current through C_2 sums up to zero. Also, since there is no change in the DC voltage across the load, output current is constant. Thus adding the two equalities yields:

$$\int_0^{T} i_2(t)dt = I_{out}T \tag{52}$$

$$\frac{1}{T}\int_0^{T} i_2(t)dt = I_{out} \tag{53}$$

where for simplicity the integration limit for $i_2(t)$ is extended to the entire cycle, even though it is not zero only during half the period. All the current that passes through D_2 is provided by capacitor C_1 since diode D_1 is reverse biased during this time. In the negative half cycle of the input voltage, D_1 must supply all the charge required by C_1 to recharge C_2 during the positive swing. A similar analysis is presented in [140]. As a result:

$$\int_0^{T} i_1(t)dt = I_{out}T \tag{54}$$

$$\frac{1}{T}\int_0^{T} i_1(t)dt = I_{out} \tag{55}$$

As shown by (53) and (55), the output DC current is equal to the average current through each diode during one period. If ideal rectifying diodes are replaced with diode-connected MOSFETs, then the integration limits in these equations must be refined to account for the forward-biased region of operation. This result may be used in the to obtain the characteristic DC equation and the equivalent resistance of the voltage doubler circuit.

Kirchhoff's law is applied to the two loops formed during each swing of the input voltage to obtain the steady state voltage across each diode (Figure 5.9). In the ideal case where the diodes have zero threshold voltage, the DC voltage across the first capacitor is the peak input voltage amplitude $\overline{V}_{in}$ and the voltage across the load capacitor is $2\overline{V}_{in}$.

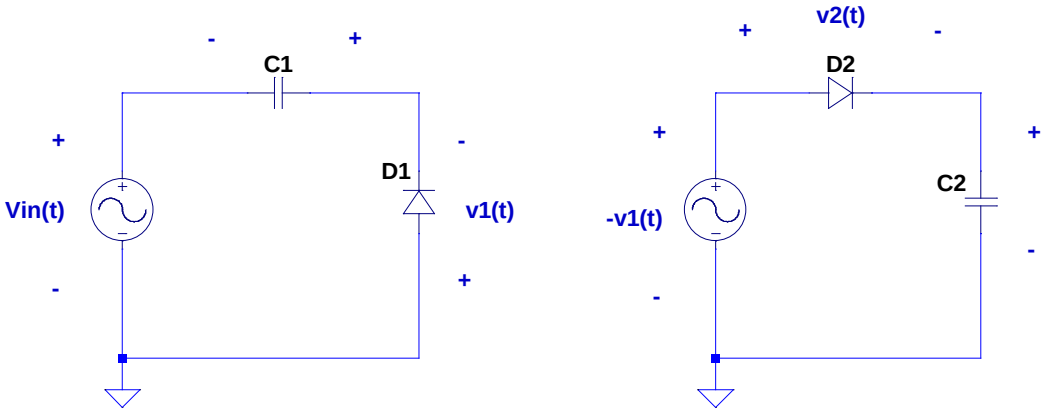

Figure 5.9 Voltage multiplier circuit during negative voltage swing (left) and positive voltage swing (right)

Denoting the voltage across D_1 and D_2 by $v_1(t)$ and $v_2(t)$ respectively, for the negative half cycle it can be expressed as:

$$v_1(t) = -V_{in}(t) - V_{C_1} \tag{56}$$

$$v_1(t) = -V_{in}(t) - \overline{V}_{in} \tag{57}$$

For the positive half cycle by considering $v_1(t)$ as the new source for the circuit:

$$v_2(t) = -v_1(t) - V_{C_2} \tag{58}$$

$$v_2(t) = V_{in}(t) + \overline{V}_{in} - 2\overline{V}_{in} \tag{59}$$

$$v_2(t) = V_{in}(t) + \overline{V}_{in} \tag{60}$$

Therefore, (57) and (60) represent voltages across diodes neglecting the drops due to threshold voltage. However, in the real case the output voltage does not reach twice the input voltage peak. In this case the voltage across each diode is shifted down (based on the polarity chosen) by a value less than $\overline{V}_{in}$ (correspondingly the first capacitor charges up to a voltage less than $\overline{V}_{in}$). In general, the second term in the right-hand side of (57) and (60) can be replaced by $V_{out}/2$, which reduces to the ideal case value $\overline{V}_{in}$ when output voltage is twice the input amplitude.

5.6.3. Multi-stage voltage multiplier

Similar analysis can be applied to an N-stage voltage multiplier (Figure 5.7). A voltage quadrupler, which is a special case of such a multiplier, is shown in Figure 5.10

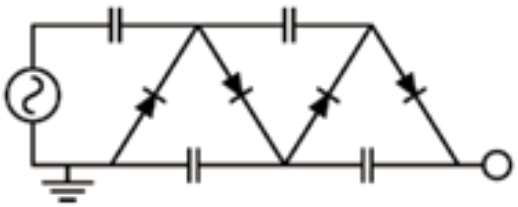

Figure 5.10 Schematic diagram of voltage quadrupler

A different, but equally valid analysis by studying the DC and AC operation of the circuit can also be employed. In the DC analysis, by considering all the coupling capacitors as open circuit, all diodes are in series, and thus the DC voltage on each diode is:

$$\overline{V}_D = \frac{V_{out}}{2N} \tag{61}$$

In the AC analysis, all the coupling capacitors are considered as short and thus the input sinusoidal voltage $\overline{V}_{in} = \cos(\omega_0 t)$ drops across each diode. Therefore, the total voltage across each diode is the sum of the DC and AC voltages:

$$v_d(t) = \pm\overline{V}_{in}\cos(\omega_0 t) - \frac{V_{out}}{2N} \tag{62}$$

where the minus sign applies to diodes with an odd subscript the plus sign applies to diodes with an even subscript. This equation (62) can be used for calculating the equivalent resistance of the voltage multiplier circuit.

One of the prototypes designed for 433MHz EH is shown in Figure 5.11. A quadrupler was used as the RF-DC convertor, so the harvested voltage was multiplied by four times in order to provide enough voltage for the LED for demonstration purposes. A 2W transmitter was used as a dedicated RF energy source at 433MHz ISM band at a distance of 5m. The goal of this experiment was twofold – firstly, to demonstrate the concept of remotely powering a low power device using UHF RF energy source, and secondly, to compare several antenna

types, hence demonstrating to what extent the antenna efficiency is influencing the overall system performance.

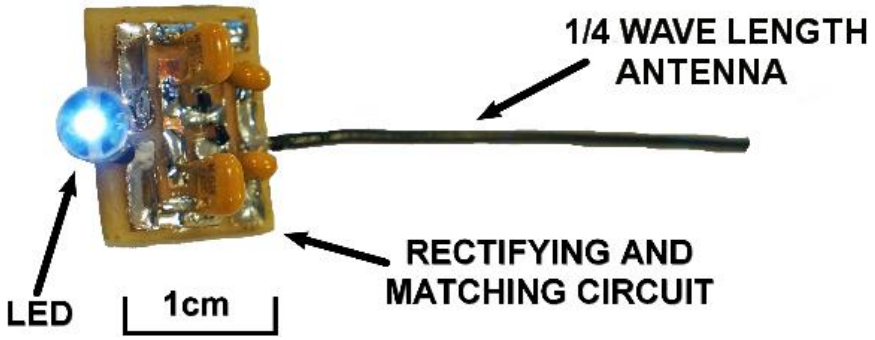

Figure 5.11 A prototype rectenna powering an LED at a distance of 3 wave lengths of a dedicated RF energy source on 433MHz.

5.7. RF energy transfer optimisation

Because of the specific characteristics of the diode, the impedance of the rectifying circuit is influenced by the input power level, the frequency of operation, and the load. In order to define the way these parameters depend on each other, we designed a series of experiments to prioritise each of the parameter's and define their importance for the power efficiency of the RFEH system.

The measurement set-up for the RF-DC impedance and efficiency is shown in Figure 5.12. The source is a signal generator (model R&S® SMC100A) connected to the RF-DC convertor under test, allowing power efficiency measurements to be performed for a range of input power levels and load resistance values. The RF-DC convertor is a standard 2-stage Villard voltage doubler (SMS7621 Schottky diode) and the output DC is measured by the oscilloscope and checked by a thermal μPower Sensor (model R&S® NRP-Z51).

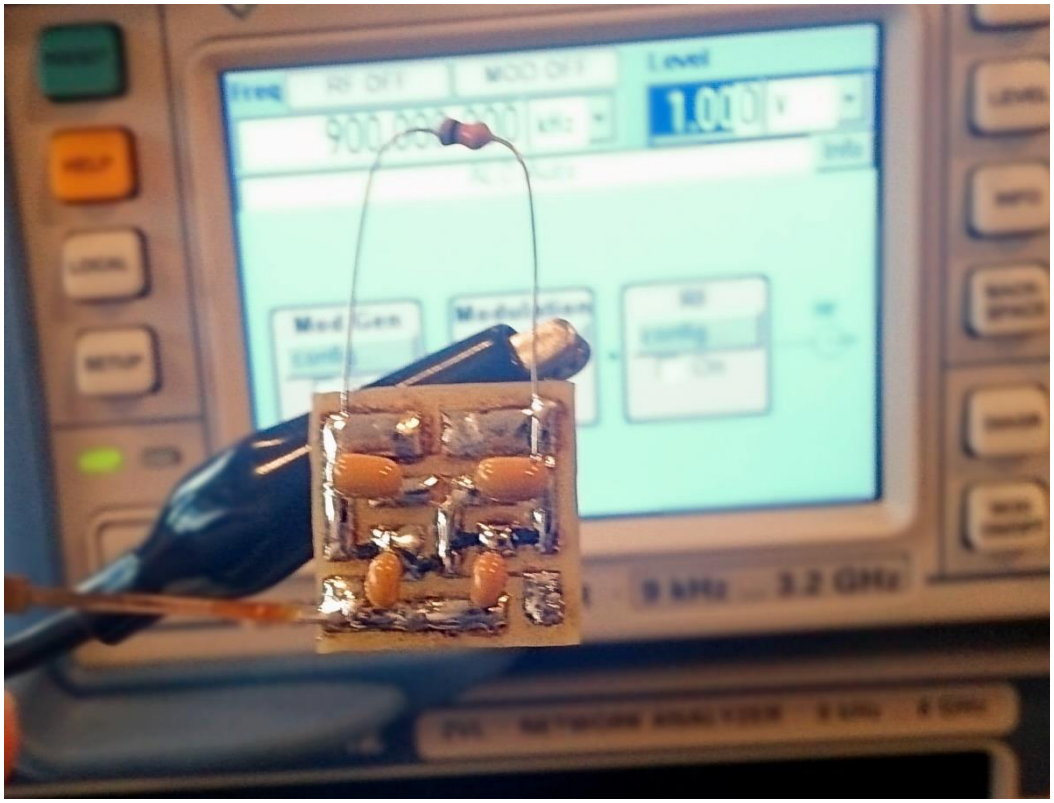

Figure 5.12 Test set-up for measuring multiplier efficiency with different load values.

For this experiment the cables and the power meter were calibrated for levels between -20dBm and 18dBm of output power. The output power of the generator, was corrected based on the calibration result and measured by the spectrum analyser and the power meter, it was then used to calculate the power at the output terminals of the convertor.

The real part of the input impedance of an RF-DC circuit as a function of the input power level an load resistance is shown in Figure 5.13.

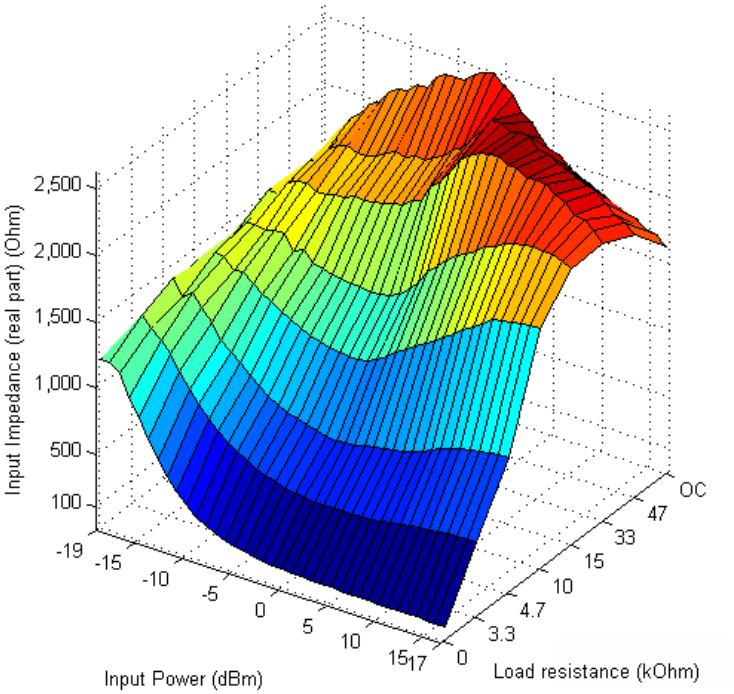

Figure 5.13 Load resistance and input power influence the input impedance, measured for power levels between -19dBm and 15dBm.

It is obvious that in the higher input power level (-5 to 17 dBm), the real part is relatively stable for load resistances between short circuit and 4.7 kΩ, hence easier to choose a suitable output impedance of the antenna. At lower input level (< -5 dBm), however, the real part of the input impedance is changing rapidly. In order to match the antenna to the rectifying circuit, the performance of the antenna is adjusted using the values of the input impedance of the rectifier.

In the second experiment, using the same set-up as shown in Figure 5.12, we have measured the efficiency of two types of voltage multipliers over the range of -11dBm to 17dBm input power. As a result (see Figure 5.14), the maximum values for both 1-stage and 3-stage voltage multipliers are plotted for different load resistances. The load resistance values for a particular configuration with the highest efficiency achieved, are defined as ‘best load resistances’.

As shown in Figure 5.14, if a voltage multiplier has been optimised for a fixed load resistance value and it reaches its maximum power efficiency at a particular

input power level, changing the incident power density will drastically affect overall power efficiency of the RFEH system.

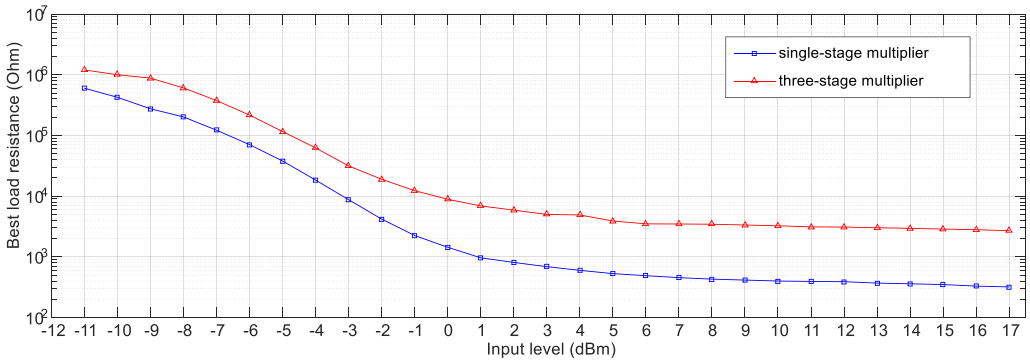

Figure 5.14 Load resistance values with the highest multiplier efficiency measured for input levels between -11dBm and 17dBm for 1 and 3 stages

Experimental results also show, that the influence of the number of the rectifier stages used, varies depending on the input power level. Moreover, we may conclude that there needs to be much more emphasis put on antenna optimisation in order to bring the power conversion to a sufficiently high level, i.e., the power level provided by the antenna to be higher than 0 dBm as this part of the curve is less affected by the load resistance value.

As shown in the simulated results in Figure 5.15, the maximum power efficiency achieved with N-stages Dickson charge pumps. The simulations were conducted with LTSpice for 1,2,4,6, and 8 stages. The drawback in using a large number of stages in a RF-DC conversion circuit is the lower power conversion efficiency at lower input power levels. However, it may be considered as an advantage if the power density of the harvested RF energy is high enough to enable the conversion circuit to achieve its maximum efficiency. Therefore, RF-DC converters can obtain maximum power efficiency only at certain input power level. For different incident density levels, the input impedance changes because of the nonlinearity of the diodes and this leads to degraded efficiency.

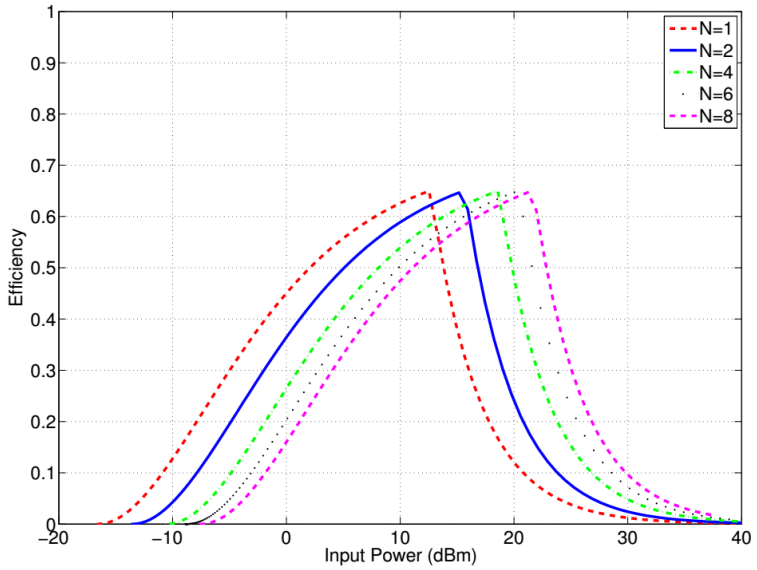

Figure 5.15 Theoretical RFEH efficiency for N-stage Dickson charge pumps.

To avoid this limitation while designing RF-DC conversion circuits, multiple rectifiers optimised at different input power levels are connected in parallel or in series to widen the operating range. The authors of [141] are proposing an adaptive rectifier (Figure 5.16) with extended input power range with two differential-type sub-rectifiers and a control circuit.

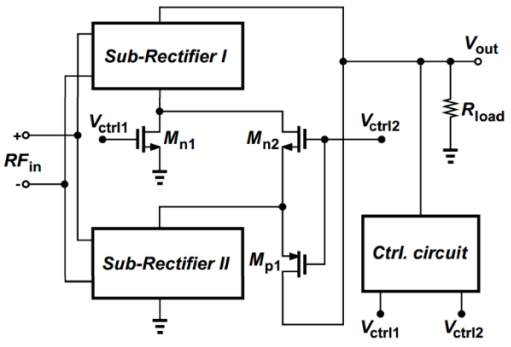

Figure 5.16 Adaptive rectifier proposed in [141]

It is switching between series and parallel modes by checking the output voltage in order to achieve optimal performance for an extended input range compared to a rectifier optimised for a fixed input power value.

Another similar approach is proposed by the authors of [142]. As shown in Figure 5.17, they designed an adaptive rectifier circuit that reconfigures itself depending on the input RF power level.

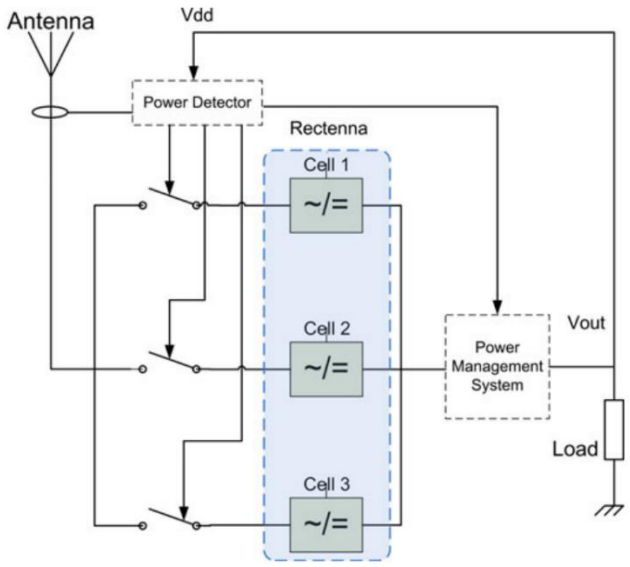

Figure 5.17 Schematics of the reconfigurable rectenna circuit, proposed in [142]

The main drawback in using a control circuit is the extra power consumption of the control component. Moreover, in both [141] and [142] precise level adjustment is required in order to achieve the stated efficiency values. Therefore, designing an efficient RF-DC convertor covering an extended range of input power levels, is a challenge which requires a novel approach.

There are two main configurations used for RFEH power combining when rectenna array is considered: RF power combining technique (Figure 5.18a) is well known in antenna array design theory as a method of combining or 'phasing' the signals of two or more antennas in order to achieve improved performance over that of a single antenna. The second technique (Figure 5.18b) is using multiple RF-DC conversion circuits, each of them connected to an antenna. In the second case,

the RF loss is minimised compared to the loss present in RF phased arrays. It is much easier to sum DC voltages instead of combining multiple RF antennas, connected together in such a way that their individual currents are in a particular phase and amplitude relationship.

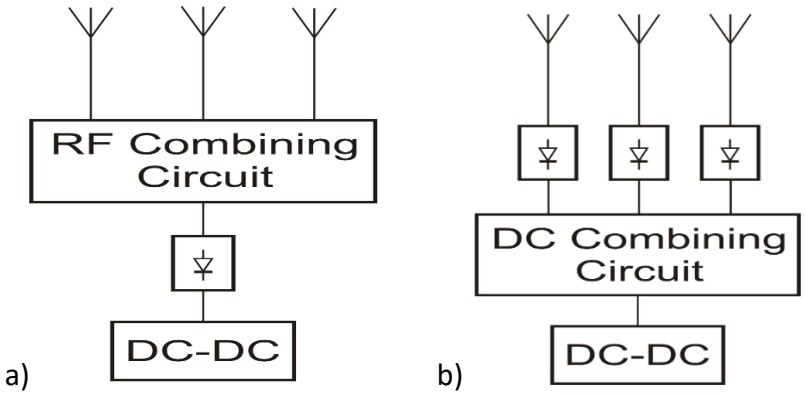

Figure 5.18 RFEH array combining configurations: a)RF power combining; b) DC voltage combining.

As the requirements for the RF-DC power conversion efficiency and the impedance matching in such rectenna configurations, may be critical for the overall effectiveness of the RFEH system, we have proposed a new technique for optimising the rectenna performance at the MW frequency band with a ferrite rod antenna array.

Ten ferrite rod antennas were prototyped. Each of them consists of a coil of 120 turns, wound onto a low loss ferrite core with Litz wire of 60 strands/46SWG of diameter. The ferrite core is MnZn material with relative permeability of 2000 and dimensions - 10mm diameter, 100m in length. The coils are placed at the end of the ferrite rods in order to improve the Q-factor as described in Section 3.5.3. and their inductances are 168μH. A diagram is shown in Figure 5.19.

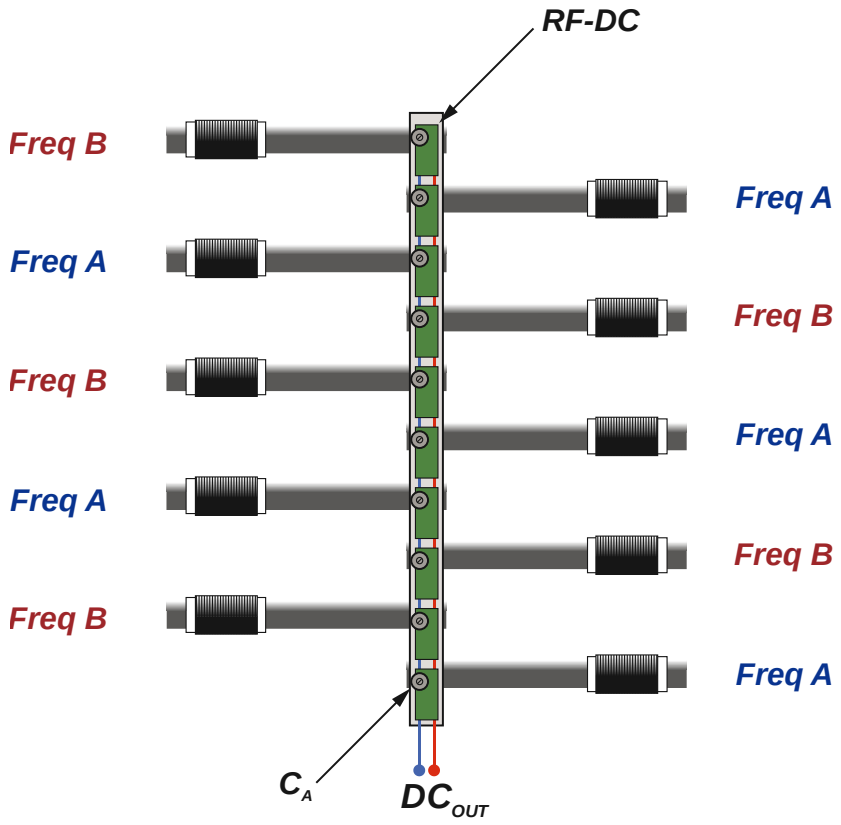

Figure 5.19 Diagram of the multi-ferrite rod rectenna

The adjustment capacitor C_A of each of the rectifying circuits, is installed in a position which is suitable for easy frequency setting. Half of the ferrite rod antennas were set to 909kHz (marked as 'Freq A'), and the other five antennas were set to 1089kHz (marked as 'Freq B'). These two frequencies are used to transmit the AM broadcast radio signals of 'BBS Radio 5' and 'Talksport London'. Using two different MW frequencies allowed us to minimise the influence of the coils by 'separating' Freq A antennas with antennas set to Freq B. The Q-factor achieved for each of the ferrite rod antenna was in the range of 180-200.

The prototype was measured in the engineering laboratory of University of Bedfordshire, University Campus of Milton Keynes (UCMK). We used a signal generator for each of the MW frequencies, and a pair of MOS-FET amplifiers to increase the power generated by the signal source by 10dB. Using two wire loop antenna prototypes, used for the experiments in Section 3.6.2. , we transmitted

500mW at both 909kHz and 1089kHz frequencies. As a result, we were able to measure voltage levels of more than 7V on 2.2k load resistance at distances of 2m from the transmitting antennas. A picture of the prototype is shown in Figure 5.20.

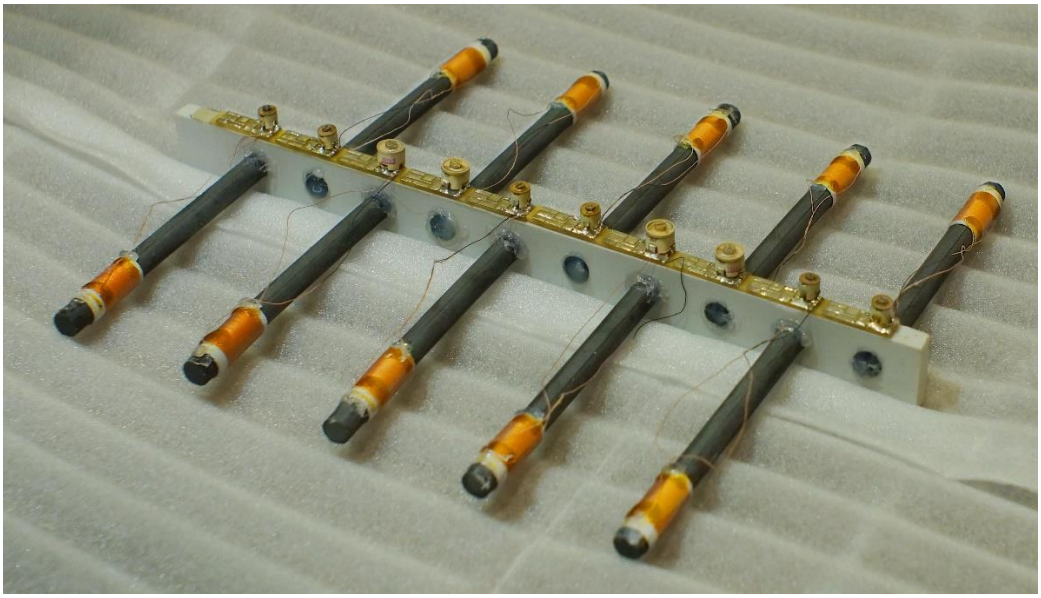

Figure 5.20 Prototype of the proposed multi-ferrite rod MW rectenna.

5.8. Summary

In current state-of-the-art different implementations of diodes have been investigated for RF harvesting. Schottky diodes were mostly used due to their inherently low turn on voltage, low junction capacitance, and low conduction resistance [143]. Since a basic requirement for diodes used in the voltage multiplier is to have a switching time which is much shorter than the cycle of the input signal, diodes such as Schottky type are preferred mainly because of their fast switching times compared to the normal diodes. Moreover, using Schottky diodes, higher saturation current is achieved and therefore a higher conversion efficiency [144],[145]. However, tunnel diodes, metal-insulator-metal (MIM) diodes, and spin diodes have recently made a re-emergence as their technologies have developed [38].

Recently, using diode-connected transistors as rectifying elements has become increasingly popular. Low- or zero-threshold voltage MOS transistors are available with threshold voltage values of less than 20 mV, and could be used in passive RF energy harvesting devices or RFID tags [146] and [147]. Figure 5.21 shows an N-stage voltage multiplier implemented by NMOS transistors each with its gate and drain connected together. In [148], p–n-junction diode rectifier circuit is analysed and the results of different validation methods are presented. Furthermore, in [138] an analysis of MOS transistor are presented, considering its size. The authors are assuming that DC loading currents are equal to the transistor currents.

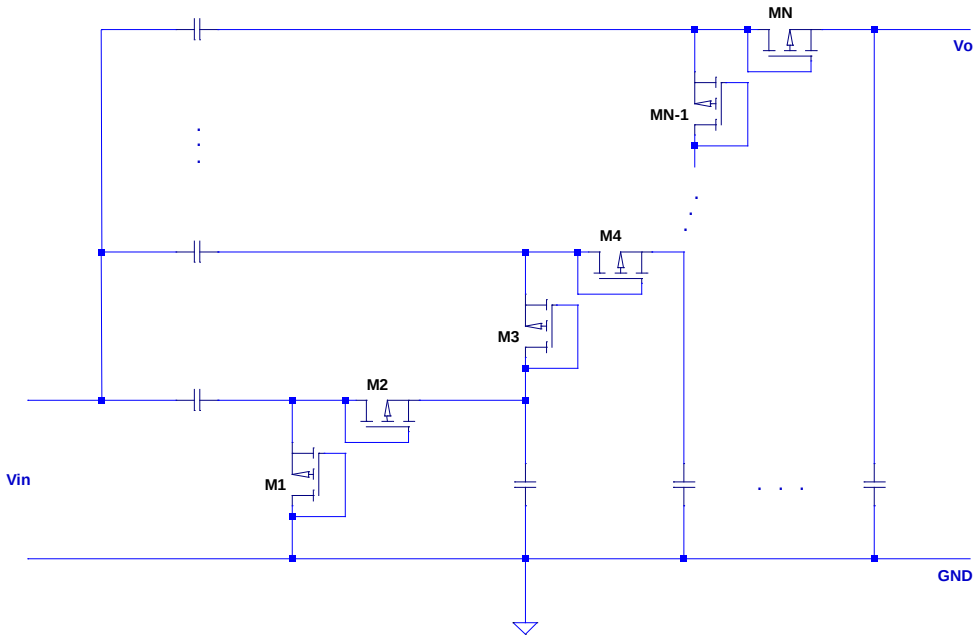

Figure 5.21 N-stage voltage multiplier using diode-connected transistors

The authors of [139] have considered different design strategies to reduce the threshold voltage of the transistors in order to fulfil the requirement of turning on the diode-connected transistors despite low input voltage amplitudes. Dynamic gate-drain biasing using an external threshold voltage compensator was discussed. The rectified output voltage was shown to have the form of:

$$V_R = 2(V_{rf} - V_{th} + V_{bth}) \quad (63)$$

Hence if the bias voltage V_{bth} was set equal to the threshold voltage of the transistors, RF to DC conversion could be achieved without the impact of V_{th}. The transistors in this rectifier are fixed in the saturation region, because the drain–source voltage V_{DS} is equal to the gate–source voltage V_{GS} with the condition of $V_R \approx 2V_{rf}$. A voltage doubler rectifier using floating gate transistors with NMOS replaced with PMOS was presented in [47]. A MOS capacitor was connected in series with the gate of each diode-connected transistor in order to design a floating gate device, using a standard CMOS fabricating procedure.

Because of the high impedance of the RF-DC conversion circuit, a big part of the RF energy delivered by the antenna might be returned in the form of reflected power. This behaviour is quantified by S11 parameter or return loss, and it shows how close the input impedance of the rectifier is to the antenna impedance. In some cases, the power loss caused by impedance mismatch may be much higher than the harvested RF energy. To minimise this loss, a matching circuit is needed, although adding such a network could add its own insertion loss to the mismatch losses [149]. The ferrite rod antennas for MW frequencies do not need any additional matching network, because of their wide range of impedance, which may be adjusted to match the input impedance of the conversion circuit. The capacitance and the inductance of the ferrite rod antenna are set to optimise the impedance of the rectifying circuit to match the antenna impedance.

Chapter 6 Conclusions and Future Work

With the recent development of radio communications, a big number of wireless systems which transmit RF energy into the air but most of it has not been used. The rectenna has attracted great attention to recycle the ambient power radiated by wireless systems. Accordingly, the major goals of this thesis are on investigating a wide range of RF energy sources, different antenna types performance, designing novel rectennas for RF wireless energy harvesting and proposing novel ways of improving rectenna conversion efficiency for low input power density with the main goal to resolve the energy supply problems faced by the autonomous systems.

6.1. Summary

To design an energy-efficient rectenna, all the components of the RFEH system must be studied, optimised and properly selected, depending on the application requirements. Designing a RFEH system requires three main steps. Firstly, power requirements of the RFEH system must be defined. It is common for the autonomous systems, the power consumption of their circuits to rise only if necessary, therefore, the time between active cycles and the average power consumed must be considered. Secondly, a suitable RF energy source must be selected based on the requirements. Dedicated RF transmission may be used for applications where no ambient RF signal is available or a RF signal is available, but its power density is not sufficient for the particular application. Factors, such as frequency of the RF source signal, physical location of the sensor, or size limitations, should be considered in that stage of the planning. In the last stage, an efficient RF-DC conversion circuit must be selected and implemented for an efficient power conversion of the incident RF power energy to DC energy suitable for the load.

The approach is validated by a number independent experimental results conducted in conditions as close as possible to the real life which also shows that the actual RFEH rectennas for a specific application scenario need to be considered in order to design a reliable RFEH system for both harvesting energy from ambient RF sources and RF harvesting using dedicated RF sources. Experimental results show that we have completed the goal of being able to power small devices remotely using both dedicated and ambient RF energy sources.

The state-of-the-art of energy harvesting technologies has been investigated and the results are presented in Chapter 2 . Also, some of the most important historical discoveries in this area were highlighted. The chapter presents a system analysis and compares different power transfer systems through several figures of merit highlighting the importance of a system optimisation approach to achieve higher end-to-end efficiencies

In Chapter 3 , different aspects of MW rectenna were discussed and new optimisation methods were proposed. It has been shown in the last part of Chapter 3 that in a distance of 3.1km from the Brookmans park broadcast centre a small digital LCD clock can be easily powered by a simple ferrite antenna without using any battery. More than 4,000 people are living in the area within this radius around the transmitting tower in Brookmans park according to the Office of National Statistics [109], proving that many people may benefit from MW RFEH power for powering small autonomous devices.

An impedance matching network has been simulated to optimise the efficiency and reduce the return loss. As a result, the power efficiency of the circuit has been increased by 10% by connecting a 2.2pF capacitor in series with the voltage rectifier. The value of the matching capacitance was achieved with an impedance matching circuit inserted.

In Chapter 4 , a highly efficient compact printed microstrip antenna for harvesting energy from mobile phone base stations at 930 MHz was designed and experimentally evaluated. The main advantages of the proposed rectenna design

are its compact and light-weight size and its high gain. In order to maximise the efficiency, a suitable matching method was considered, which could provide the estimated efficiency of more than 65% for input power between 0.02 to 5 mW. The simulated gain of the antenna was higher than 8.2 dBi at 930 MHz. The coplanar stripline circuit and the antenna were measured individually, and they were in good agreement with the simulation results. At the end of this chapter a comparison of the main parameters between similar rectenna designs and the proposed rectenna design is presented.

In Chapter 5 , several aspects RF-DC power conversion efficiency are analysed with the aim to propose novel optimisation techniques for improving the overall RFEH system efficiency. In-depth analysis has been presented to investigate diode performance. Different types of voltage multipliers are discussed in details, highlighting their properties. On the topic of optimal RF-DC conversion efficiency, it was shown how the main external parameters, such as input power density, load resistance, and rectifier impedance, are dependent on each other as well as their influence on the power conversion efficiency. Therefore, one of the challenges for maximising the RF-DC efficiency lies in decreasing the variations of the external factors by selecting suitable rectifier design. Comparing two ways of combining the harvested signals delivered by several antennas, it was proven that the DC combining method achieves a higher conversion efficiency at wider bandwidth and higher flexibility for RF EH applications. In addition, several ways of RF energy transfer optimisation are analysed and a novel rectenna design is proposed in order to proof the concept of improved RFEH system performance at MW frequencies by using an array of ferrite rod antennas with DC combining circuit.

6.2. Future work

Considering the conclusions and the design challenges in the work presented, future work can be suggested in the following areas:

- → ***Integrated design*** – A big part of the modern Printed Circuit Board (PCB) layouts is the power supply network which may include thousands of nodes, tracks, vias, etc. Implementing a RFEH approach to the individual component's design may contribute to the improvement of the integration factor. Using a dedicated RF energy source located in the device compartment may power hundreds of electronic components at the same time. Moreover, using different frequencies as RF energy sources for distinguished modules, would let us optimise and better control the resources.
- → ***Solar Powered Satellite*** – Though still in the experimental stage, researchers working in Solar Powered Satellite (SPS) (see Figure 6.1) have made advancements in energy conversion at great distances and high powers (greater than 1 Watt) to enable electricity to be transferred via radio waves, collecting solar energy in geostationary stations around the earth using big solar panels, and beaming it to ground stations via microwave power transfer [20],[24],[150]

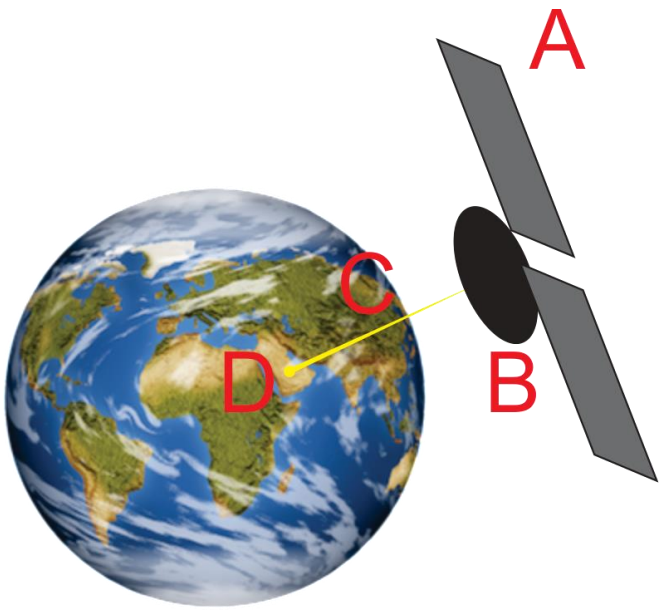

Figure 6.1 Solar Power Satellite (SPS) main components: A - solar panels; B - DC-uWave; C - RF beam; D - Rectenna

Space-based solar collectors in geosynchronous orbit could generate power nearly 24 hours a day. Moreover, the solar energy available at such altitudes is ten times more than the one available on the ground. While there are a number of technological challenges that need to be resolved before this idea can be implemented, results so far are promising [151],[152]. In 2015, Mitsubishi Heavy Industries (MHI) announced 'A successful ground test' [153] of a system designed to be a part of a future space solar power systems (SSPS). However, the experiment demonstrated only a single element of the system - wireless power transfer of 10 kilowatts sent at microwave frequencies from a transmitting unit to a receiver 500 meters away, conducted at the ground level. This shows that the research in this area is still in its early experimental stage. The concept of transferring energy at very long distances, as required for a typical SSPS, hasn't been proofed yet. The research investment in this area can be justified for a country like Japan with limited natural resources, that's still reeling from the

Fukushima nuclear disaster, however, the most of the physical difficulties within the context of such a technology haven't been mitigated yet.

→ ***Maximum Power Point Tracking*** – More techniques for optimising the rectification process should be investigated. Power conversion efficiency values in the range of 30-40% are proved to be the lowest efficiency achieved in a RFEH system, compared to the efficiencies of the other components. There is a method called Maximum Power Point Tracking (MPPT) which is already popular in solar energy harvesting. It is an electronic system that varies the electrical operating point of the Photovoltaic (PV) modules so that they are able to deliver maximum available power. A similar system may be considered in RFEH aspect by controlling at least one of the parameters affecting the conversion efficiency. However, as the power available in RFEH systems is limited, passive MPPT optimisation methods may be considered.

Continuing research into RFEH technologies will enable numerous new applications in the area of health, space power, IoT, Bluetooth Low Energy (BLE), and in many more.

References:

[1] V. Raghunathan, a. Kansal, J. Hsu, J. Friedman, and M. Srivastava, “Design considerations for solar energy harvesting wireless embedded systems,” *IPSN 2005. Fourth Int. Symp. Inf. Process. Sens. Networks, 2005.*, pp. 457–462, 2005.

[2] B. P. D. Mitcheson, M. Ieee, E. M. Yeatman, S. M. Ieee, G. K. Rao, S. M. Ieee, A. S. Holmes, and T. C. Green, “Human and Machine Motion for Wireless Electronic Devices,” vol. 96, no. 9, pp. 1457–1486, 2008.

[3] S. Dalola, M. Ferrari, V. Ferrari, M. Guizzetti, D. Marioli, and a. Taroni, “Characterization of Thermoelectric Modules for Powering Autonomous Sensors,” *IEEE Trans. Instrum. Meas.*, vol. 58, no. 1, pp. 99–107, Jan. 2009.

[4] M. A. Green, “Thin-film solar cells: Review of materials, technologies and commercial status,” in *Journal of Materials Science: Materials in Electronics*, 2007, vol. 18, no. SUPPL. 1, pp. 15–19.

[5] R. Kappel, W. Pachler, M. Auer, W. Pribyl, G. Hofer, and G. Holweg, “Using thermoelectric energy harvesting to power a self-sustaining temperature sensor in body area networks,” *Proc. IEEE Int. Conf. Ind. Technol.*, pp. 787–792, 2013.

[6] A. Khaligh, P. Zeng, and C. Zheng, “Kinetic Energy Harvesting Using Piezoelectric and Electromagnetic Technologies,” *Ind. Electron. IEEE Trans.*, vol. 57, no. 3, pp. 850–860, 2010.

[7] “Circuit Design Tools & Calculators | Design Center | Analog Devices,” *Analog Devices*. [Online]. Available: http://www.analog.com/en/design-center/design-tools-and-calculators.html#LTspice. [Accessed: 10-Sep-2018].

[8] S. Jalbrzykowski and a Bogdan, “A Dual Full Bridge Resonant Class-E Bidirectional DC-DC Converter,” *, IEEE Trans.*, vol. 57, no. 4, pp. 1478–1486, 2011.

[9] G. Wakte and H. K. Naidu, “Wireless Transmission of Electrical Energy by using Inductive Coupling,” pp. 1779–1785, 2016.

[10] N. A. Wahab, Z. M. Yasin, N. Hamzah, Z. I. Khan, and M. K. M. Salleh, “Investigation on Magnetic Resonant Coupling for Low Voltage Application,” no. Rfm, pp. 14–16, 2015.

[11] T. Imura, “Superiority of Magnetic Resonant Coupling at Large Air Gap in Wireless Power Transfer,” pp. 0–5, 2016.

[12] A. P. Sample, D. A. Meyer, and J. R. Smith, “Analysis, Experimental Results, and Range Adaptation of Magnetically Coupled Resonators for Wireless

Power Transfer," *IEEE Trans. Ind. Electron.*, vol. 58, no. 2, pp. 544–554, Feb. 2011.

[13] J. O. McSpadden and J. C. Mankins, "Space solar power programs and microwave wireless power transmission technology," *IEEE Microw. Mag.*, vol. 3, no. 4, pp. 46–57, 2002.

[14] Y. S. Hwang and H. C. Lin, "A new CMOS analog front end for RFID tags," *IEEE Trans. Ind. Electron.*, vol. 56, no. 7, pp. 2299–2307, 2009.

[15] "WiGLE: Wireless Network Mapping." [Online]. Available: https://www.wigle.net/. [Accessed: 21-Jan-2017].

[16] a L. Allègre, a Bouscayrol, and R. Trigui, "Influence of control strategies on battery / supercapacitor hybrid Energy Storage Systems for traction applications," pp. 213–220, 2009.

[17] R. Lu, C. Zhu, L. Tian, and Q. Wang, "Super-capacitor stacks management system with dynamic equalization techniques," *IEEE Trans. Magn.*, vol. 43, no. 1, pp. 254–258, 2007.

[18] J. B. Goodenough, "US Patent," 4302518, 1980.

[19] H. Kato, Y. Yamamoto, M. Nagamine, and Y. Nishi, "Lithium ion rechargeable batteries," *Proc. WESCON '93*, pp. 210–214.

[20] P. E. Glaser, "Power from the Sun: Its Future," *Science (80-.).*, vol. 162, no. 3856, pp. 857–861, Nov. 1968.

[21] W. Brown, J. Mims, and N. Heenan, "An experimental microwave-powered helicopter," *IRE Int. Conv. Rec.*, vol. 13, no. October, 1965.

[22] M. M. Hossain, V. R. Prybutok, and A. Radiofrequency, "Consumer Acceptance of RFID Technology: An Exploratory Study," *IEEE Trans. Eng. Manag.*, vol. 55, no. 2, pp. 316–328, 2008.

[23] I. Bose and S. Yan, "Potencial da RFID em projetos verdes (IEEE Explore): estudos de casos," *IT Prof.*, vol. 13, pp. 41–47, 2011.

[24] G. R. Woodcock, "Solar Power Satllite System Definition Study," Seattle, WA, 1979.

[25] John Griffiths, *Radio Wave Propagation and Antennas: An Introduction*. Prentice-Hall International Ltd., 1987.

[26] V. Trainotti and S. Member, "Short Medium Frequency AM Antennas," *IEEE Trans. Broadcast.*, vol. 47, no. 3, pp. 263–284, 2001.

[27] "MW channels in the UK." [Online]. Available: http://www.mediumwaveradio.com/uk.php. [Accessed: 21-Jan-2017].

[28] FCC, "Broadcast Station Totals as of December 31, 2000," Washington, 2000.

[29] FCC, “Broadcast Station Totals as of December 31, 2017,” Washington, 2018.

[30] I. Kuzle, H. Pandzic, and D. Bosnjak, “The true inventor of the radio communications,” *IEEE Hist. Telecommun. Conf. HISTELCON 2008*, pp. 20–23, 2008.

[31] V. Dyo, B. Allen, D. Jazani, I. Ivanov, and T. Ajmal, “Design of a ferrite rod antenna for harvesting energy from medium wave broadcast signals,” *J. Eng.*, pp. 1–8, 2013.

[32] B. Allen, D. Jazani, V. Dyo, T. Ajmal, and I. Ivanov, “Design and optimisation of compact RF energy harvesting device for smart applications,” *Electron. Lett.*, vol. 50, no. 2, pp. 111–113, Jan. 2014.

[33] N. Tesla, “Experiments with alternate currents of very high frequency and their application to methods of artificial illumination,” *Trans. Am. Soc. Agric. Eng.*, vol. 8, no. 1, pp. 267–319, 1891.

[34] J. D. Kraus, “Heinrich Hertz-theorist and experimenter,” *IEEE MTT-S Int. Microw. Symp. Dig.*, vol. 36, no. 5, pp. 1–6, 1988.

[35] H. Hertz, “Electric Waves,” English Tr., D. E. Jones, Ed. MacMillan and Co., 1893.

[36] J. Maxwell, “A Dynamical Theory of the Electromagnetic Field.,” *Proc. R. Soc. …*, no. 1, 1863.

[37] M. B. Farriz, A. Din, A. A. Rahman, M. S. Yahaya, and J. M. Herman, “A simple design of a mini tesla coil with DC voltage input,” *Proc. - Int. Conf. Electr. Control Eng. ICECE 2010*, pp. 4556–4559, 2010.

[38] S. Hemour and K. Wu, “Radio-frequency rectifier for electromagnetic energy harvesting: Development path and future outlook,” *Proc. IEEE*, vol. 102, no. 11, pp. 1667–1691, 2014.

[39] H. H. Scott, “A new type of selective circuit and some applications* by h. h. scott,” vol. 26, no. 2, pp. 226–235, 1938.

[40] a Khaligh, P. Zeng, and C. Zheng, “Kinetic Energy Harvesting Using Piezoelectric and Electromagnetic Technologies #x2014;State of the Art,” *Ind. Electron. IEEE Trans.*, vol. 57, no. 3, pp. 850–860, 2010.

[41] A. F. A. Facen and a. Boni, “A CMOS Analog Frontend for a Passive UHF RFID Tag,” *ISLPED’06 Proc. 2006 Int. Symp. Low Power Electron. Des.*, vol. 1, no. 1, pp. 280–285, 2006.

[42] S. Gregori, Y. Li, H. Li, J. Liu, and F. Maloberti, “2.45 GHz Power and Data Transmission for a Low-Power Autonomous Sensors Platform,” *Proc. Int. Symp. Low Power Electron. Des.*, vol. 2004–Janua, no. January, pp. 269–273, 2004.

[43] J. A. Hagerty, S. Member, F. B. Helmbrecht, W. H. Mccalpin, R. Zane, and Z. B. Popovic, “Broad-Band Rectenna Arrays,” vol. 3, no. March, pp. 1014–1024, 2004.

[44] P. B. Koeneman, I. J. Busch-Vishniac, and K. L. Wood, “Feasibility of micro power supplies for MEMS,” *J. Microelectromechanical Syst.*, vol. 6, no. 4, pp. 355–362, 1997.

[45] R. M. LaFollette, J. N. Harb, and P. Humble, “Microfabricated secondary batteries for remote, autonomous, electronic devices,” *Sixt. Annu. Batter. Conf. Appl. Adv.*, pp. 349–354, 2001.

[46] A. Kansal, J. Hsu, S. Zahedi, and M. B. Srivastava, “Power Management in Energy Harvesting Sensor Networks,” pp. 1–35, 2002.

[47] T. Le, K. Mayaram, and T. Fiez, “Efficient Far-Field Radio Frequency Energy Harvesting for Passively Powered Sensor Networks,” *IEEE J. Solid-State Circuits*, vol. 43, no. 5, pp. 1287–1302, May 2008.

[48] Z. W. Sim, R. Shuttleworth, and B. Grieve, “Investigation of PCB Microstrip Patch Receiving Antenna for Outdoor RF Energy Harvesting in Wireless Sensor Networks,” no. November, pp. 129–132, 2009.

[49] M. T. Penella-Lopez and M. Gasulla-Forner, *Powering Autonomous Sensors*. Springer, 2011.

[50] Z. W. Sim, “Radio Frequency Energy Harvesting for Embedded Sensor Networks in the Natural Environment,” University of Manchester, 2011.

[51] F. Philipp, F. a. Samman, M. Glesner, K. B. Dassanayake, S. Maheswararajah, and S. Halgamuge, “Adaptive wireless sensor networks powered by hybrid energy harvesting for environmental monitoring,” *2012 IEEE 6th Int. Conf. Inf. Autom. Sustain.*, pp. 285–289, Sep. 2012.

[52] C. Mikeka and H. Arai, “Notched Circular Microstrip Patch Antenna integrated with a single diode rectifier for energy-harvesting prosthetic leg,” *2011 IEEE Top. Conf. Biomed. Wirel. Technol. Networks, Sens. Syst.*, pp. 31–34, Jan. 2011.

[53] A. Georgiadis, G. Andia, and A. Collado, “Rectenna design and optimization using reciprocity theory and harmonic balance analysis for electromagnetic (EM) energy harvesting,” *IEEE Antennas Wirel. Propag. Lett.*, vol. 9, no. 12, pp. 444–446, Dec. 2010.

[54] V. Dyo, T. Ajmal, B. Allen, D. Jazani, and I. Ivanov, “Design of a ferrite rod antenna for harvesting energy from medium wave broadcast signals,” *J. Eng.*, pp. 1–8, 2013.

[55] U. Olgun, S. Member, C. Chen, S. Member, and J. L. Volakis, “Investigation of Rectenna Array Configurations for Enhanced RF Power Harvesting,” no. 2, pp. 262–265, 2011.

[56] R. Zhang and C. K. Ho, “MIMO Broadcasting for Simultaneous Wireless Information and Power Transfer,” *IEEE Trans. Wirel. Commun.*, vol. 12, no. May, pp. 1989–2001, 2013.

[57] S. Timotheou, I. Krikidis, G. Zheng, and B. Ottersten, “Beamforming for MISO interference channels with QoS and RF energy transfer,” *IEEE Trans. Wirel. Commun.*, vol. 13, no. 5, pp. 2646–2658, 2014.

[58] H. Lee, S. R. Lee, K. J. Lee, H. B. Kong, and I. Lee, “Transmit Beamforming Techniques for Wireless Information and Power Transfer in MISO Interference Channels,” *2015 IEEE Glob. Commun. Conf.*, vol. 14, no. 9, pp. 1–6, 2015.

[59] Q. Sun, G. Zhu, C. Shen, X. Li, and Z. Zhong, “Joint Beamforming Design and Time Allocation for Wireless Powered Communication Networks,” *IEEE Commun. Lett.*, vol. 18, no. 10, pp. 1783–1786, Oct. 2014.

[60] X. Lu, P. Wang, D. Niyato, D. I. Kim, and Z. Han, “Wireless Networks With RF Energy Harvesting: A Contemporary Survey,” *IEEE Commun. Surv. Tutorials*, vol. 17, no. 2, pp. 757–789, 2015.

[61] U. Olgun, C.-C. Chen, and J. L. Volakis, “Design of an efficient ambient WiFi energy harvesting system,” *IET Microwaves, Antennas Propag.*, vol. 6, no. May, p. 1200, 2012.

[62] M. Piñuela, S. Member, P. D. Mitcheson, and S. Member, “Ambient RF Energy Harvesting in Urban and Semi-Urban Environments,” vol. 61, no. 7, pp. 2715–2726, 2013.

[63] P. Nintanavongsa, M. Y. Naderi, and K. R. Chowdhury, “A dual-band wireless energy transfer protocol for heterogeneous sensor networks powered by RF energy harvesting,” *2013 Int. Comput. Sci. Eng. Conf.*, pp. 387–392, 2013.

[64] K. Huang and V. K. N. Lau, “Enabling Wireless Power Transfer in Cellular Networks: Architecture, Modeling and Deployment,” pp. 5555–5560, Jul. 2012.

[65] A. H. Sakr and E. Hossain, “Analysis of multi-tier uplink cellular networks with energy harvesting and flexible cell association,” *2014 IEEE Glob. Commun. Conf. GLOBECOM 2014*, pp. 4525–4530, 2014.

[66] J. Guo, S. Durrani, X. Zhou, and H. Yanikomeroglu, “Outage Probability of Ad Hoc Networks with Wireless Information and Power Transfer,” *IEEE Wirel. Commun. Lett.*, vol. 4, no. 4, pp. 409–412, 2015.

[67] O. Ozel and S. Ulukus, “Achieving AWGN capacity under stochastic energy harvesting,” *IEEE Trans. Inf. Theory*, vol. 58, no. 10, pp. 6471–6483, 2012.

[68] F. Ozcelik, G. Uctu, and E. Uysal-Biyikoglu, “Optimal Packet Scheduling on an Energy Harvesting Fading Channel,” *arXiv Prepr. arXiv1202.0690*, vol. 60, no. 1, pp. 220–230, 2012.

[69] M. A. Zafer and E. Modiano, “A calculus approach to energy-efficient data transmission with quality-of-service constraints,” *IEEE/ACM Trans. Netw.*, vol. 17, no. 3, pp. 898–911, 2009.

[70] A. Sinha and P. Chaporkar, “Optimal Power Allocation for a Renewable Energy Source,” 2012.

[71] P. Mitran, “On optimal online policies in energy harvesting systems for compound poisson energy arrivals,” *IEEE Int. Symp. Inf. Theory - Proc.*, pp. 960–964, 2012.

[72] S. Asmussen, *Applied probability and queues*. Chichester: Wiley, 1987.

[73] M. B. Khuzani, H. E. Saffar, E. H. M. Alian, and P. Mitran, “On optimal online power policies for energy harvesting with finite-state Markov channels,” *IEEE Int. Symp. Inf. Theory - Proc.*, pp. 1586–1590, 2013.

[74] M. B. Khuzani and P. Mitran, “On online energy harvesting in multiple access communication systems,” *IEEE Trans. Inf. Theory*, vol. 60, no. 3, pp. 1883–1898, 2014.

[75] S. M. Mann, T. G. Cooper, S. G. Allen, R. P. Blackwell, and A. J. Lowe, “Exposure to Radio Waves Near Mobile Phone Base Stations,” Oxon OX11 0RQ, 2000.

[76] S. I. Henderson and M. J. Bangay, “Survey of RF exposure levels from mobile telephone base stations in Australia,” *Bioelectromagnetics*, vol. 27, no. 1, pp. 73–76, Jan. 2006.

[77] C. Bornkessel, M. Schubert, M. Wuschek, and P. Schmidt, “Measurement and Calculation of General Public Electromagnetic Exposure Around GSM and UMTS Cellular Base Stations,” in *2007 2nd International ITG Conference on Antennas*, 2007, pp. 225–229.

[78] G. Thuróczy, F. Molnár, J. Szabó, G. Jánossy, N. Nagy, G. Kubinyi, and J. Bakos, “Public exposure to RF from installed sources: Site measurements and personal exposimetry,” *Eur. Sp. Agency, (Special Publ. ESA SP*, vol. 626 SP, 2006.

[79] “IEEE Standard for Safety Levels with Respect to Human Exposure to Radio Frequency Electromagnetic Fields, 3 kHz to 300 GHz,” *IEEE Std C95.1-2005 (Revision IEEE Std C95.1-1991)*, pp. 1–238, Apr. 2006.

[80] X. Cao, W. J. Chiang, Y. C. King, and Y. K. Lee, “Electromagnetic energy harvesting circuit with feedforward and feedback dc-dc PWM boost converter for vibration power generator system,” *IEEE Trans. Power Electron.*, vol. 22, no. 2, pp. 679–685, 2007.

[81] R. Dayal, S. Dwari, and L. Parsa, “Design and implementation of a direct ACDC boost converter for low-voltage energy harvesting,” *IEEE Trans. Ind. Electron.*, vol. 58, no. 6, pp. 2387–2396, 2011.

[82] P. S. Carter and H. H. Beverage, “Early History of the Antennas and Propagation Field until the End of World War I, Part I - Antennas,” *Proc. IRE*, vol. 50, p. 679, 1962.

[83] J. A. Hora, N. M. Mapula, E. D. Talagon, M. B. Bate, R. S. Berido, and G. F. P. Palencia, “Design of RF to DC Converter in 90nm CMOS Technology for Ultra-Low Power Application,” *Humanoid, Nanotechnology, Inf. Technol. Control. Environ. Manag. (HNICEM), 2015 Int. Conf.*, no. December, pp. 1–6, 2015.

[84] J. Salomaa, M. Pulkkinen, T. Haapala, M. Nurmi, and K. Halonen, “Power Management System for Ultra-Low Power Energy Harvesting Applications,” *2015 IEEE Int. Symp. Circuits Syst.*, pp. 1086–1089, 2015.

[85] A. Richelli, L. Colalongo, S. Tonoli, and Z. M. KovÁcs-Vajna, “A 0.2-1.2V DC/DC Boost Converter for Power Harvesting Applications,” *IEEE Trans. Power Electron.*, vol. 24, no. 6, pp. 1541–1546, 2009.

[86] J. Jia and K. N. Leung, “Improved active-diode circuit used in voltage doubler,” *Int. J. Circuit Theory Appl.*, vol. 40, no. 2, pp. 1650–1659, Feb. 2012.

[87] Z. Hameed and K. Moez, “Hybrid forward and backward threshold-compensated RF-DC power converter for RF energy harvesting,” *IEEE J. Emerg. Sel. Top. Circuits Syst.*, vol. 4, no. 3, pp. 335–343, 2014.

[88] Q. W. Lin and X. Y. Zhang, “Differential Rectifier Using Resistance Compression Network for Improving Efficiency Over Extended Input Power Range,” *IEEE Trans. Microw. Theory Tech.*, vol. 64, no. 9, pp. 2943–2954, Sep. 2016.

[89] J. Taneja, J. Jeong, and D. Culler, “Design, modeling and capacity planning for micro-solar power sensor networks,” *Proc. - 2008 Int. Conf. Inf. Process. Sens. Networks, IPSN 2008*, pp. 407–418, 2008.

[90] X. Jiang, J. Polastre, and D. Culler, “Perpetual environmentally powered sensor networks,” *2005 4th Int. Symp. Inf. Process. Sens. Networks, IPSN 2005*, vol. 2005, pp. 463–468, 2005.

[91] R. A. Dougal, S. Liu, and R. E. White, “Power and life extension of battery-ultracapacitor hybrids,” *IEEE Trans. Components Packag. Technol.*, vol. 25, no. 1, pp. 120–131, 2002.

[92] M. Hata, “Empirical formula for propagation loss in land mobile radio services,” *Veh. Technol. IEEE Trans.*, vol. 29, no. 3, pp. 317–325, 1980.

[93] W. H. Tu, S. H. Hsu, and K. Chang, “Compact 5.8-GHz rectenna using stepped-impedance dipole antenna,” *IEEE Antennas Wirel. Propag. Lett.*, vol. 6, pp. 282–284, 2007.

[94] J. O. McSpadden, L. F. L. Fan, and K. C. K. Chang, “Design and experiments

of a high-conversion-efficiency 5.8-GHz\nrectenna," *IEEE Trans. Microw. Theory Tech.*, vol. 46, no. 12, pp. 2053–2060, 1998.

[95] H. Sun, Y. X. Guo, M. He, and Z. Zhong, "Design of a high-efficiency 2.45-GHz rectenna for low-input-power energy harvesting," *IEEE Antennas Wirel. Propag. Lett.*, vol. 11, pp. 929–932, 2012.

[96] T. C. Yo, C. M. Lee, C. M. Hsu, and C. H. Luo, "Compact circularly polarized rectenna with unbalanced circular slots," *IEEE Trans. Antennas Propag.*, vol. 56, no. 3, pp. 882–886, 2008.

[97] J. Heikkinen and M. Kivikoski, "A Novel Dual-Frequency Circularly Polarized Rectenna," vol. 2, pp. 330–333, 2003.

[98] Y. J. Ren, M. F. Farooqui, and K. Chang, "A compact dual-frequency rectifying antenna with high-orders harmonic-rejection," *IEEE Trans. Antennas Propag.*, vol. 55, no. 7, pp. 2110–2113, 2007.

[99] Y. H. Suh and K. Chang, "A high-efficiency dual-frequency rectenna for 2.45- and 5.8-GHz wireless power transmission," *IEEE Trans. Microw. Theory Tech.*, vol. 50, no. 7, pp. 1784–1789, 2002.

[100] V. Dyo, B. Allen, D. Jazani, I. Ivanov, and T. Ajmal, "Design of a ferrite rod antenna for harvesting energy from medium wave broadcast signals," *J. Eng.*, vol. 51, no. 6, pp. 1347–1356, Jan. 2013.

[101] J. Kraus, *Antennas*, Second. McGraw-Hill, 1988.

[102] "Ferroxcube Ltd." [Online]. Available: http://www.ferroxcube.com/.

[103] T. Simpson and Y. Zhu, "The Electrically Small Multi-Turn Loop Antenna with a Spheroidal Core," vol. 48, no. 5, 2006.

[104] J. G. Van Bladel, *Electromagnetic Fields: Second Edition*. 2006.

[105] B. Thide, *Electromagnetic Field Theory*. 2000.

[106] J. A. Stratton, *Electromagnetic Theory*, vol. 14, no. 11. 1941.

[107] T. Simpson and J. Cahill, "The electrically small elliptical loop with an oblate spheroidal core," *IEEE Antennas Propag. Mag.*, vol. 49, no. 5, pp. 83–92, 2007.

[108] Y. T. Lo and S. W. Lee, *Antenna Handbook*, 1st ed., vol. 44, no. 8. Boston, MA: Springer US, 1988.

[109] "Home - Office for National Statistics." [Online]. Available: https://www.ons.gov.uk/. [Accessed: 21-Jan-2017].

[110] B. Allen, T. Ajmal, V. Dyo, and D. Jazani, "Harvesting energy from ambient radio signals: a load of hot air?," *Antennas Propag. …*, no. November, pp. 8–11, 2012.

[111] “Heritage Retrofit Project,” 2014. [Online]. Available: http://www.cewales.org.uk/latest-news/heritage-retrofit/. [Accessed: 08-Nov-2018].

[112] S. Dey, P. Venugopalan, K. A. Jose, C. K. Aanandan, P. Mohanan, and K. G. Nair, “Bandwidth enhancement by flared microstrip dipole antenna,” in *Antennas and Propagation Society Symposium 1991 Digest*, 1991, pp. 342–345 vol.1.

[113] S. Barrette, S. K. Podilchak, and Y. M. M. Antar, “Ultrawideband double-sided printed dipole arrays,” in *2012 IEEE International Conference on Ultra-Wideband*, 2012, pp. 232–235.

[114] H. Sun, Y. x. Guo, M. He, and Z. Zhong, “Design of a High-Efficiency 2.45-GHz Rectenna for Low-Input-Power Energy Harvesting,” *IEEE Antennas Wirel. Propag. Lett.*, vol. 11, pp. 929–932, 2012.

[115] H. Yagi, “Beam transmission of ultra short waves,” *Proc. IEEE*, vol. 85, pp. 1864–1874, 1997.

[116] Y. Qian, W. R. Deal, N. Kaneda, and T. Itoh, “Microstrip-fed quasi-Yagi antenna with broadband characteristics,” *Electronics Letters*, vol. 34. p. 2194, 1998.

[117] N. Kaneda, W. R. Deal, Y. Qian, R. Waterhouse, and T. Itoh, “A broad-band planar quasi-Yagi antenna,” *IEEE Trans. Antennas Propag.*, vol. 50, pp. 1158–1160, 2002.

[118] I. K. Ivanov, M. U. Rehman, and B. Allen, “Printed Microstrip Antenna for Harvesting Energy from Mobile Phone Base Stations,” in *Antennas and Propagation (EuCAP), 2016 10th European Conference on*, pp. 2–6.

[119] David M. Pozar, “Considerations for Millimeter Wave Printed Antennas,” *IEEE Trans. Antennas Propag.*, vol. AP-31, no. 5, pp. 740–747, 1983.

[120] S. Keyrouz, H. J. Visser, and A. G. Tijhuis, “Novel Empirical Equations to Calculate the Impedance of a Strip Dipole Antenna,” pp. 1258–1261.

[121] R. S. Elliott, *Antenna Theory & Design*, Revised Ed. Wiley-IEEE Press, 2003.

[122] B. C. Wadell, *Transmission line design handbook*. 1991.

[123] J. I. K. J. Il Kim, J. M. K. J. M. Kim, Y. J. Y. Y. J. Yoon, and C. S. P. C. S. Pyo, “Wideband printed fat dipole fed by tapered microstrip balun,” *IEEE Antennas Propag. Soc. Int. Symp. Dig. Held conjunction with Usn. North Am. Radio Sci. Meet. (Cat. No.03CH37450)*, vol. 3, 2003.

[124] K. Sen Ang and L. D. Robertson, “Analysis and design of impedance-transforming planar marchand baluns,” *IEEE Trans. Microw. Theory Tech.*, vol. 49, pp. 402–406, 2001.

[125] C. Song, Y. Huang, S. Member, J. Zhou, J. Zhang, and S. Yuan, “A High-

Efficiency Broadband Rectenna for Ambient Wireless Energy Harvesting," vol. 63, no. MAY, pp. 3486–3495, 2015.

[126] M. Nie, X. Yang, G. Tan, and B. Han, "A Compact 2 . 45-GHz Broadband Rectenna Using," vol. 14, pp. 986–989, 2015.

[127] M. Arrawatia, M. S. Baghini, and G. Kumar, "Broadband Bent Triangular Omnidirectional Antenna for RF Energy Harvesting," *IEEE Antennas Wirel. Propag. Lett.*, vol. 15, pp. 36–39, 2016.

[128] M. Steer, *Microwave and RF Design: A Systems Approach*. 2010.

[129] J. A. G. Akkermans, M. C. Van Beurden, G. J. N. Doodeman, and H. J. Visser, "Analytical models for low-power rectenna design," *IEEE Antennas Wirel. Propag. Lett.*, vol. 4, no. 1, pp. 187–190, 2005.

[130] N. O. Sokal and a. D. Sokal, "Class E-A new class of high-efficiency tuned single-ended switching power amplifiers," *IEEE J. Solid-State Circuits*, vol. 10, no. 3, pp. 168–176, 1975.

[131] W. A. Nitz, W. C. Bowman, F. T. Dickens, F. M. Magalhaes, W. Strauss, W. B. Suiter, and N. G. Ziesse, "A new family of resonant rectifier circuits for high frequency DC-DC converter applications," *APEC '88 Third Annu. IEEE Appl. Power Electron. Conf. Expo.*, pp. 12–22, 1988.

[132] T. B. Mader and Z. B. Popovi??, "The Transmission-Line High-Efficiency Class-E Amplifier," *IEEE Microw. Guid. Wave Lett.*, vol. 5, no. 9, pp. 290–292, 1995.

[133] F. H. Raab, "Class-E, class-C, and class-F power amplifiers based upon a finite number of harmonics," *IEEE Trans. Microw. Theory Tech.*, vol. 49, no. 8, pp. 1462–1468, 2001.

[134] R. E. Barnett, J. Liu, and S. Lazar, "A RF to DC voltage conversion model for multi-stage rectifiers in UHF RFID transponders," *IEEE J. Solid-State Circuits*, vol. 44, no. 2, pp. 354–370, 2009.

[135] A. S. Sedra and K. C. Smith, "Microelectronic Circuits Revised Edition," *Oxford Ser. Electr. Comput. Eng.*, p. 1392, 2007.

[136] D. W. Harrist, "Wireless Battery Charging System Using Radio Frequency Energy Harvesting," 2001.

[137] T. S. Salter, "Low Power Smartdust Receiver with Novel Applications and Improvements of an RF Power Harvesting Circuit," University of Maryland, 2009.

[138] Y. Yao, Y. Shi, and F. F. Dai, "A novel low-power input-independent MOS AC/DC charge pump," *Proc. - IEEE Int. Symp. Circuits Syst.*, pp. 380–383, 2005.

[139] T. Umeda, H. Yoshida, S. Sekine, Y. Fujita, T. Suzuki, and S. Otaka, "A 950-

MHz rectifier circuit for sensor network tags with 10-m distance," *IEEE J. Solid-State Circuits*, vol. 41, no. 1, pp. 35–41, 2006.

[140] J. P. Curty, N. Joehl, F. Krummenacher, C. Dehollain, and M. J. Declercq, "A model for u-power rectifier analysis and design," *IEEE Trans. Circuits Syst. I Regul. Pap.*, vol. 52, no. 12, pp. 2771–2779, 2006.

[141] C.-J. Li and T.-C. Lee, "2.4-GHz High-Efficiency Adaptive Power Harvester," *IEEE Trans. Very Large Scale Integr. Syst.*, vol. 22, no. 2, pp. 434–438, Feb. 2014.

[142] V. Marian, B. Allard, C. Vollaire, and J. Verdier, "Strategy for Microwave Energy Harvesting From Ambient Field or a Feeding Source," *IEEE Trans. Power Electron.*, vol. 27, no. 11, pp. 4481–4491, Nov. 2012.

[143] C. R. Valenta, "Fundamental limitations for Schottky diode RF energy harvesting," *RFID Technol. Appl. (RFID-TA), 2015 IEEE Int. Conf.*, pp. 188–193, 2015.

[144] G. De Vita and G. Lannaccone, "Design criteria for the RF section of long range passive RFID systems," *Proc. Norchip Conf. 2004.*, vol. 53, no. 9, pp. 2978–2990, 2004.

[145] U. Karthaus and M. Fischer, "Fully Integrated Passive UHF RFID Transponder IC with 16.7-μ W Minimum RF Input Power," *IEEE J. Solid-State Circuits*, vol. 38, no. 10, pp. 1602–1608, 2003.

[146] F. Kocer and M. P. Flynn, "A new transponder architecture for long-range telemetry applications," *Proc. 2005 Eur. Conf. Circuit Theory Des.*, vol. 2, no. 5, pp. 177–180, 2005.

[147] Y. S. L. Wooi Gan Yeoh, Yeung Bun Choi, Kok Yin Tham, Sheng Xi Diao, "A CMOS 2.45-GHz Radio Frequency Identification Tag IC with Rea/Write Memory," *IEEE Rad0 Freq. Integr. Circuits Symp.*, vol. 00, no. C, pp. 365–368, 2005.

[148] K. Wing-Hung, S. Feng, and T. Chi-Ying, "Charge redistribution loss consideration in optimal charge pump design," *Proc. - IEEE Int. Symp. Circuits Syst.*, vol. 2, no. 8, pp. 1895–1898, 2005.

[149] A. M. Niknejad, *Electromagnetics for High-Speed Analog and Digital Communication Circuits*. Cambridge: Cambridge University Press, 2007.

[150] S. Sasaki and K. Tanaka, "Wireless power transmission technologies for solar power satellite," *2011 IEEE MTT-S Int. Microw. Work. Ser. Innov. Wirel. Power Transm. Technol. Syst. Appl. IMWS-IWPT 2011 - Proc.*, pp. 3–6, 2011.

[151] X. Li, B. Duan, L. Song, Y. Zhang, and W. Xu, "Study of Stepped Amplitude Distribution Taper for Microwave Power Transmission for SSPS," *IEEE Trans. Antennas Propag.*, vol. 65, no. 10, pp. 5396–5405, 2017.

[152] Y. Yang, Y. Zhang, B. Duan, D. Wang, and X. Li, “A novel design project for space solar power station (SSPS-OMEGA),” *Acta Astronaut.*, vol. 121, pp. 51–58, 2016.

[153] MHI, “MHI Successfully Completes Ground Demonstration Testing of Wireless Power Transmission Technology for SSPS | Mitsubishi Heavy Industries, Ltd. Global Website,” 2015. [Online]. Available: https://www.mhi.com/news/story/1503121879.html. [Accessed: 08-Nov-2018].

APPENDIX A Ofcom MW Licence

Ofcom

Non-Operational Development

SCHEDULE 1 TO LICENCE NUMBER 1005614/1

This schedule forms part of Licence **1005614/1**, issued to **University of Bedfordshire**, the Licensee on **27/08/2014,** and describes the Radio Equipment covered by the Licence and the purpose for which the Radio Equipment may be used.

1. Description of the Radio Equipment licensed

In this Licence, the Radio Equipment means sending and receiving station(s) ("base stations") and sending and receiving station(s) ("mobile stations) for wireless telegraphy as defined in paragraph 2 below.

2. Purpose of the Radio Equipment

Subject to the administrative and technical requirements set out in this and the subsequent schedule(s) to this Licence, the Licensee and any person authorised to act on the Licensee's behalf is hereby authorised to:

(a) send and receive transmissions between the base station(s) and the mobile station(s); and/or

(b) send and receive transmissions between the mobile stations.

3. Licence Term

(a) The Licence shall continue in force for the period stated in the schedule (to a maximum of twelve months) unless revoked earlier by Ofcom or surrendered by the Licensee.

(b) This Licence is not renewable

4. Radio Equipment Use

The Licensee must ensure that the Radio Equipment is established, installed and operated in accordance with the provisions of this Licence including the schedules to the Licence.

5. Special Conditions Relating To The Activities Of The Licensee

The Licensee shall:

(a) Only operate Radio Equipment on a Non Protected and Non Interference basis

(b) Only operate equipment on a Non-Operational basis

(c) Use measurement equipment to verify from time to time that the Radio Equipment is operating at the frequency and within the frequency tolerance, with the class of emission and at or below the maximum power specified in schedule 2;

(d) Not transmit until it has been confirmed as far as reasonably possible that the proposed frequency is not in use at the time of the proposed transmission;

Wireless Telegraphy Act 2006

Non-Operational Development

Sector/class/product	Science and Technology / Non-Operational Development / 601010
Licence number	1005614/1
Licensee	University of Bedfordshire
Licensee address	Park Square LUTON LU1 3JU
Date	27/08/2014
Valid from	22/08/2014
End Date	21/08/2015

1. This Licence is issued by the Office of Communications ("Ofcom") on **27 August 2014** and replaces any previous authority granted in respect of the service subject to this Licence by Ofcom or by the Secretary of State.

2. This Licence authorises **University of Bedfordshire** to establish, install and/or use Innovative radio transmitting and/or receiving stations and/or radio apparatus as described in the schedule(s) (hereinafter together called "the Radio Equipment") subject to the terms set out below and subject to the terms of the General Licence Conditions booklet.(Version OF195.1).

ISSUED BY OFCOM

Riverside House
2a Southwark Bridge Road
London SE1 9HA

Telephone +44 (0)20 7981 3000
Facsimile +44 (0)20 7981 3333

www.ofcom.org.uk

(e) Not transmit for longer than the minimum necessary for the purpose of the particular project or operation being performed; and

(f) Use the Radio Equipment:

i) As far as possible under suppressed radiation conditions; and

ii) Where this is not possible at the minimum power necessary for a particular project or operation being performed and only use the maximum power permitted, not exceeding that specified in the Schedule(s), when necessary

6. Interpretation

In the Licence, unless the context otherwise requires:

(a) "Non-Operational" means non-commercial and not for (or in connection with) the provision of any services or sale of goods

(b) "Development" means experimentation and/or innovation

(c) "Innovative" means new or not currently in general use

(d) "Non Protected" means that protection will not be given from harmful interference receied from other authorised services

(e) "Non Interference" means that the Radio Equipment must not cause harmful interference to any other authorised services

Ofcom

Non-Operational Development

SCHEDULE 2

Licence No	1005614/1	Valid from	22/08/2014	End Date	21/08/2015

Purpose of Licence

Investigate the feasibility of using radio transmissions to charge electronic devices.

Station 1 details

Base Station Address	University Campus, 502 Avebury Boulevard, Milton Keynes, MK9 3HS
Base Station NGR	SP 854 385
Maximum ERP (dbW)	-7.00

Site Contact Name	Ben Allen
Telephone No: 01582 489212	Fax No:

Antenna details

Antenna Type	01 - Directional
Antenna Gain (dB)	-20.00
Antenna Tilt (degrees)	0°
Antenna Height above ground (m)	0.5

Transmitting frequency	Channel width	Class of Emission
1,071.000000 kHz		1H00N0N

APPENDIX B Q-factor measurements

Detailed results from the measurements presented in Section 3.6

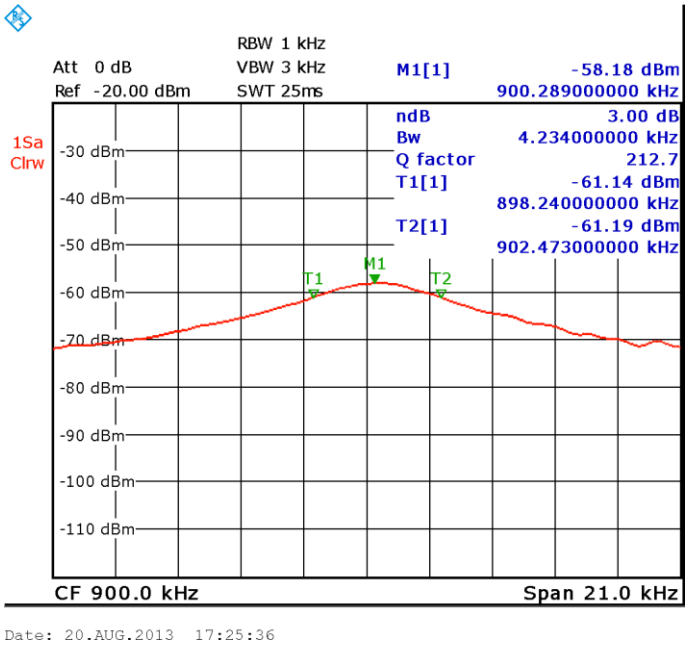

Figure B.1 Coil positions 0: Q = 212.7; L = 99µH; f_0 = 900kHz

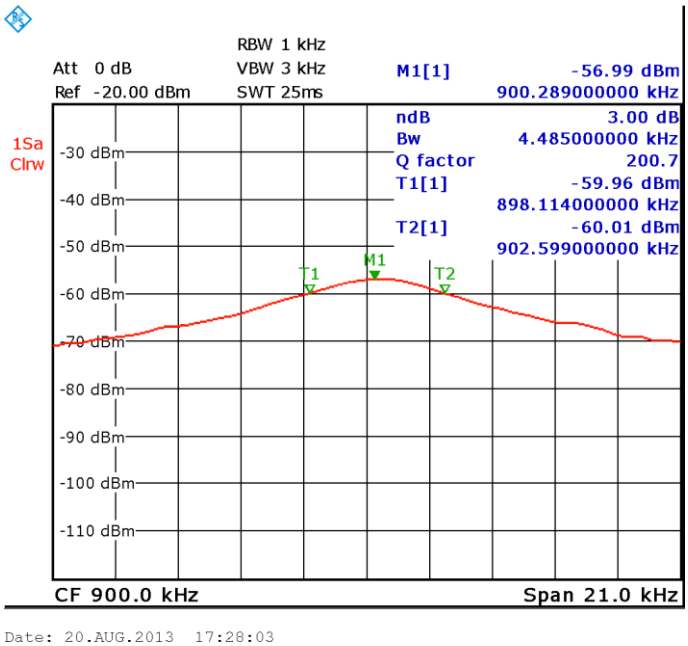

Figure B.2 Coil positions 0.1: Q = 200.7; L = 136µH; f_0 = 900kHz

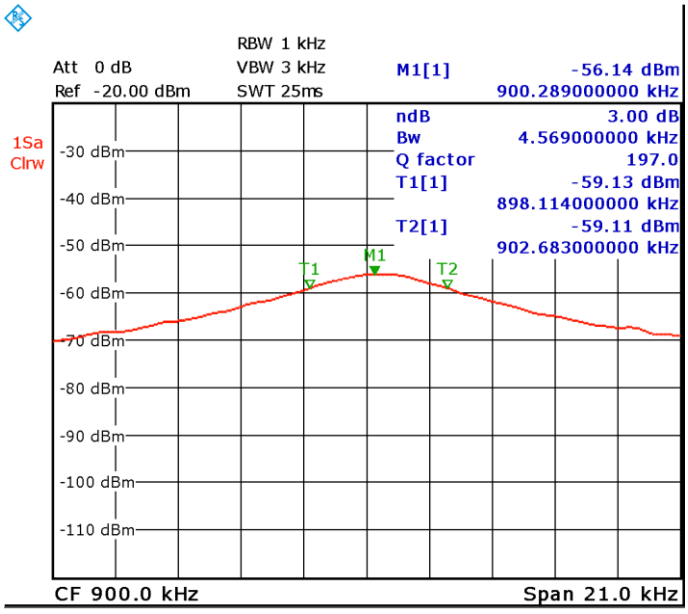

Figure B.3 Coil positions 0.2: Q = 197; L = 152µH; f_0 = 900kHz

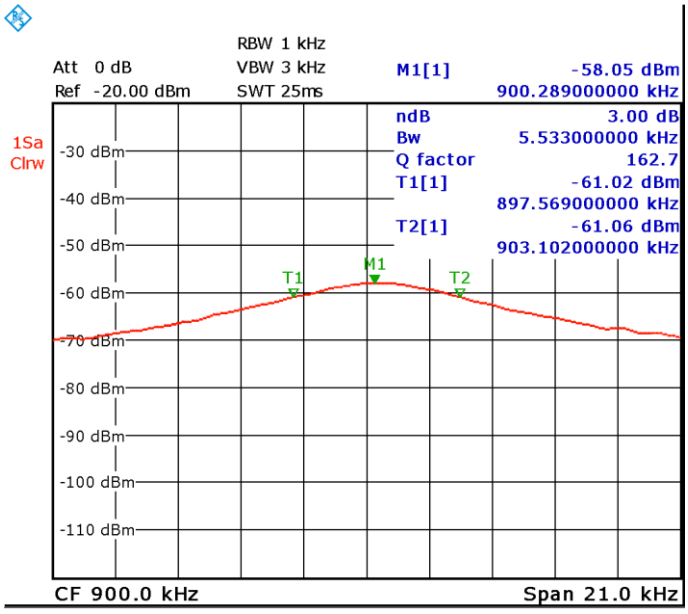

Figure B.4 Coil positions 0.3: Q = 162.7; L = 189µH; f_0 = 900kHz

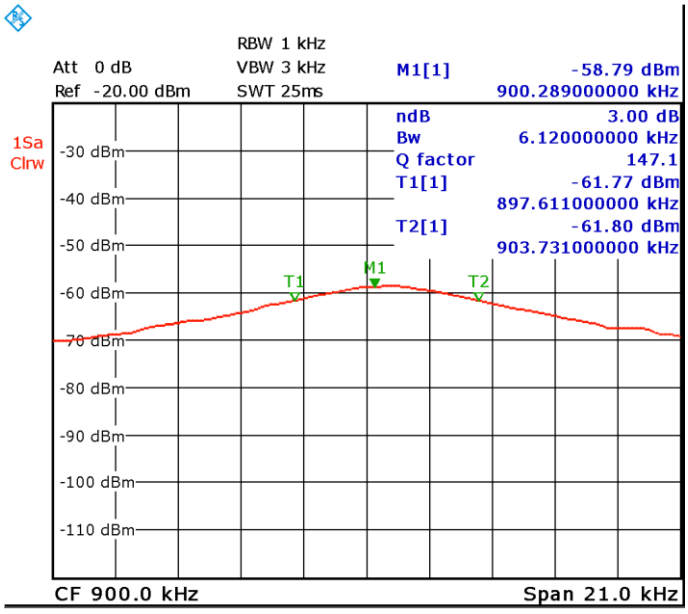

Figure B.5 Coil positions 0.4: Q = 147.1; L = 230µH; f_0 = 900kHz

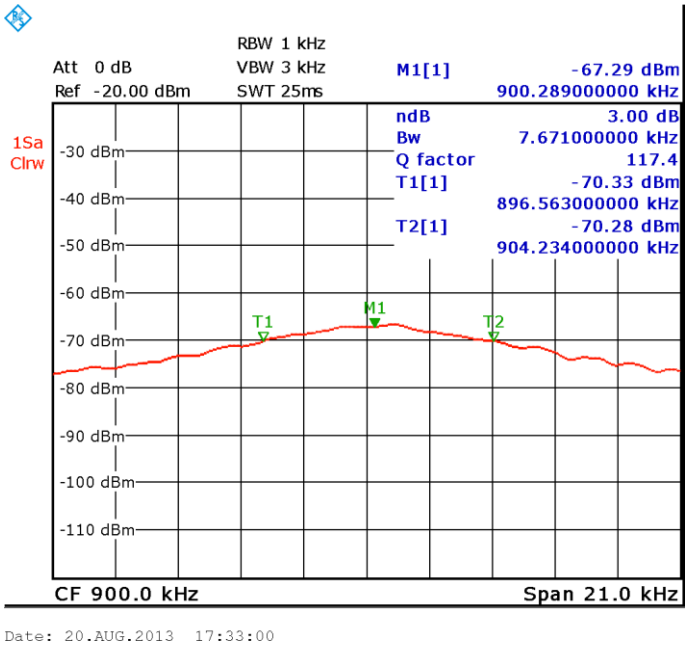

Figure B.6 Coil positions 0.5: Q = 117.47; L = 245µH; f_0 = 900kHz

APPENDIX C Impedance multimodal dependency

Table XV Multiplier's input impedance (real part) measured with different load values.

P_{in} (dBm)	SC	3.3kΩ	4.7kΩ	10kΩ	15kΩ	33kΩ	47kΩ	OC
-19	1200	1220	1320	1400	1370	1400	1320	1460
-18	1200	1380	1470	1350	1470	1600	1550	1500
-17	1140	1300	1350	1510	1550	1600	1660	1620
-16	980	1230	1410	1500	1570	1700	1680	1820
-15	850	1160	1320	1420	1540	1730	1800	1880
-14	712	1050	1230	1430	1570	1750	1850	1980
-13	593	940	1120	1370	1570	1700	1870	2020
-12	480	845	1060	1310	1460	1700	1840	2120
-11	387	760	1005	1285	1490	1730	1840	2160
-10	313	693	930	1225	1420	1730	1860	2180
-9	248	630	870	1200	1400	1770	1910	2250
-8	203	579	821	1158	1375	1760	1940	2250
-7	169	540	778	1123	1370	1770	1920	2350
-6	142	501	745	1100	1360	1780	1960	2400
-5	123	474	720	1080	1360	1800	1950	2400
-4	107	451	696	1070	1340	1820	2000	2400
-3	94	429	675	1065	1350	1880	2030	2470
-2	83	414	663	1060	1357	1900	2100	2500
-1	74	401	653	1075	1392	2020	2150	2520
0	68	395	660	1110	1450	2090	2240	2460
1	63	392	668	1160	1530	2180	2320	2400
2	59	395	684	1215	1635	2300	2420	2300
3	55	396	700	1262	1703	2350	2420	2250
4	53	399	710	1310	1770	2400	2380	2150
5	51	403	727	1356	1835	2410	2400	2080
6	49	406	741	1390	1870	2430	2390	2060
7	47	413	763	1440	1915	2380	2320	2000
8	46	424	789	1490	1970	2380	2300	1955
9	45	437	821	1545	2000	2330	2260	1920
10	45	450	851	1600	2040	2340	2230	1890
11	44	463	878	1645	2060	2330	2200	1860
12	44	473	900	1695	2080	2280	2160	1820
13	43	480	920	1712	2090	2250	2140	1800
14	43	488	932	1725	2080	2170	2080	1780
15	42	491	945	1735	2080	2160	2016	1720
16	42	495	952	1750	2045	2100	1980	1710
17	41	499	959	1745	2020	2030	1910	1640

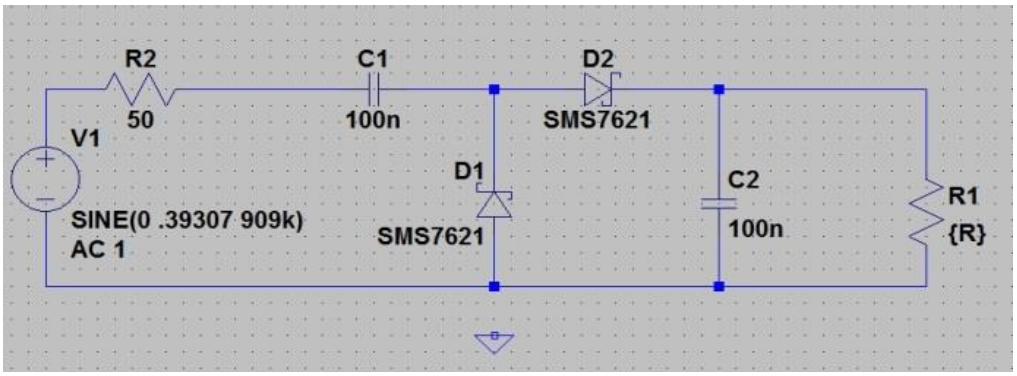

Figure C.1 Single-stage voltage doubler as presented in LTspice for the simulations in Section 5.3

APPENDIX D Detailed pictures of prototypes and trials

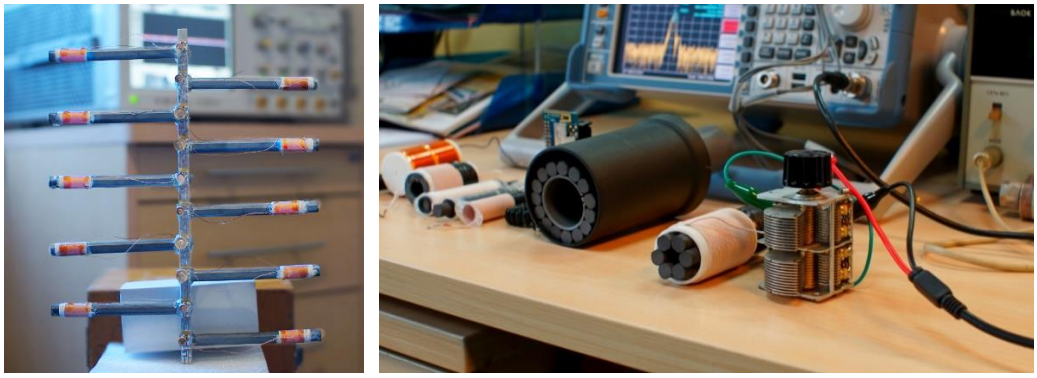

Figure D.1 Photographs of ferrite rod antenna prototypes

Figure D.2 Photographs taken during the first field trial

Figure D.3 Photographs taken during the third field trial

APPENDIX E List of UK AM Broadcast Radio Stations

Table XVI UK AM broadcast radio stations with transmitting power between 2kW and 500kW

Freq(kHz)	Station Name	Location	Power (W)	Station ID
1053	Talk Sport	Droitwich	500000	SO929663
1089	Talk Sport	Brookmans Park	400000	TL259050
1089	Talk Sport	Moorside Edge	400000	SE070154
648	BBC World Service	Orfordness	200000	
909	Radio 5 Live	Moorside Edge	200000	SE070154
1215	Virgin AM	Moorside Edge	200000	SE070154
1296	BBC World Service DRM	Orfordness	200000	
693	Radio 5 Live	Droitwich	150000	SO929663
909	Radio 5 Live	Brookmans Park	150000	TL259050
1089	Talk Sport	Westerglen	125000	NS868773
1215	Virgin AM	Brookmans Park	125000	TL259050
1458	Sunrise Radio	Brookmans Park	125000	TL259050
1215	Virgin AM	Droitwich	105000	SO929663
810	R Scotland	Burghead	100000	NJ125685
810	R Scotland	Westerglen	100000	NS868773
882	R Wales	Washford	100000	ST058410
1215	Virgin AM	Washford	100000	ST058410
1215	Virgin AM	Westerglen	100000	NS868773
1341	R Ulster	Lisnagarvey	100000	J258619
1548	Capital Gold	Saffron Green	97500	TQ216977
1089	Talk Sport	Washford	80000	ST058410
693	Radio 5 Live	Stagshaw	50000	NY986709
693	Radio 5 Live	Start Point	50000	SX814378
909	Radio 5 Live	Westerglen	50000	NS868773
909	Radio 5 Live	Clevedon	50000	ST400697
693	Radio 5 Live	Burghead	25000	NJ125685
1152	LBC News 1152	Saffron Green	23500	TQ216977
1368	Manx Radio	Foxdale	20000	SC292778
1053	Talk Sport	Postwick	18000	TG303086
1215	Virgin AM	Lisnagarvey	16000	IJ258619
1089	Talk Sport	Lisnagarvey	12500	J258619
693	Radio 5 Live	Postwick	10000	TG303086
720	BBC Radio 4	Lisnagarvey	10000	J258619
882	R Wales	Penmon	10000	SH615789
909	Radio 5 Live	Lisnagarvey	10000	J258619
1053	Talk Sport	Dumfries	10000	NY055714
1296	Radio XL	Langley Mill B	10000	SP163966
810	R Scotland	Redmoss	5000	NJ942024

882	R Wales	Tywyn	5000	SH581004
1458	BBC Asian Network	Langley Mill	5000	SP160968
1458	Big 1458 AM	Ashton Moss (NGW)	5000	SJ915985
1548	R Bristol	Mangotsfield	5000	ST672780
1053	Talk Sport	Tonbridge	4000	TQ557401
1152	Clyde 2	Dechmont Hill	3600	NS647578
1152	Capital Gold 1152	Langley Mill	3000	SP160968
1035	Kismat Asian Talk Radio	Crystal Palace	2500	TQ339712
1215	Virgin AM	Redmoss	2300	NJ942024
1053	Talk Sport	Southwick Brighton	2200	TQ234051
1089	Talk Sport	Redmoss	2200	NJ942024
1215	Virgin AM	Wrekenton	2200	NZ274598
1548	Forth 2	Colinswell	2200	NT221861
585	R Scotland (Solway)	Dumfries	2000	NY055714
603	BBC Radio 4	Wrekenton	2000	NZ274598
630	R Cornwall	Redruth	2000	SW709403
657	R Wales (Clwyd)	Wrexham	2000	SJ312497
756	BBC Radio 4	Redruth	2000	SW709403
801	R Devon	Barnstaple	2000	SS519298
909	Radio 5 Live	Redruth	2000	SW709403
1089	Talk Sport	Redruth	2000	SW709403
1107	Talk Sport	Lydd	2000	TR049208
1197	Virgin AM	Hoo	2000	TQ790720
1215	Virgin AM	Redruth	2000	SW709403
1242	Virgin AM	Boston	2000	TF260448
1368	R Lincolnshire	Swan Pool Lincoln	2000	SK956710
1449	BBC Radio 4	Redmoss	2000	NJ942024
1458	R Devon	Occombe Torbay	2000	SX878630
1458	R Newcastle	Wrekenton	2000	NZ274598
1485	R Humberside	Hull	2000	TA169258
1485	R Merseyside	Wallasey	2000	SJ305926